Summer 8-15-2019

Regulation of the Yeast Cell Cycle Checkpoint Kinase Tel1 at Double-Strand DNA Breaks and at Telomeres

Sarem Hailemariam
Washington University in St. Louis

WASHINGTON UNIVERSITY IN ST. LOUIS

Division of Biology and Biomedical Sciences
Molecular Cell Biology

Dissertation Examination Committee:

Peter Burgers, Chair
Eric Galburt
Roberto Galletto
John Majors
Alessandro Vindigni
Zhongsheng You

Regulation of the Yeast Cell Cycle Checkpoint Kinase Tel1 at Double-Strand DNA Breaks and at Telomeres

by
Sarem S. Hailemariam

A dissertation presented to
The Graduate School
of Washington University in
partial fulfillment of the
requirements for the degree
of Doctor of Philosophy

August 2019

St. Louis, Missouri

Table of contents

List of Figures

Acknowledgments

This dissertation required the unwavering support and encouragement of so many people over the last six years. To my advisor, Peter, thank you for being one of a kind mentor to me. You are an incredibly thorough scientist who is not only invested in the scientific development of your students but also their well-being. I have learned so much by paying attention to the type of questions you ask. Your enjoyment of designing and doing experiments is infectious and has always been one of my favorite qualities about you. Thank you for the confidence you have instilled in me and embodying the qualities of a great mentor I aspire to acquire one day!

To my committee members; Drs. Eric Galburt, Roberto Galletto, John Majors, Alessandro Vindigni, and Zhongsheng You: thank you for your time, help, and insightful suggestions. I would like to specifically thank John and Roberto. John, having you as an honorary member of the Burgers lab and being able to interact with you on a regular basis was a real treat. Thank you for always being a source of encouragement and for the numerous impromptu discussions about my project. Roberto, I very much enjoyed working on the Rif2 project with you. I always walk away learning something new from our discussions. Thank you for being generous with your time and reagents.

To all the members of the Burgers lab past and present, thank you immensely! Joe, thank you for being there to discuss ambiguous results and provide insightful suggestions and for being a great friend overall. Rachel, Elias, and Tanumoy – thank you for being a valuable source of scientific expertise and making the lab a fun place to work. Kim, you are one of my favorite people to talk science with. Thank you for your support and killer sense of humor. Bonnie, thank you for always offering to help in all the ways you can. Thank you for being so caring and making me feel at home. Carrie or the do-it-all and know-it-all member of the Burgers lab, thank

for all your help over the years. A few days go by where I don't need your assistance. Thank you for the countless discussions whether it's about science, current events, or podcasts.

Thank you to all my great friends, Caitlin, Mike, Bhavna, Youjin, Anshu, Scott, Jeff, and Dana, who made this process fun and memorable. Getting to the finish line of this journey would not have been possible without you all. I love you and I cherish the friendships we've built.

Thank you to my wonderful parents, siblings, and the rest of my family. Thank you for your unwavering support, encouragement, and love. I wouldn't be where I am today without your dedication and investment in my education! I love you all dearly.

Sarem S. Hailemariam

Washington University in St. Louis

August 2019

ABSTRACT OF THE DISSERTATION

Regulation of the Yeast Cell Cycle Checkpoint Kinase Tel1at Double-Strand DNA Breaks and at Telomeres

by

Sarem S. Hailemariam

Doctor of Philosophy in Biology and Biomedical Sciences

Molecular Cell Biology

Washington University in St. Louis, 2019

Professor Peter Burgers, Chair

The work discussed in this dissertation focuses on two distinct areas that are critical for genome maintenance. Both areas are focused on the regulation of the *Saccharomyces cerevisiae* checkpoint kinase Tel1 by the MRX complex. Tel1 kinase initiates cell cycle checkpoint in response to double-strand DNA breaks. Tel1 also plays a major role in telomere maintenance. Tel1's function both in checkpoint signaling and telomere regulation is dependent on the Mre11-Rad50-Xrs2 complex. In Chapter II, I describe a robust biochemical approach aimed at reconstituting the initial stages of double-strand DNA break response using purified proteins in order to address how the MRX complex and DNA orchestrate to activate Tel1 kinase. Our results demonstrate that double-stranded DNA and MRX activate Tel1 synergistically. This work revealed a DNA length dependent stimulation of Tel1, with long, nucleosome-free duplex DNA being the preferred effector for full Tel1 activation. Our work also highlights there is no requirement for double-stranded DNA ends for Tel1 activation by MRX *in vitro.* Our data show Rad50 is the most critical subunit as no stimulation of Tel1 is seen with the Mre11-Xrs2 pair and DNA, which is in agreement with reported genetic observations. This stimulatory effect of

Rad50 is absolutely dependent on its ATP binding activity. This work provides a comprehensive model into how individual subunits of MRX collaborate with DNA to activate Tel1 kinase.

The second portion of this thesis discusses work employing the biochemical assay described in Chapter II to investigate the regulation of Tel1 kinase and MRX at telomeres. Similar to several other checkpoint and DNA repair factors, Tel1 and MRX are involved in telomere regulation. Unique architectural organization and remodeling of telomeric DNA by telomere binding proteins prevents telomeres from inappropriate recognition and repair as intrachromosomal DNA breaks. In budding yeast, Rif2 is one of the main proteins involved in checkpoint response suppression at long telomeres. MRX has been shown to recruit Tel1 specifically to short telomeres, resulting in the recruitment of telomerase and the elongation of short telomeres. Conversely, based on genetic observations Rif2 has been suggested to attenuate elongation of long telomeres through the MRX-Tel1 pathway. Our studies show Rif2 directly inhibits MRX-dependent activation of Tel1 kinase. The inhibitory role of Rif2 is mediated through its conserved N-terminal domain. Our data demonstrate that Rif2 exerts its inhibition by modulating the ATPase activity of Rad50. Investigation of an allosteric Rad50 ATPase mutant that maps outside of the conserved ATP binding domain suggest Rif2 discharges the ATP-bound form of Rad50, which is a state conducive for Tel1 activation. Taken together these data point to a novel role of Rif2 in regulating Tel1 kinase through the Rad50 subunit of MRX

Chapter I

DNA Damage response mechanisms

Genome maintenance is central for the survival and proper functioning of all organisms. Genome instability is a biological phenomenon characterized by reduced fidelity with which genetic information is passed onto daughter cells. It is caused when cells fail to detect DNA damage and properly repair the damage in the parental DNA before cell division. Genome integrity is under constant assault both from endogenous and exogenous DNA damaging agents that result in different types of DNA lesions. Endogenous DNA damaging agents can be byproducts of normal cellular metabolic processes such as free radicals. Exogenous damaging agents include ultraviolet light (UV), alkylating agents like methymethane sulfonate (MMS), and antitumor drugs like bleomycin. Maintenance of genome integrity relies on the DNA damage response (DDR), which is an intricate network of signal transduction, cell cycle regulation, and DNA damage repair mechanisms.

DNA double-strand breaks

DNA double-strand breaks (DSBs) are one of the most cytotoxic forms of DNA lesions and are generated from breakage of the two complementary DNA strands. The hazardous nature of DSBs is highlighted by the observation that failure to repair a single DSB was shown to lead to cell death (Malkova and Haber, 2012). Misrepair of DSBs on the other has catastrophic consequences such as chromosomal rearrangements. Defects in DSB repair pathways are implicated in a number of disorders including cancer and immunodeficiency diseases (McKinnon and Caldecott, 2007; Prochazkova and Loizou, 2016; Rulten and Caldecott, 2013).

Causes of DNA double-strand breaks

Although DSBs are the most hazardous types of DNA lesions, their formation can be intrinsic to normal cellular functions. Programmed DSBs are formed as intermediates during immune system development in class switch and V(D)J recombination. DSBs are also induced during meiosis and mating type switching in yeast. In addition, intrinsic DSBs can arise spontaneously during DNA replication and mitosis. Replication fork collapse can lead to the formation of single-ended DSBs. The physical stress of chromosome segregation during mitosis can form DSBs as well. DNA-damaging agents used for therapeutic approaches, such as ionizing radiation (IR), and chemotherapeutic drugs like camptothecin and etoposide cause DSBs. Therefore, the formation and metabolism of DSBs is an integral part of cellular development and underscores the genesis of a plethora of disorders (Mehta and Haber, 2014).

DSB repair pathways

Cells employ two major pathways to repair DSBs – nonhomologous end joining (NHEJ) and homologous recombination (HR) **Figure 1**. The repair choice between these two pathways is tightly regulated and is dependent on the structure of the broken DNA ends and cell cycle phase (Mehta and Haber, 2014; Shibata, 2017).

Non-homologous end joining

As implied by the name NHEJ, the two broken DNA ends are directly ligated, sometimes after minimal processing. There is little to no homology between the ligated DNA ends. A subset of NHEJ known as microhomology-mediated end joining (MMEJ) relies on short homologous sequences of a few base-pairs generated by the end resection machinery to align DNA ends before ligation. Although NHEJ provides the simplest approach to repair DSBs, it is closely related with illegitimate recombination and chromosomal rearrangements. Thus, NHEJ is a less proficient and error-prone repair pathway. In *S. cerevisiae* NHEJ is dependent on the heterodimeric protein complex YKu70 and YKu80 and the DNA ligase Dnl4, and its cofactors Lif1 and Nej1 (mammalian Xrcc4 and Xlf4 respectively). The Ku proteins are the defining protein complex in NHEJ and avidly bind DNA ends in a sequence-independent manner. Association of Ku dimers with DNA ends protects them from nucleolytic degradation. Loading of Ku at DNA ends inhibits resection and prevents formation of long stretches of single-stranded DNA, which is needed for homologous recombination. Ku-mediated inhibition of resection is the initial step in successful NHEJ. In *S. cerevisiae* there are no DNA end processing nucleases associated with NHEJ pathway. Therefore, NHEJ can only function with high proficiency and fidelity in repair of "clean"

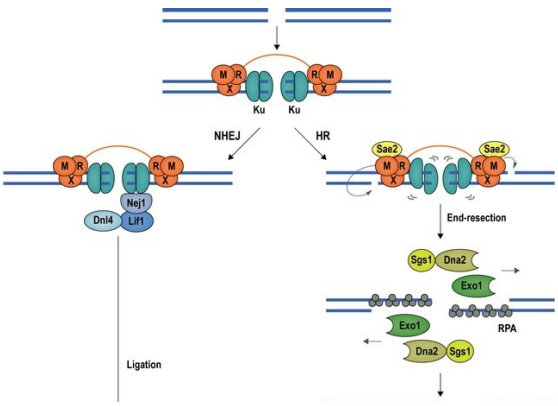

Figure 1. Mechanisms of DSB repair by NHEJ and HR in yeast. The Ku hetrodimer initiates NHEJ and recruits Lif1-Dnl4 and Nej1 ligase complex. The MRX complex along with Sae2 promotes HR by initiating end-resection. Exo1, Dna2, and Sgs1 carry out long-range resection (Fontana et al., 2018).

compatible DNA ends. Complex and "dirty" DNA ends like the ones generated by IR require processing prior to ligation (reviewed in (Emerson and Bertuch, 2016; Mehta and Haber, 2014).

Homologous Recombination

The homologous recombination repair pathway uses undamaged sister chromatids or homologous chromosomes as a template to guide DNA synthesis across the break. HR is carried out by the Rad52 epistasis group of proteins, which includes Rad50, Rad51, Rad52, Rad54, Rad57, and Mre11. After damage recognition, the initial step in HR is nucleolytic processing of DNA ends in the 5' to 3'direction to generate 3' single-stranded DNA overhangs, a process called end resection. As a critical early step in HR, end resection serves as a governing point in DSB repair pathway choice. DNA end resection is cell cycle regulated to makes sure HR occurs primarily in S and G2 phases when a sister chromatid is present to be used as a repair template. In *S. cerevisiae*, initial end resection is initiated by the Mre11/Rad50/Xrs2 (MRX) complex. MRX along with Sae2 (mammalian CtIP) carry out limited end resection. The MRX complex is also required for the recruitment of additional resection nucleases, Exo1, Sgs1, and Dna2. More extensive resection is done by Exo1 or the concerted effort of Sgs1 and Dna2. The resulting ssDNA overhangs are bound by the ssDNA binding protein RPA (replication protein A). Rad52 (orthologous to mammalian BRCA 2) facilitates the exchange of RPA with Rad51. Rad51 recombinase forms a nucleoprotein filament that performs a homology search to identify an intact donor DNA with sequence homology to Rad51-bound single-stranded DNA. This nucleoprotein filament catalyzes strand invasion leading to the formation of a

D-loop where the ssDNA is paired with the homologous donor DNA. The 3' end of the invading ssDNA serves as a primer to synthesize DNA enabling the information within the donor template to be used to replace sequence information lost from the damaged DNA (reviewed in (San Filippo et al., 2008)).

Cellular response to DNA double-strand breaks

Faithful transmission of genetic information from one cell to the other during cell division is essential for survival, and is an ongoing challenge to cells. It is crucial that progression of cell cycle is stalled to allow cells to properly and efficiently repair DNA lesions. In incidents of irreparable DNA damage, the DDR can trigger apoptosis or senescence to prevent the passage of damaged DNA to daughter cells. Failure to trigger apoptosis in these cells can result in improper segregation of chromosomes, accumulation of mutation and ultimately genomic instability (Malkova and Haber, 2012). Weinert and Hartwell elucidated surveillance mechanisms that enable cells to delay cell cycle progression in response to DNA damage (Weinert and Hartwell, 1988). These mechanisms are known as cell cycle checkpoints and comprise the cellular response to DNA breaks. Three DNA repair checkpoints have been characterized in *Saccharomyces cerevisiae*, G1/S, intra-S, and G2/M. Checkpoint proteins are categorized into four major groups; damage sensors, signal mediators, signal transducers, and effectors (reviewed in (Barnum and O'Connell, 2014).

The cellular response to DSBs relies on sensor proteins to detect the damage and elicit a signal. This signal is relayed to effectors through the action of intermediates known as transducers. Transducers control cell cycle arrest, DNA repair, and apoptosis.

Transducers coordinate these processes through posttranslational modification of effector proteins. In *S. cerevisiae,* DNA damage checkpoints are initiated by two major transducer kinases, Tel1 and Mec1. In response to double-strand breaks the Mre11-Rad50-Xrs2 is the DNA damage sensor. The MRX complex is discussed in more detail later in this chapter. In addition to sensing the damage, MRX also recruits the transducer checkpoint kinase Tel1 to break sites (reviewed in (Abraham, 2001; Oh and Symington, 2018).

Tel1 kinase

TEL1 (Telomere maintenance 1) was first identified in a genetic screen for genes that affect telomere length in *Saccharomyces cerevisiae* (Lustig and Petes, 1986). Tel1 is a serine-threonine checkpoint kinase that is activated in response to DSBs and is the ortholog of mammalian Ataxia telangiectasia mutated (ATM) kinase. *TEL1* encodes a large (320KDa) protein that shares a 40% amino-acid sequence identity in the kinase domain and 20% amino-acid sequence identity in the rest of the protein with the mammalian ATM gene (Greenwell et al., 1995; Morrow et al., 1995).

Structural organization of Tel1

Tel1 belongs to the phosphoinositide 3-kinase-related protein kinase (PIKK) family of kinases and mediates checkpoint response by phosphorylating downstream targets. Other members of PIKK family kinases involved in checkpoint signaling include yeast Mec1 (mammalian ATR), DNA-

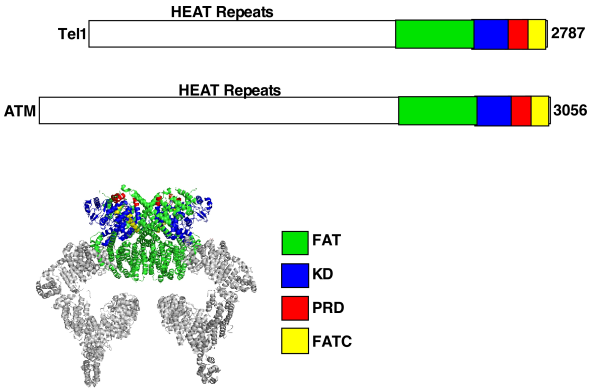

Figure 2. Domain organization of the yeast Tel1 and mammalian ATM kinases. Both Tel1 and ATM exist as a dimer. FAT and Kinase Domains mediate an interaction between two Tel1 molecules. (PDB ID:4JSV)

dependent protein kinase (DNA-PK), and ATM (Lempiainen and Halazonetis, 2009). The canonical motif recognized for phosphorylation by these kinases is S/T-Q cluster domain (SCD), which is characterized by serine (S) or threonine (T) followed by a glutamine (Q) (Traven and Heierhorst, 2005). Members of PIKK family are very large enzymes (270–460 kDa) that share structural homology. The N-terminal and central regions are made up of tandem HEAT (Huntigton, Elongation factor 3, A subunit of protein phosphatese 2A, and TOR1) repeats, with a single HEAT domain comprised of anti-parallel helices joined by a flexible loop (Perry and Kleckner, 2003; Shiloh, 2003). These regions show very little sequence homology even within subfamilies (**Figure 2**). Structural studies have revealed that HEAT repeats attain a super helical conformation that is believed to mediate protein-protein and protein-DNA interaction. A relatively small C-terminal kinase domain follows these tandem HEAT repeats (Perry and Kleckner, 2003). The kinase domain makes up only 5-10% of the total sequence and is flanked by two highly conserved domains known as FAT (FRAP, ATM, TRRAP) and FATC (FAT C-terminus) domains. FAT and FATC domains are believed to play a role in regulating the kinase domain (Bosotti et al., 2000; Ogi et al., 2015). Recent structural studies from both *S.pombe* and *S.cerevisiae* have shown that the kinase and FATC domains mediate interactions between two Tel1 proteins to form a dimer (Sawicka et al., 2016; Wang et al., 2016; Xin et al., 2019).

Tel1-dependent checkpoint response to DSBs

Tel1 and Mec1 are both activated in response to DNA lesions but respond to distinctly different types of DNA damage. Tel1 primarily responds to double-strand breaks, while Mec1 is activated by stretches of ssDNA coated with the ssDNA binding protein RPA (Sanchez et al., 1996; Usui et al., 2001; Zou and Elledge, 2003). Upon recruitment to damage sites, Tel1 phosphorylates histone H2A. This phosphorylation event is important for marking the chromatin surrounding the DNA lesion, and also facilitates recruitment and retention of DNA repair factors (Downs et al., 2000). Phosphorylated H2A is recognized by the BRCT-containing adaptor protein, Rad9 (mammalian 53BP1) (Hammet et al., 2007). Rad9 itself is a substrate of Tel1 and this Tel1-dependent phosphorylation upon damage transforms it into a binding partner for Rad53 (Hammet et al., 2007). Rad53 undergoes autophosphorylation, an event required for its full activation and release from phospho-Rad9 (Usui et al., 2009). Rad53 is the master effector kinase that couples cell cycle arrest with DNA repair and is the budding yeast sequence homologue of mammalian Chk2 kinase. Rad53

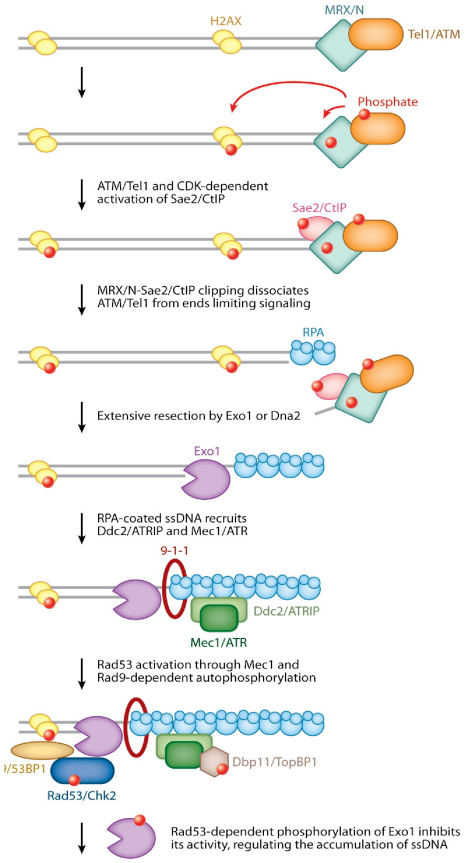

Figure 3. Tel1-mediated checkpoint response. MRX recruits Tel1 to DSBs. Extensive resection of DSBs orchestrates the switch from Tel1-dependent checkpoint response to that of Mec1 (Symington and Gautier, 2011).

is essential for normal cell growth, replication stress response, and DNA damage checkpoints (**Figure 3**). Rad53 is required for arrest in G1/S, intra-S, and G2/M checkpoints. It is also important for the replication checkpoint that monitors progression of DNA synthesis. Rad53 has several downstream targets required for DNA repair and induces an array of transcriptional changes in response to damage. Some of these Rad53-controlled events include downregulation of the ribonucleotide reductase (RNR) inhibitor, Sml1, to increase deoxyribonucleotide pools to facilitate DNA synthesis, phosphorylation of Dbf4 to stall late origin-firing in response to replication stress, and phosphorylation of Exonuclease 1 to turn off DNA end resection (Lee et al., 2003; Usui et al., 2009; Usui et al., 2001).

Activation of Tel1 kinase: lessons from higher eukaryotes

Both Tel1 and ATM primarily respond to DSBs. However, the specific signal that activates Tel1 and ATM after double-strand breaks is still unknown. Studies of ATM have lead to a proposal where changes and chromatin modification near break sites serve as the initial triggering signal that leads to activation of the kinase. Mammalian ATM has been shown to exist as an inactive dimer in unperturbed cells. Upon DSB induction or treatment with agents that alter chromatin structure, ATM undergoes an autophosphorylation event on serine 1981 leading to dimer to monomer transition (Bakkenist and Kastan, 2003). Bakkenist & Kastan showed that phosphorylation on S1981 occurs in trans and phosphomimetic mutants are not able to form dimers, indicating that phosphorylation on S1981 disrupts the ATM dimer. Although the functional significance of Serine 1981 is still ambiguous and ATM recruitment occurs

independent of autophosphorylation, it's been shown to be important to stabilize ATM at break sites (Daniel et al., 2008; So et al., 2009). S1981A ATM mutants act as dominant negative for autophosphorylation, S-phase checkpoint, and localization to DNA breaks, further highlighting that autophosphorylation, and hence monomerization are important for ATM functions in DNA damage response (Bakkenist and Kastan, 2003; Berkovich et al., 2007).

In addition to autophosphorylation on serine 1981, complete activation of ATM requires its association with the MRN complex. Biochemical studies have shown that the MRN complex is able to fully activate ATM monomer in the absence of DNA (Lee and Paull, 2004). DNA is required only when the dimeric ATM form is present in kinase reactions. This observation suggested that DNA mediates the autophosphorylation of ATM at serine 1981. In mammalian cells it was also shown that tethering of sufficient amount of Mre11, Nbs1 or ATM to a specific chromosome locus leads to activation of ATM, suggesting one possible function of the interaction between the MRN complex and ATM is to facilitate the accumulation of ATM at DNA breaks (Soutoglou and Misteli, 2008).

DNA end resection and Tel1-dependent checkpoint response

Although Mec1/ATR primarily responds to replication stress, it is also a key regulator of DSBs. However, in humans, ATR activation is slower than that of ATM and mainly takes place in the S/G2 phase of the cell cycle (Jazayeri et al., 2006). Homology directed DSB repair mechanisms involve nucleolytic processing of the DNA ends to generate 3' single-stranded DNA overhangs. These ssDNA overhangs are bound by RPA

(Symington and Gautier, 2011). Both in yeast and mammalian cells, recruitment of Mec1/ATR requires RPA-coated single-stranded DNA overhangs (Zou and Elledge, 2003). Tel1 and ATM are required for DNA end resection and their activation leads to accumulation of ssDNA at DSB ends, suggesting sequential activation of these two kinases (Jazayeri et al., 2006; Mantiero et al., 2007; Myers and Cortez, 2006; Shiotani and Zou, 2009). Shiotani and Zou showed in *Xenopus* extracts that while activations of both ATM and ATR are dependent on ss/dsDNA junctions, they are oppositely regulated by single-stranded overhang length. They showed that blunt ended dsDNA and DNA ends with short overhangs are the preferred substrates for ATM. As single-stranded tails grow in length, it leads to ATM kinase inactivation and simultaneously triggers ATR signaling (Shiotani and Zou, 2009). Mantiero *et al* proposed a similar mechanism in *S. cerevisiae*, where Tel1-mediated signaling dampens when DSB ends are subjected to 5'-3' exonucleolytic processing. These observations suggest that the nature of DNA ends command whether it is Tel1/ATM or Mec1/ATR that is engaged (Mantiero et al., 2007).

S. cerevisiae strains defective in resection such as *sae2*Δ and *exo1*Δ are unable to turn off checkpoint signaling in response to unrepaired DSB. In addition, deletion of Sae2 enhances Tel1-dependent activation of Rad53 after DNA damage. This increased Rad53 activation appears to be due to prolonged association of MRX with DNA breaks, leading to sustained Tel1 activity (Clerici et al., 2006; Usui et al., 2001). These data taken together indicate that generation of ssDNA by the resection machinery leads to the displacement of MRX, which in turn attenuates Tel1 signaling. These data are also consistent with a working model where extensive DNA resection orchestrates the transition from a Tel1-mediated checkpoint to that of Mec1 (**Figure 3**).

The Mre11-Rad50-Xrs2 Complex

The metabolism of DNA double-strand breaks administered by the DDR is crucial for genome integrity and cell viability. DDR triggered by DSBs involves three distinct parts/functionalities: 1) detection of the damage, 2) induction of a signaling cascade to control cell cycle and transcriptional responses to the damage, and 3) mechanisms to efficiently repair the lesion. The Mre11 complex made up of meiotic recombination 11 (Mre11), Rad50, X-Ray Sensitive 2 (Xrs2) complex sits at the hub of the DSB-mediated damage response and is a critical player in all three aspects of DSB repair. The MRX complex acts as a damage sensor, governs DSB-induced cell cycle checkpoint, and facilitates lesion repair in both NHEJ and HR pathways (Gobbini et al., 2016; Paull, 2018).

Mre11, Rad50, and Xrs2 were first identified in *Saccharomyces cerevisiae.* The *MRE11* gene was identified in a genetic screen for mutants defective in meiotic recombination (Ajimura et al., 1993). *RAD50* and *XRS2* were identified in a genetic screen for mutants sensitive to ionizing radiation (Game and Mortimer, 1974; Ivanov et al., 1992). Xrs2 is the yeast homologue of mammalian Nijmegen breakage syndrome 1 (Nbs1). The Mre11 and Rad50 subunits are conserved in all forms of life where as Xrs2 has only been found in eukaryotes. *Mre11*, *rad50*, and *xrs2* deletion strains exhibit similar phenotypes and these three proteins were later shown to form a complex (Usui et al., 1998).

Components of the MRX Complex

Mre11

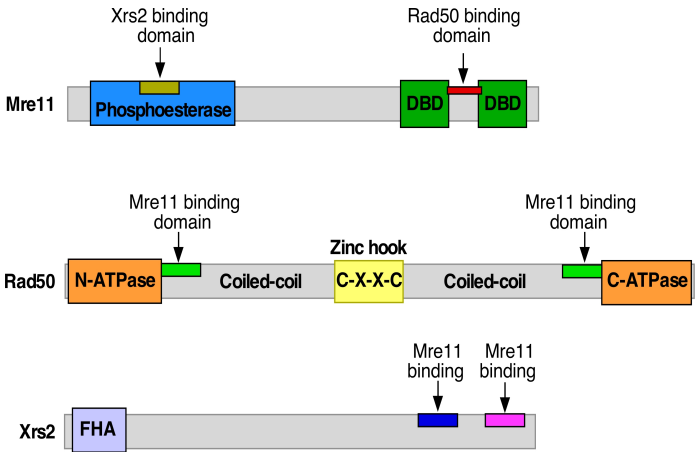

Figure 3. Domain organization of Mre11, Rad50, and Xrs2.

Mre11 is a highly conserved 70-90 KDa protein and is a member of the lambda phosphatase family of phosphoesterases. The N-terminal region contains manganese-dependent phosphodiesterase activity while two distinct DNA-binding domains are located in the C-terminus (**Figure 4**). Mre11 has been shown to form a stable dimer and interacts with both Rad50 and Xrs2/Nbs1 individually (Gobbini et al., 2016; Krogh and Symington, 2004; Syed and Tainer, 2018). It displays ssDNA endonuclease and 3'-5' dsDNA exonuclease activities. The endonuclease and exonuclease activities of Mre11 do not depend on Rad50 and Xrs2 but are enhanced when Mre11 is in complex with them (Paull and Gellert, 1998; Trujillo et al., 1998). MRX along with Sae2 has been proposed to initiate DNA end resection. *S. cerevisiae* strains lacking Sae2 or any of the MRX components delay resection of an endonuclease-induced DSB (Clerici et al., 2006). Surprisingly, Mre11 lacks the 5'-3' exonuclease activity required to generate 3'-ssDNA tails for the initiation of HR (Paull and Gellert, 1998; Trujillo et al., 1998). Its weak endonuclease activity is stimulated by Sae2 and by a protein block at DNA ends. MRX along with Sae2 cleaves 20 nucleotides from linear DNA ends bound to biotin-streptavidin at the 5' end (Cannavo and Cejka, 2014; Garcia et al., 2011). In addition, *sae2*Δ and *mre11* nuclease mutant strains are defective in the

removal of Spo11, a protein that generates meiotic DSBs and stays covalently bound to the 5'- ends of the resulting breaks. These strains are also hypersensitive to camptothecin, a drug that extends the half-life of DNA-topoisomerase protein complexes. These studies suggest MRX, through its Mre11 subunit; initiates end resection by generating a nick that serves as an entry site for additional nucleases to DNA in 5' – 3' polarity (Keeney and Kleckner, 1995; Neale et al., 2005).

Rad50

Rad50 is a 152 KDa ATPase that shares sequence and structural homology to the structural maintenance of chromosomes (SMC) family of proteins that control dynamics of chromatin (Kinoshita et al., 2009). The N-terminal Walker A and C-terminal Walker B nucleotide binding motifs associate with each other to generate a functional bipartite ATP binding pocket. This interaction is ATP-dependent, where two ATP molecules are sandwiched between the Rad50-Rad50 dimer interfaces. This globular domain has been shown to preferentially bind and partially unwind dsDNA (de Jager et al., 2001; Hopfner et al., 2001; Hopfner et al., 2000). The intervening amino acids between the ATPase form two anti-parallel coiled-coil domains that are separated by a zinc-hook (CXXC) motif (**Figure 4**). The coiled-coil domains fall back on themselves, juxtaposing the ATP binding pockets. The zinc motif facilitates dimerization of two Rad50 molecules. Interactions between adjacent amino acids near the zinc hook provide additional coiled-coil dimer interface and stabilize hook-mediated dimerization. Zinc hook and coiled-coil mediated dimerization is implicated in tethering two DSBs and holding sister chromatids together, preventing the damaged chromatin physically separating. This sister chromatid

bridging activity is believed to mediate homology search during HR and averts the DSB from becoming a chromosome break (Hohl et al., 2011; Hopfner et al., 2002; Wiltzius et al., 2005). A stable Mre11-Rad50 core complex is formed when Mre11 binds a Rad50 molecule at the intersection of its globular ATP binding pocket and coiled-coil domains. The ATPase domain, along with the nuclease and DNA binding motifs of Mre11 comprise the catalytic core of the MRX complex. In *S. cerevisiae*, the ATP-dependent activities of Rad50 are required for all of its function in DNA repair as ATPase dead mutants show similar phenotype to *rad50* null strains (Chen et al., 2005; de Jager et al., 2001; Hopfner et al., 2001).

Xrs2/Nbs1

Xrs2/Nbs1 is the least conserved subunit and has only been identified in eukaryotes. It has been shown to stimulate the ATPase, DNA binding, and nuclease activities of the Mre11-Rad50 dimer but it does not have any reported enzymatic activity (Carney et al., 1998). The N-terminal domain of Xrs2 contains a phosphopeptide recognition motif known as fork-head associated (FHA) domain (**Figure 4**). The mammalian Nbs1 has two BRCT domains in addition to a FHA domain. The FHA domain binds to phosphorylated threonine residues within SCDs (Becker et al., 2006; Matsuzaki et al., 2008). Through these phosphorylation-dependent interactions, Xrs2/Nbs1 mediates the recruitment and retention of repair factors to DNA break sites. It is the only subunit that contains a nuclear localization signal (NLS) and its association with Mre11 is important for the translocation of the Mre11-Rad50 dimer complex to the nucleus (Tsukamoto et al., 2005). Genetic studies in *S. cerevisiae* have shown that alteration of residues within the Mre11 binding domain that abrogate the Xrs2 interaction

with Mre11, result in identical phenotypes as *xrs2* and *mre11* deletion strains (Tsukamoto et al., 2005). Similar mutations lead to embryonic lethality in mice (Kim et al., 2017). In budding yeast, the requirement for Xrs2 to translocate Mre11-Rad50 to the nucleus is partially restored by fusing Mre11 to the NLS domain. Expression of this fusion protein suppressed the DNA damage sensitivity of *xrs2Δ* strains but was unable to compensate for defects in Tel1 signaling (Oh et al., 2016; Tsukamoto et al., 2005).

The C-terminal domain of Xrs2/Nbs1 contains a conserved FXF/Y motif that mediates the interaction with Tel1/ATM. Disruption of this Xrs2-Tel1 interaction confers similar phenotypes as Tel1 null strains, which are characterized by defective Tel1-mediated DNA damage response and short telomeres. Attaching the Tel1 interacting domain of Xrs2 to Mre11-NLS restores Tel1 checkpoint signaling and telomere length (Nakada et al., 2003). These data highlight the role of Xrs2/Nbs1 in recruiting Tel1 to DNA break sites.

Role of ATP on the structural architecture of MRX

The MRX complex integrates both its enzymatic and structural functions in DNA damage signaling. As a damage sensor and one of the initial protein complexes that bind to broken DNA ends, it is involved in the structural tethering of DNA ends. It also recruits Tel1 kinase and

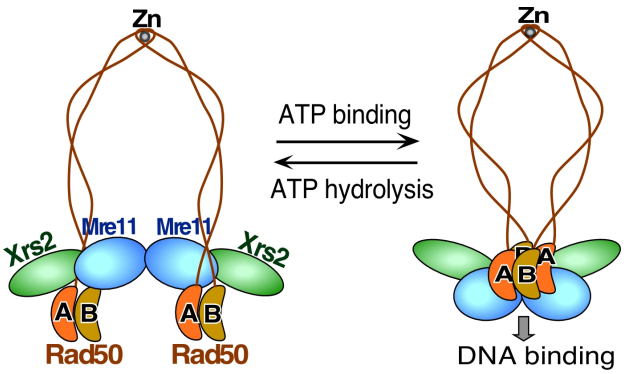

Figure 4. Structural architecture of the MRX complex in the presence of ATP. ATP binding by Rad50 transforms MRX from an open to closed conformation.

initiates nucleolytic degradation of DNA ends. Structural studies from bacterial and archaeal complexes have provided substantial insight into how the structural organization of MRX governs its catalytic activities (reviewed in (Stracker and Petrini, 2011).

MRX has been designated as an ATP-controlled molecular switch, with distinct ATP-induced conformations possessing different cellular functions. The DNA binding domain of MRX is made up of the Mre11 dimer along with the ATP binding pocket of the Rad50 dimer. In the presence of ATP, the Mre11-Rad50 dimer adopts a closed confirmation. Upon ATP binding, the nucleotide binding domains of Mre11 and Rad50 engage with one another by sandwiching two ATP molecules in their dimer interface (Deshpande et al., 2014). In the ATP bound state, the dimer interacts with the DNA binding cleft of the Mre11 dimer, resulting in the partial blockage of the Mre11 nuclease active site. Biochemical studies have suggested that the exonuclease activity of Mre11 is hindered in this conformation while the endonuclease activity is unaffected (Herdendorf et al., 2011; Lim et al., 2011).

Role of MRX in damage detection and checkpoint activation

The MRX complex is among the first protein complexes to sense DNA double-strand breaks (Lisby et al., 2004). MRX binding to the broken DNA ends marks the beginning of the cellular response to DSBs. Both in mammalian and yeast cells, MRX/N was shown to be present evenly diffused throughout the nucleus, suggesting MRX serves as a surveillance factor that scans along the genome to detect broken DNA ends. Upon DSB formation, the complex rapidly relocalizes from the diffuse pool to the site of DNA damage to form repair foci (Lisby et al., 2004; Myler et al., 2017). In agreement with its

role as a damage sensor, concentrations of MRX/N components remain constant throughout the cell cycle. Lisby *et al* showed that in yeast cells, Mre11 is the first protein detected at DSBs and that a 50-fold higher concentration of MRX protein is detected near the vicinity of DNA breaks. This redistribution of MRX and other repair proteins to DSB foci in high concentrations is suggested to facilitate lesion repair and coordinate cell cycle progression with repair status (Lisby et al., 2004).

After MRX has detected DNA lesions and is bound to DNA ends, it recruits Tel1 checkpoint kinase (Falck et al., 2005). The presence of a functional relationship between MRN and ATM came from the observation of nearly indistinguishable clinical phenotypes between ATLD (hypomorphic for Mre11 activity) and AT patients, suggesting that it is likely that these two protein complexes function in the same pathway. ATLD cells show reduced activation of ATM kinase after DSBs, indicating MRN is required for full activation of ATM after DSB induction and therefore describing the clinically similar phenotypes between AT and ATLD patients (Stewart et al., 1999). Subsequent studies both in yeast and mammalian cells showed that localization of Tel1/ATM to DNA damage sites depends at a minimum on the interaction between Tel1/ATM and Xrs2/Nbs1. Removal of Tel1/ATM interacting motif in Xrs2/Nbs1 attenuates Tel1/ATM signaling (Nakada et al., 2003; You et al., 2005). However, both the Mre11 and Rad50 subunits also interact with Tel1, suggesting that the required interaction network may be more complex (Hailemariam et al., 2019).

Biochemical and genetic studies in mammalian cells and *Xenopus* egg extracts have shown direct role of MRN in activation of ATM kinase. Using purified proteins Lee *et al* showed MRN facilitates conversion of inactive ATM dimers into active monomers.

MRN interaction with ATM induces an intermolecular autophosphorylation in ATM leading to dissociation of the dimer into monomers (Lee and Paull, 2004, 2005). In budding yeast, Tel1 activation is directly coupled with its localization to DSB ends *in vivo*. Oh *et al* showed the Xrs2 subunit of MRX is indispensible for Tel1-mediated checkpoint signaling is *S. cerevisiae (Oh et al., 2016)*. Tel1 checkpoint function is redundant with Mec1 kinase. Due to this redundancy DNA damage-induced activation of Rad53 effector kinase in *Tel1* delete cells is unperturbed. The checkpoint function of Tel1 is discernable in cells that fail to initiate DNA end resection. In fact, a delay in DNA end resection initiation and persistence of MRX at DNA ends results in hyperactivation of Tel1 kinase (Oh et al., 2016). Dampening of Tel1-mediated signaling correlates with the initiation of DNA end resection, which in turn activates the Mec1 pathway. Therefore, in addition to sensing DNA lesions and initiating a Tel1 signaling, the MRX complex plays a role in orchestrating the transition from Tel1 to Mec1-mediated pathway (Mantiero et al., 2007; Shiotani and Zou, 2009).

The role of MRX in DNA repair

MRX is a key factor that controls the initiation of DNA end resection and keeps DNA ends tethered to each other before repair through homologous recombination and non-homologous end joining begins. Several lines of work have shown that inactivation of Mre11, Rad50, or Xrs2 affects a number of DNA metabolic processes, including HR and NHEJ, indicating that the MRX complex has a role in both HR and NHEJ in yeast (Adelman and Petrini, 2009). Consistent with the compactness of its genomes and the relative absence of repetitive sequences, HR is the dominant pathway during lesion repair in yeast. In mammalian cells, where repetitive sequences and intergenic regions are more

abundant, NHEJ is suggested to be quicker and more efficient repair choice. Moore & Haber and Boulton & Jackson independently showed that MRX is essential for NHEJ in budding yeast (Boulton and Jackson, 1998; Moore and Haber, 1996). The Xrs2 subunit was shown to directly interact with Lif1, suggesting that MRX facilitates the recruitment of DNA Ligase IV to DNA breaks. Hence, MRX has been suggested to play a structural role in NHEJ as an end-joining factor rather than an enzymatic role, because Mre11 nuclease-deficient cells show no defects in NHEJ (Moreau et al., 1999).

All three subunits of the MRX complex are classified under the Rad52 epistasis group of proteins, which are essential players in HR repair pathway. Budding yeast lacking all components of MRX are still able to carry out HR, although resection initiation is delayed (San Filippo et al., 2008). In meiotic recombination, MRX is believed to be involved in the initial formation of DSBs at regions of recombination hotspots. MRX then aids in the resection of these breaks to generate 3' overhangs, which serves as a substrate for the HR repair machinery. During DNA end resection in response to damage, the MRX complex is aided by its cofactor Sae2. MRX along with Sae2 catalyze cleavage internal to the 5' end, generating a single-stranded nick. This nick serves as an entry point for additional resection machineries such as Exo1, Sgs1, and Dna2 to resect DNA in the 5' to 3' direction. MRX employs its 3' to 5' nuclease activity to degrade from an internal nick towards the 5'-termini of broken DNA ends. This activity of MRX is suggested to be important for removing hairpin structures and covalently bound proteins from DNA ends (reviewed in (Mimitou and Symington, 2009).

In addition to its endonucleolytic activity in end resection, MRX also recruits Exo1, Sgs1, and Dna2 to DNA ends. Yeast cells expressing a nuclease dead mutant of

mre11 exhibit a mild resection defect at clean DSBs lacking covalently modified ends, with a delay in resection initiation. On the other hand, *mre11Δ* and *rad50Δ* cells show more severe defects, likely due to an impaired recruitment of Sgs1 and Dna2. DNA damage sensitivity of *mre11Δ* and *rad50Δ* cells is rescued by deletion of Ku70/80 in a process that requires, indicating that Ku70/80 inhibits Exo1 from getting access to DNA ends (Shim et al., 2010). In fission yeast and mammalian cells, Mre11 nuclease-dead mutants show more severe defects in resection and HR than in budding yeast. This severe phenotype is due to the requirement for Mre11 nuclease to remove Ku from DNA ends and the inability of Sgs1-Dna2 to compensate for the lack of Mre11 nuclease activity in those organisms (Shim et al., 2010). MRX/N has also been shown to stimulate the nuclease activities of Exo1, Sgs1, and Dna2 *in vitro*, highlighting the collaboration between short-range and long-range resection factors (Niu et al., 2010; Shim et al., 2010).

Roles of Tel1 kinase and the MRX complex in telomere regulation and maintenance

Telomeres

Telomeres are DNA-protein complexes that define the physical ends of linear eukaryotic chromosomes. Proper establishment and maintenance of telomeres is critical for genome stability and cell survival. Telomeres progressively shorten as cells divide. Telomere shortening is counteracted by telomerase, a reverse transcriptase enzyme that synthesizes TG-rich telomere repeats using an AC repeat motif-containing RNA subunit as template. Both yeast cells and primary mammalian cells that are unable to maintain telomeres initiate senescence, which is mediated by a DNA damage-signaling pathway.

Telomere-induced senescence underlies a plethora of human genetic disorders that share short telomere as a common molecular defect. On the other hand, inappropriate elongation of telomere leads to cancer predisposition and aids the survival of cancer cells.In most species, telomeric DNA is made up of tandem arrays of short repeated sequences that are guanine-rich in the strand running 5'- 3' from the centromere to chromosome ends. Some telomeric DNAs are made of perfect repeats such as TTAGGG repeats in metazoans, or can be heterogenic repeats of $(TG)_{1-4}G_{2-3}$ repeats in *Saccharomyces cerevisiae*. The size of duplex telomeric DNA per chromosome end varies from organism to organism, ranging from 300-350 bp in budding and fission yeast to 2-50 kb in humans (reviewed in (Palm and de Lange, 2008; Wellinger and Zakian, 2012).

Telomeric DNA is divided into three regions; a sub telomeric domain, the double-stranded repeat region, and a 3' single-stranded tail. Sub-telomeric regions contain repetitive telomere associated sequences. The heterogeneous nature of sub-telomeric confers distinct behaviors by individual telomeres. The extreme ends of telomeres are not blunt ended, rather made up of 3'-overhang. The G-strand at both ends of a chromosome extends over the C-strand to form this 3'-overhang (Dionne and Wellinger, 1996). Mammalian 3'-G-tails vary in size from 50-500nt while *Saccharomyces cerevisiae* is between 12-15nt throughout the cell cycle, although it temporarily extends to 100nt in late S and G2 phases during telomere replication (Makarov et al., 1997; McElligott and Wellinger, 1997). The 3'-tail is subjected to nucleolytic degradation. This nucleolytic processing converts telomere ends to preferred substrate for telomerase, which cannot act on blunt ended DNA substrates. This nucleolytic degradation also generates a ssDNA

substrate that is bound by the telomere-specific ssDNA binding protein, Cdc13.

The double-stranded region of telomeres in *Saccharomyces cerevisiae* is made up of 300-350 bp $(TG)_{1\text{-}4}G_{2\text{-}3}$-repeats and is bound by telomere-associated proteins. Unlike mammalian telomeres, the sequence of budding yeast telomeric repeats is heterogeneous in nature. Sequence analysis of the same telomere driven from a given colony has revealed that the end region shows sequence diversity while the internal region of telomeres maintains sequence identity during DNA replication. This indicates that the extreme ends of telomeric DNA are more susceptible to recombination and telomerase-mediated extension (Wellinger and Zakian, 2012).

Telomere maintenance

In most eukaryotes, telomeres are extended using telomerase. The telomerase holoenzyme is a ribonucleoprotein complex with reverse transcriptase catalytic subunit (*s.c*Est2 and *hs*TERT) and RNA component (*s.c*TLC1 and *hs*TERC) used as a template for telomere extension. The 3' end of chromosome ends serve as a primer for Est2 and is located adjacent to the short template sequence in TLC1 (Lundblad and Szostak, 1989). A single extension round of telomere termini adds one telomere repeat. Repeated cycles of extension enable telomere length maintenance. In many unicellular organisms telomerase is constitutively active, which is in contrast with human somatic cells where telomerase is suppressed. Tumor cells, like human primary cells, are dependent on telomerase activity for telomere maintenance. The progressive proliferation of cancer cells in several cancers has been associated with unregulated telomerase activity (Palm and de Lange, 2008).

Telomerase-mediated extension is not the only mechanism that eukaryotes employ to maintain telomere homeostasis. Telomerase negative yeast cells rely on the homologous recombination proteins, Rad50, Rad51, and Rad52 to maintain telomere length. Yeast cells that are dependent on the Rad51 recombinase in order to survive in the absence of telomerase are classified as Type I survivors (Lundblad and Blackburn, 1993; Teng and Zakian, 1999). Rad51 is a Rec-A like recombinase and acts in conjunction with Rad54, Rad55, and Rad57 to extend telomeres. The other group of survivors is called Type II survivors and exhibit comparable telomere lengths seen in human tumor cells and immortal cell lines. Type II survivors use a telomerase independent pathway known as alternative telomere lengthening (ALT) pathway to extend telomeres. The ALT pathway is dependent on Rad50-mediated homologous recombination. This pathway requires MRX and Sgs1 (Teng and Zakian, 1999).

Telomere length regulation

Regulation of telomere length involves a negative feedback loop that keeps telomeres within a broad range size. Newly synthesized telomeric repeats are bound by protein complexes that negatively regulate telomerase, leading to this feedback loop. In budding yeast, Rap1, Rif1, and

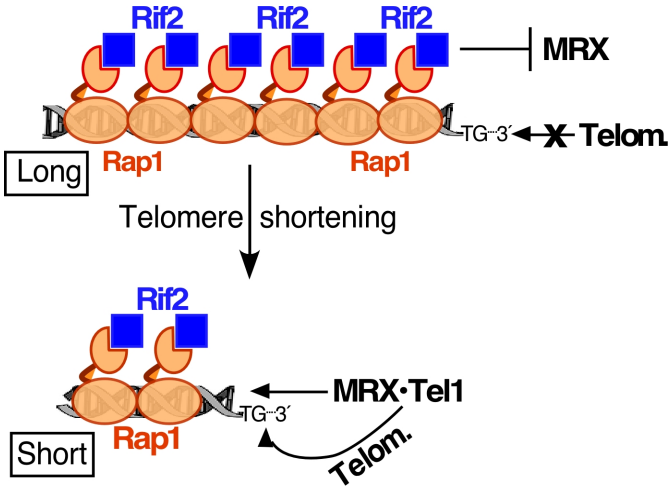

Figure 5. The protein counting model. High concentrations of Rif2 at long telomeres inhibits functions of Tel1 and MRX.

Rif2 make up the major double-stranded telomeric DNA binding protein complex and are negative regulators of telomere length. *RAP1* (Repressor Activator Protein 1) is an essential gene in *Saccharomyces cerevisiae* and plays a role in gene regulation in addition to its critical role in telomere length maintenance (Shore and Nasmyth, 1987). Consistent with its telomere regulatory role, the double-stranded regions of yeast telomeres contain multiple arrays of high affinity Rap1 binding sites (Gilson et al., 1993).

Rap1 also recruits Rif1 and Rif2 to telomeres. As indicated by their names, Rap1 interacting factor 1 and 2, both of these proteins bind to the C-terminal domain of Rap1 and this interaction is required for their recruitment. Deletion of Rif1 and Rif2 leads to telomere elongation and deletion of both has an additive effect, resulting in even longer telomeres. Strains that express a Rap1 variant lacking the C-terminal domain confer telomere phenotypes similar to *rif1Δ rif2Δ* double deletion strains (Hardy et al., 1992; Wotton and Shore, 1997). Based on these genetic observations, a protein-counting model has been proposed to describe how these factors coordinate to negatively regulate telomere length (Levy and Blackburn, 2004; Marcand et al., 1997). The model suggests that long telomeres, by the virtue of their size, are able to support the binding of multiple Rap1-Rif1-Rif2 complexes (**Figure 6**). This large number of Rap1-Rif1-Rif2 molecules leads to a larger repressive effect on telomere elongation. On the other hand, short telomeres have fewer of these repressive factors bound and are more frequently elongated. Tethering Rif1 and Rif2 to telomeres by fusing these proteins to other DNA binding domains, rather than to Rap1, also limits telomere elongation. This suggests that Rif1 and Rif2, rather than Rap1, facilitate repression of telomere elongation and the number of telomere associated Rif1 and Rif2 proteins serve as a sensor for telomere

length (Levy and Blackburn, 2004).

No orthologs for Rif2 have been found outside of closely related yeast species. Sequence comparisons of the genomes of *S. cerevisiae* and *Kulyveromyces polysporus* revealed that *RIF2* is syntenic to *ORC4*. Based on sequence alignment, Rif2 was predicted to possess a general AAA+ ATPase fold similar to Orc4. The Walker A lysine in Rif2 is replaced by a histidine and the Walker B aspartate residue is substituted by glutamic acid, indicating the two motifs that are responsible for ATPase activity in AAA+ proteins are absent in Rif2. As a result, Rif2 lacks any detectable ATPase activity (Marcand et al., 2008).

Tel1 kinase and MRX complex in telomere regulation

Yeast cells lacking Tel1 or *tel1* kinase dead mutants exhibit short telomeres in comparison to wild-type cells. This suggests that the telomere regulatory role of Tel1 depends on its kinase activity (Lustig and Petes, 1986; Mallory and Petes, 2000). In wild-type cells, Tel1 association with telomeres is weak and mainly restricted to late S-G2 phase of the cell cycle. As telomeres shorten over time Tel1 binding to telomeres increases, indicating preferential binding to short telomeres (Hector et al., 2007; Sabourin et al., 2007). Tel1 phosphorylates Cdc13 and this phosphorylation event is thought to facilitate the recruitment of telomerase (Tseng et al., 2006). However, data contradicting this interpretation have been reported (Arneric and Lingner, 2007; Gao et al., 2010). Preferential elongation of short telomeres at native telomeres is reported to occur in cells lacking Tel1, suggesting an alternative mechanism, in which reduced telomere shortening in these cells is due to reduced telomere resection. Hence, it remains unclear whether

Tel1 directly phosphorylates telomere-binding factors to facilitate telomerase recruitment or whether it plays an indirect role in mediating G-tail extension to provide a better substrate for telomerase binding.

The MRX complex is required for maintenance of telomere length in *S. cerevisiae*. Null mutations in any of the subunits of MRX confer telomere phenotypes similar to Tel1-deficient cells, indicating that Tel1 and MRX function in the same epistatic telomere regulation pathway (Ritchie and Petes, 2000). Consistent with this, binding of Tel1 to telomeres is dependent on the interaction between Tel1 and Xrs2 (Hirano et al., 2009).

Interplays between DDR factors and telomere regulatory factors

The ends of chromosomes bare resemblance to one half of a DNA double-strand break. The unique architectural organization of telomeres enables cells to distinguish chromosome ends from intrachromosomal DNA breaks and help confer genome stability. Telomeres protect chromosome ends from nucleolytic degradation and prevent their improper recognition by DNA repair machineries and subsequent activation of a DNA-damage checkpoint response. In yeast, loss of a single telomere elevates the risk loss of a whole chromosome (Sandell and Zakian, 1993). Proper "capping" of telomeres is therefore essential for genome maintenance. The Rap1-Rif1-Rif2 protein complex is the one of major telomere capping factors involved in restricting checkpoint response at telomeres.

Despite the bulk of genetic evidence on checkpoint responses to deregulated telomeres, the exact mechanism of how the Rap1-Rif1-Rif2 complex exerts it anti-

checkpoint function at telomeres remains unclear. Several studies have proposed a model where Rap1-Rif1-Rif2 protein complex acts through the Tel1-MRX pathway to regulate telomere length in yeast (Cassani et al., 2016; Hirano et al., 2009). Rif2 has been shown to physically interact with the Xrs2 C-terminus, counteracting Xrs2-Tel1 interaction. Abrogating Xrs2-Tel1 interaction reduces telomere association of MRX, suggesting a feedback loop regulation where Tel1 enhances MRX retention at telomeres (Hirano et al., 2009).

Chapter II of this thesis describes a biochemical assay for MRX-dependent and DNA-dependent activation of Tel1 in the phosphorylation of downstream checkpoint factors. Our data demonstrate the requirement of double-stranded DNA and the Rad50 subunit for optimal stimulation of Tel1 kinase. The work described in Chapter III make use of this biochemical assay to investigate the role of Rif2 in modulating the activity of the MRX-DNA-Tel1 complex in the regulation of telomere length. We show Rif2-induced ATPase activity has a negative role in MRX-dependent Tel1 stimulation.

Reference:

Abraham, R.T. (2001). Cell cycle checkpoint signaling through the ATM and ATR kinases. Genes & development *15*, 2177-2196.

Adelman, C.A., and Petrini, J.H. (2009). Division of labor: DNA repair and the cell cycle specific functions of the Mre11 complex. Cell cycle (Georgetown, Tex) *8*, 1510-1514.

Ajimura, M., Leem, S.H., and Ogawa, H. (1993). Identification of new genes required for meiotic recombination in Saccharomyces cerevisiae. Genetics *133*, 51-66.

Arneric, M., and Lingner, J. (2007). Tel1 kinase and subtelomere-bound Tbf1 mediate preferential elongation of short telomeres by telomerase in yeast. EMBO reports *8*, 1080-1085.

Bakkenist, C.J., and Kastan, M.B. (2003). DNA damage activates ATM through intermolecular autophosphorylation and dimer dissociation. Nature *421*, 499-506.

Barnum, K.J., and O'Connell, M.J. (2014). Cell cycle regulation by checkpoints. Methods in molecular biology (Clifton, NJ) *1170*, 29-40.

Becker, E., Meyer, V., Madaoui, H., and Guerois, R. (2006). Detection of a tandem BRCT in Nbs1 and Xrs2 with functional implications in the DNA damage response. Bioinformatics (Oxford, England) *22*, 1289-1292.

Berkovich, E., Monnat, R.J., Jr., and Kastan, M.B. (2007). Roles of ATM and NBS1 in chromatin structure modulation and DNA double-strand break repair. Nature cell biology *9*, 683-690.

Bosotti, R., Isacchi, A., and Sonnhammer, E.L. (2000). FAT: a novel domain in PIK-related kinases. Trends in biochemical sciences *25*, 225-227.

Boulton, S.J., and Jackson, S.P. (1998). Components of the Ku-dependent non-homologous end-joining pathway are involved in telomeric length maintenance and telomeric silencing. The EMBO journal *17*, 1819-1828.

Cannavo, E., and Cejka, P. (2014). Sae2 promotes dsDNA endonuclease activity within Mre11-Rad50-Xrs2 to resect DNA breaks. Nature *514*, 122-125.

Carney, J.P., Maser, R.S., Olivares, H., Davis, E.M., Le Beau, M., Yates, J.R., 3rd, Hays, L., Morgan, W.F., and Petrini, J.H. (1998). The hMre11/hRad50 protein complex and Nijmegen breakage syndrome: linkage of double-strand break repair to the cellular DNA damage response. Cell *93*, 477-486.

Cassani, C., Gobbini, E., Wang, W., Niu, H., Clerici, M., Sung, P., and Longhese, M.P. (2016). Tel1 and Rif2 Regulate MRX Functions in End-Tethering and Repair of DNA Double-Strand Breaks. PLoS biology *14*, e1002387.

Chen, L., Trujillo, K.M., Van Komen, S., Roh, D.H., Krejci, L., Lewis, L.K., Resnick, M.A., Sung, P., and Tomkinson, A.E. (2005). Effect of amino acid substitutions in the rad50 ATP binding domain on DNA double strand break repair in yeast. The Journal of biological chemistry *280*, 2620-2627.

Clerici, M., Mantiero, D., Lucchini, G., and Longhese, M.P. (2006). The Saccharomyces cerevisiae Sae2 protein negatively regulates DNA damage checkpoint signalling. EMBO reports *7*, 212-218.

Daniel, J.A., Pellegrini, M., Lee, J.H., Paull, T.T., Feigenbaum, L., and Nussenzweig, A. (2008). Multiple autophosphorylation sites are dispensable for murine ATM activation in vivo. The Journal of cell biology *183*, 777-783.
de Jager, M., van Noort, J., van Gent, D.C., Dekker, C., Kanaar, R., and Wyman, C. (2001). Human Rad50/Mre11 is a flexible complex that can tether DNA ends. Molecular cell *8*, 1129-1135.
Deshpande, R.A., Williams, G.J., Limbo, O., Williams, R.S., Kuhnlein, J., Lee, J.H., Classen, S., Guenther, G., Russell, P., Tainer, J.A*., et al.* (2014). ATP-driven Rad50 conformations regulate DNA tethering, end resection, and ATM checkpoint signaling. The EMBO journal *33*, 482-500.
Dionne, I., and Wellinger, R.J. (1996). Cell cycle-regulated generation of single-stranded G-rich DNA in the absence of telomerase. Proceedings of the National Academy of Sciences of the United States of America *93*, 13902-13907.
Downs, J.A., Lowndes, N.F., and Jackson, S.P. (2000). A role for Saccharomyces cerevisiae histone H2A in DNA repair. Nature *408*, 1001-1004.
Emerson, C.H., and Bertuch, A.A. (2016). Consider the workhorse: Nonhomologous end-joining in budding yeast. Biochemistry and cell biology = Biochimie et biologie cellulaire *94*, 396-406.
Falck, J., Coates, J., and Jackson, S.P. (2005). Conserved modes of recruitment of ATM, ATR and DNA-PKcs to sites of DNA damage. Nature *434*, 605-611.
Fontana, G.A., Reinert, J.K., Thoma, N.H., and Rass, U. (2018). Shepherding DNA ends: Rif1 protects telomeres and chromosome breaks. Microbial cell (Graz, Austria) *5*, 327-343.
Game, J.C., and Mortimer, R.K. (1974). A genetic study of x-ray sensitive mutants in yeast. Mutation research *24*, 281-292.
Gao, H., Toro, T.B., Paschini, M., Braunstein-Ballew, B., Cervantes, R.B., and Lundblad, V. (2010). Telomerase recruitment in Saccharomyces cerevisiae is not dependent on Tel1-mediated phosphorylation of Cdc13. Genetics *186*, 1147-1159.
Garcia, V., Phelps, S.E., Gray, S., and Neale, M.J. (2011). Bidirectional resection of DNA double-strand breaks by Mre11 and Exo1. Nature *479*, 241-244.
Gilson, E., Roberge, M., Giraldo, R., Rhodes, D., and Gasser, S.M. (1993). Distortion of the DNA double helix by RAP1 at silencers and multiple telomeric binding sites. Journal of molecular biology *231*, 293-310.
Gobbini, E., Cassani, C., Villa, M., Bonetti, D., and Longhese, M.P. (2016). Functions and regulation of the MRX complex at DNA double-strand breaks. Microbial cell (Graz, Austria) *3*, 329-337.
Greenwell, P.W., Kronmal, S.L., Porter, S.E., Gassenhuber, J., Obermaier, B., and Petes, T.D. (1995). TEL1, a gene involved in controlling telomere length in S. cerevisiae, is homologous to the human ataxia telangiectasia gene. Cell *82*, 823-829.
Hailemariam, S., Kumar, S., and Burgers, P.M. (2019). Activation of Tel1(ATM) kinase requires Rad50 ATPase and long nucleosome-free DNA but no DNA ends. The Journal of biological chemistry *294*, 10120-10130.
Hammet, A., Magill, C., Heierhorst, J., and Jackson, S.P. (2007). Rad9 BRCT domain interaction with phosphorylated H2AX regulates the G1 checkpoint in budding yeast. EMBO reports *8*, 851-857.

Hardy, C.F., Sussel, L., and Shore, D. (1992). A RAP1-interacting protein involved in transcriptional silencing and telomere length regulation. Genes & development *6*, 801-814.
Hector, R.E., Shtofman, R.L., Ray, A., Chen, B.R., Nyun, T., Berkner, K.L., and Runge, K.W. (2007). Tel1p preferentially associates with short telomeres to stimulate their elongation. Molecular cell *27*, 851-858.
Herdendorf, T.J., Albrecht, D.W., Benkovic, S.J., and Nelson, S.W. (2011). Biochemical characterization of bacteriophage T4 Mre11-Rad50 complex. The Journal of biological chemistry *286*, 2382-2392.
Hirano, Y., Fukunaga, K., and Sugimoto, K. (2009). Rif1 and rif2 inhibit localization of tel1 to DNA ends. Molecular cell *33*, 312-322.
Hohl, M., Kwon, Y., Galvan, S.M., Xue, X., Tous, C., Aguilera, A., Sung, P., and Petrini, J.H. (2011). The Rad50 coiled-coil domain is indispensable for Mre11 complex functions. Nature structural & molecular biology *18*, 1124-1131.
Hopfner, K.P., Craig, L., Moncalian, G., Zinkel, R.A., Usui, T., Owen, B.A., Karcher, A., Henderson, B., Bodmer, J.L., McMurray, C.T.*, et al.* (2002). The Rad50 zinc-hook is a structure joining Mre11 complexes in DNA recombination and repair. Nature *418*, 562-566.
Hopfner, K.P., Karcher, A., Craig, L., Woo, T.T., Carney, J.P., and Tainer, J.A. (2001). Structural biochemistry and interaction architecture of the DNA double-strand break repair Mre11 nuclease and Rad50-ATPase. Cell *105*, 473-485.
Hopfner, K.P., Karcher, A., Shin, D.S., Craig, L., Arthur, L.M., Carney, J.P., and Tainer, J.A. (2000). Structural biology of Rad50 ATPase: ATP-driven conformational control in DNA double-strand break repair and the ABC-ATPase superfamily. Cell *101*, 789-800.
Ivanov, E.L., Korolev, V.G., and Fabre, F. (1992). XRS2, a DNA repair gene of Saccharomyces cerevisiae, is needed for meiotic recombination. Genetics *132*, 651-664.
Jazayeri, A., Falck, J., Lukas, C., Bartek, J., Smith, G.C., Lukas, J., and Jackson, S.P. (2006). ATM- and cell cycle-dependent regulation of ATR in response to DNA double-strand breaks. Nature cell biology *8*, 37-45.
Keeney, S., and Kleckner, N. (1995). Covalent protein-DNA complexes at the 5' strand termini of meiosis-specific double-strand breaks in yeast. Proceedings of the National Academy of Sciences of the United States of America *92*, 11274-11278.
Kim, J.H., Grosbart, M., Anand, R., Wyman, C., Cejka, P., and Petrini, J.H.J. (2017). The Mre11-Nbs1 Interface Is Essential for Viability and Tumor Suppression. Cell reports *18*, 496-507.
Kinoshita, E., van der Linden, E., Sanchez, H., and Wyman, C. (2009). RAD50, an SMC family member with multiple roles in DNA break repair: how does ATP affect function? Chromosome research : an international journal on the molecular, supramolecular and evolutionary aspects of chromosome biology *17*, 277-288.
Krogh, B.O., and Symington, L.S. (2004). Recombination proteins in yeast. Annual review of genetics *38*, 233-271.
Lee, J.H., and Paull, T.T. (2004). Direct activation of the ATM protein kinase by the Mre11/Rad50/Nbs1 complex. Science (New York, NY) *304*, 93-96.

Lee, J.H., and Paull, T.T. (2005). ATM activation by DNA double-strand breaks through the Mre11-Rad50-Nbs1 complex. Science (New York, NY) *308*, 551-554.
Lee, S.J., Schwartz, M.F., Duong, J.K., and Stern, D.F. (2003). Rad53 phosphorylation site clusters are important for Rad53 regulation and signaling. Molecular and cellular biology *23*, 6300-6314.
Lempiainen, H., and Halazonetis, T.D. (2009). Emerging common themes in regulation of PIKKs and PI3Ks. The EMBO journal *28*, 3067-3073.
Levy, D.L., and Blackburn, E.H. (2004). Counting of Rif1p and Rif2p on Saccharomyces cerevisiae telomeres regulates telomere length. Molecular and cellular biology *24*, 10857-10867.
Lim, H.S., Kim, J.S., Park, Y.B., Gwon, G.H., and Cho, Y. (2011). Crystal structure of the Mre11-Rad50-ATPgammaS complex: understanding the interplay between Mre11 and Rad50. Genes & development *25*, 1091-1104.
Lisby, M., Barlow, J.H., Burgess, R.C., and Rothstein, R. (2004). Choreography of the DNA damage response: spatiotemporal relationships among checkpoint and repair proteins. Cell *118*, 699-713.
Lundblad, V., and Blackburn, E.H. (1993). An alternative pathway for yeast telomere maintenance rescues est1- senescence. Cell *73*, 347-360.
Lundblad, V., and Szostak, J.W. (1989). A mutant with a defect in telomere elongation leads to senescence in yeast. Cell *57*, 633-643.
Lustig, A.J., and Petes, T.D. (1986). Identification of yeast mutants with altered telomere structure. Proceedings of the National Academy of Sciences of the United States of America *83*, 1398-1402.
Makarov, V.L., Hirose, Y., and Langmore, J.P. (1997). Long G tails at both ends of human chromosomes suggest a C strand degradation mechanism for telomere shortening. Cell *88*, 657-666.
Malkova, A., and Haber, J.E. (2012). Mutations arising during repair of chromosome breaks. Annual review of genetics *46*, 455-473.
Mallory, J.C., and Petes, T.D. (2000). Protein kinase activity of Tel1p and Mec1p, two Saccharomyces cerevisiae proteins related to the human ATM protein kinase. Proceedings of the National Academy of Sciences of the United States of America *97*, 13749-13754.
Mantiero, D., Clerici, M., Lucchini, G., and Longhese, M.P. (2007). Dual role for Saccharomyces cerevisiae Tel1 in the checkpoint response to double-strand breaks. EMBO reports *8*, 380-387.
Marcand, S., Gilson, E., and Shore, D. (1997). A protein-counting mechanism for telomere length regulation in yeast. Science (New York, NY) *275*, 986-990.
Marcand, S., Pardo, B., Gratias, A., Cahun, S., and Callebaut, I. (2008). Multiple pathways inhibit NHEJ at telomeres. Genes & development *22*, 1153-1158.
Matsuzaki, K., Shinohara, A., and Shinohara, M. (2008). Forkhead-associated domain of yeast Xrs2, a homolog of human Nbs1, promotes nonhomologous end joining through interaction with a ligase IV partner protein, Lif1. Genetics *179*, 213-225.
McElligott, R., and Wellinger, R.J. (1997). The terminal DNA structure of mammalian chromosomes. The EMBO journal *16*, 3705-3714.
McKinnon, P.J., and Caldecott, K.W. (2007). DNA strand break repair and human genetic disease. Annual review of genomics and human genetics *8*, 37-55.

Mehta, A., and Haber, J.E. (2014). Sources of DNA double-strand breaks and models of recombinational DNA repair. Cold Spring Harbor perspectives in biology *6*, a016428.
Mimitou, E.P., and Symington, L.S. (2009). DNA end resection: many nucleases make light work. DNA repair *8*, 983-995.
Moore, J.K., and Haber, J.E. (1996). Cell cycle and genetic requirements of two pathways of nonhomologous end-joining repair of double-strand breaks in Saccharomyces cerevisiae. Molecular and cellular biology *16*, 2164-2173.
Moreau, S., Ferguson, J.R., and Symington, L.S. (1999). The nuclease activity of Mre11 is required for meiosis but not for mating type switching, end joining, or telomere maintenance. Molecular and cellular biology *19*, 556-566.
Morrow, D.M., Tagle, D.A., Shiloh, Y., Collins, F.S., and Hieter, P. (1995). TEL1, an S. cerevisiae homolog of the human gene mutated in ataxia telangiectasia, is functionally related to the yeast checkpoint gene MEC1. Cell *82*, 831-840.
Myers, J.S., and Cortez, D. (2006). Rapid activation of ATR by ionizing radiation requires ATM and Mre11. The Journal of biological chemistry *281*, 9346-9350.
Myler, L.R., Gallardo, I.F., Soniat, M.M., Deshpande, R.A., Gonzalez, X.B., Kim, Y., Paull, T.T., and Finkelstein, I.J. (2017). Single-Molecule Imaging Reveals How Mre11-Rad50-Nbs1 Initiates DNA Break Repair. Molecular cell *67*, 891-898.e894.
Nakada, D., Matsumoto, K., and Sugimoto, K. (2003). ATM-related Tel1 associates with double-strand breaks through an Xrs2-dependent mechanism. Genes & development *17*, 1957-1962.
Neale, M.J., Pan, J., and Keeney, S. (2005). Endonucleolytic processing of covalent protein-linked DNA double-strand breaks. Nature *436*, 1053-1057.
Niu, H., Chung, W.H., Zhu, Z., Kwon, Y., Zhao, W., Chi, P., Prakash, R., Seong, C., Liu, D., Lu, L.*, et al.* (2010). Mechanism of the ATP-dependent DNA end-resection machinery from Saccharomyces cerevisiae. Nature *467*, 108-111.
Ogi, H., Goto, G.H., Ghosh, A., Zencir, S., Henry, E., and Sugimoto, K. (2015). Requirement of the FATC domain of protein kinase Tel1 for localization to DNA ends and target protein recognition. Molecular biology of the cell *26*, 3480-3488.
Oh, J., Al-Zain, A., Cannavo, E., Cejka, P., and Symington, L.S. (2016). Xrs2 Dependent and Independent Functions of the Mre11-Rad50 Complex. Molecular cell *64*, 405-415.
Oh, J., and Symington, L.S. (2018). Role of the Mre11 Complex in Preserving Genome Integrity. Genes *9*.
Palm, W., and de Lange, T. (2008). How shelterin protects mammalian telomeres. Annual review of genetics *42*, 301-334.
Paull, T.T. (2018). 20 Years of Mre11 Biology: No End in Sight. Molecular cell *71*, 419-427.
Paull, T.T., and Gellert, M. (1998). The 3' to 5' exonuclease activity of Mre 11 facilitates repair of DNA double-strand breaks. Molecular cell *1*, 969-979.
Perry, J., and Kleckner, N. (2003). The ATRs, ATMs, and TORs are giant HEAT repeat proteins. Cell *112*, 151-155.
Prochazkova, J., and Loizou, J.I. (2016). Programmed DNA breaks in lymphoid cells: repair mechanisms and consequences in human disease. Immunology *147*, 11-20.

Ritchie, K.B., and Petes, T.D. (2000). The Mre11p/Rad50p/Xrs2p complex and the Tel1p function in a single pathway for telomere maintenance in yeast. Genetics *155*, 475-479.
Rulten, S.L., and Caldecott, K.W. (2013). DNA strand break repair and neurodegeneration. DNA repair *12*, 558-567.
Sabourin, M., Tuzon, C.T., and Zakian, V.A. (2007). Telomerase and Tel1p preferentially associate with short telomeres in S. cerevisiae. Molecular cell *27*, 550-561.
San Filippo, J., Sung, P., and Klein, H. (2008). Mechanism of eukaryotic homologous recombination. Annual review of biochemistry *77*, 229-257.
Sanchez, Y., Desany, B.A., Jones, W.J., Liu, Q., Wang, B., and Elledge, S.J. (1996). Regulation of RAD53 by the ATM-like kinases MEC1 and TEL1 in yeast cell cycle checkpoint pathways. Science (New York, NY) *271*, 357-360.
Sandell, L.L., and Zakian, V.A. (1993). Loss of a yeast telomere: arrest, recovery, and chromosome loss. Cell *75*, 729-739.
Sawicka, M., Wanrooij, P.H., Darbari, V.C., Tannous, E., Hailemariam, S., Bose, D., Makarova, A.V., Burgers, P.M., and Zhang, X. (2016). The Dimeric Architecture of Checkpoint Kinases Mec1ATR and Tel1ATM Reveal a Common Structural Organization. The Journal of biological chemistry *291*, 13436-13447.
Shibata, A. (2017). Regulation of repair pathway choice at two-ended DNA double-strand breaks. Mutation research *803-805*, 51-55.
Shiloh, Y. (2003). ATM and related protein kinases: safeguarding genome integrity. Nature reviews Cancer *3*, 155-168.
Shim, E.Y., Chung, W.H., Nicolette, M.L., Zhang, Y., Davis, M., Zhu, Z., Paull, T.T., Ira, G., and Lee, S.E. (2010). Saccharomyces cerevisiae Mre11/Rad50/Xrs2 and Ku proteins regulate association of Exo1 and Dna2 with DNA breaks. The EMBO journal *29*, 3370-3380.
Shiotani, B., and Zou, L. (2009). Single-stranded DNA orchestrates an ATM-to-ATR switch at DNA breaks. Molecular cell *33*, 547-558.
Shore, D., and Nasmyth, K. (1987). Purification and cloning of a DNA binding protein from yeast that binds to both silencer and activator elements. Cell *51*, 721-732.
So, S., Davis, A.J., and Chen, D.J. (2009). Autophosphorylation at serine 1981 stabilizes ATM at DNA damage sites. The Journal of cell biology *187*, 977-990.
Soutoglou, E., and Misteli, T. (2008). Activation of the cellular DNA damage response in the absence of DNA lesions. Science (New York, NY) *320*, 1507-1510.
Stewart, G.S., Maser, R.S., Stankovic, T., Bressan, D.A., Kaplan, M.I., Jaspers, N.G., Raams, A., Byrd, P.J., Petrini, J.H., and Taylor, A.M. (1999). The DNA double-strand break repair gene hMRE11 is mutated in individuals with an ataxia-telangiectasia-like disorder. Cell *99*, 577-587.
Stracker, T.H., and Petrini, J.H. (2011). The MRE11 complex: starting from the ends. Nature reviews Molecular cell biology *12*, 90-103.
Syed, A., and Tainer, J.A. (2018). The MRE11-RAD50-NBS1 Complex Conducts the Orchestration of Damage Signaling and Outcomes to Stress in DNA Replication and Repair. Annual review of biochemistry *87*, 263-294.
Symington, L.S., and Gautier, J. (2011). Double-strand break end resection and repair pathway choice. Annual review of genetics *45*, 247-271.

Teng, S.C., and Zakian, V.A. (1999). Telomere-telomere recombination is an efficient bypass pathway for telomere maintenance in Saccharomyces cerevisiae. Molecular and cellular biology *19*, 8083-8093.
Traven, A., and Heierhorst, J. (2005). SQ/TQ cluster domains: concentrated ATM/ATR kinase phosphorylation site regions in DNA-damage-response proteins. BioEssays : news and reviews in molecular, cellular and developmental biology *27*, 397-407.
Trujillo, K.M., Yuan, S.S., Lee, E.Y., and Sung, P. (1998). Nuclease activities in a complex of human recombination and DNA repair factors Rad50, Mre11, and p95. The Journal of biological chemistry *273*, 21447-21450.
Tseng, S.F., Lin, J.J., and Teng, S.C. (2006). The telomerase-recruitment domain of the telomere binding protein Cdc13 is regulated by Mec1p/Tel1p-dependent phosphorylation. Nucleic acids research *34*, 6327-6336.
Tsukamoto, Y., Mitsuoka, C., Terasawa, M., Ogawa, H., and Ogawa, T. (2005). Xrs2p regulates Mre11p translocation to the nucleus and plays a role in telomere elongation and meiotic recombination. Molecular biology of the cell *16*, 597-608.
Usui, T., Foster, S.S., and Petrini, J.H. (2009). Maintenance of the DNA-damage checkpoint requires DNA-damage-induced mediator protein oligomerization. Molecular cell *33*, 147-159.
Usui, T., Ogawa, H., and Petrini, J.H. (2001). A DNA damage response pathway controlled by Tel1 and the Mre11 complex. Molecular cell *7*, 1255-1266.
Usui, T., Ohta, T., Oshiumi, H., Tomizawa, J., Ogawa, H., and Ogawa, T. (1998). Complex formation and functional versatility of Mre11 of budding yeast in recombination. Cell *95*, 705-716.
Wang, X., Chu, H., Lv, M., Zhang, Z., Qiu, S., Liu, H., Shen, X., Wang, W., and Cai, G. (2016). Structure of the intact ATM/Tel1 kinase. Nature communications *7*, 11655.
Weinert, T.A., and Hartwell, L.H. (1988). The RAD9 gene controls the cell cycle response to DNA damage in Saccharomyces cerevisiae. Science (New York, NY) *241*, 317-322.
Wellinger, R.J., and Zakian, V.A. (2012). Everything you ever wanted to know about Saccharomyces cerevisiae telomeres: beginning to end. Genetics *191*, 1073-1105.
Wiltzius, J.J., Hohl, M., Fleming, J.C., and Petrini, J.H. (2005). The Rad50 hook domain is a critical determinant of Mre11 complex functions. Nature structural & molecular biology *12*, 403-407.
Wotton, D., and Shore, D. (1997). A novel Rap1p-interacting factor, Rif2p, cooperates with Rif1p to regulate telomere length in Saccharomyces cerevisiae. Genes & development *11*, 748-760.
Xin, J., Xu, Z., Wang, X., Tian, Y., Zhang, Z., and Cai, G. (2019). Structural basis of allosteric regulation of Tel1/ATM kinase. Cell research.
You, Z., Chahwan, C., Bailis, J., Hunter, T., and Russell, P. (2005). ATM activation and its recruitment to damaged DNA require binding to the C terminus of Nbs1. Molecular and cellular biology *25*, 5363-5379.
Zou, L., and Elledge, S.J. (2003). Sensing DNA damage through ATRIP recognition of RPA-ssDNA complexes. Science (New York, NY) *300*, 1542-1548.

Chapter II

JBC Papers in Press. Published on May 9, 2019 as Manuscript RA119.008410
The latest version is at http://www.jbc.org/cgi/doi/10.1074/jbc.RA119.008410

Activation of Tel1^{ATM} kinase requires Rad50 ATPase and long nucleosome-free DNA, but no DNA ends

Sarem Hailemariam[1], Sandeep Kumar[1,2], and Peter M. Burgers[1]*

[1]From the Department of Biochemistry and Molecular Biophysics, Washington University School of Medicine, Saint Louis, Missouri, USA.

Running title: *Activation of yeast Tel1 kinase by MRX and DNA*

[2]current address: Intellia Therapeutics, Cambridge, MA 02139.

*Corresponding author: TEL (314) 362-3772; FAX (314) 362-7183; burgers@wustl.edu

Keywords: checkpoint control, ataxia telangiectasia, DNA damage response, phosphorylation, PI3-kinase like kinase, ATM, MRX

ABSTRACT

In *Saccharomyces cerevisiae*, Tel1 protein kinase, the ortholog of human ATM is activated in response to DNA double-strand breaks. Biochemical studies with human ATM, and genetic studies in yeast suggest that recruitment and activation of Tel1^{ATM} is dependent on the heterotrimeric MRX^{MRN} complex, composed of Mre11, Rad50 and Xrs2 (human Nbs1). However, the mechanism of activation of Tel1 by MRX remains unclear, as does the role of effector DNA. Here, we demonstrate that double-stranded DNA and MRX activate Tel1 synergistically. While minimal activation was observed with 80-mer duplex DNA, the optimal effector for Tel1 activation is long, nucleosome-free DNA. However, there is no requirement for DNA double-stranded termini. The ATPase activity of Rad50 is critical to activation. In addition to DNA and Rad50, either Mre11 or Xrs2 but not both, is also required. Each of the three MRX subunits shows a physical association with Tel1. Our studies provide a model how the individual subunits of MRX and DNA regulate Tel1 kinase activity.

Genome stability mechanisms are essential for the normal function of cells. Genomic integrity can be disrupted due to errors caused during DNA replication, and by both endogenous and exogenous DNA damaging agents. Double-strand DNA breaks (DSBs) are among the most cytotoxic and deleterious forms of DNA lesions. The efficient repair of DSBs is essential for genome integrity. DSBs can be formed by exogenous agents, but they can also occur during normal cellular processes such as during meiosis, immunoglobulin gene rearrangement, and during DNA replication. Defective DSB repair is associated with developmental and immunological disorders, and promotes carcinogenesis in humans (1). To avoid chromosomal alterations and rearrangements, cells must detect and repair DSBs timely and properly. Eukaryotes respond to DSBs by promptly initiating a multipronged DNA damage response, which involves the initiation of a cell cycle checkpoint and DNA repair. The cell cycle checkpoint is an intricate signal transduction pathway that involves DNA damage sensing, a slow-down or inhibition of cell cycle progression, and DNA repair (2).

The yeast *Saccharomyces cerevisiae* Tel1 and Mec1 protein kinases are orthologs of mammalian ATM and ATR respectively. They are essential regulators of cell cycle checkpoint initiation yeast (3,4). Tel1 and Mec1 belong to a superfamily of protein kinases that share a common C-terminal phosphatidylinositol-3′-OH kinase-like kinase (PIKK) domain. All members of the PIKK family are very large proteins (>250 kDa), in which the C-terminal catalytic kinase domain makes up only 5-10% of the total sequence. The non-kinase regions of PIKKs are comprised largely of tandem HEAT (Huntington, Elongation factor 3, A subunit of protein phosphatase 2A, and TOR1) repeats and show very little sequence homology even within subfamilies. Structural analyses have revealed that HEAT repeats form helical structures that form large curved superstructures (5-7). In addition to harboring the kinase domain, the C-terminal region of PIKKs contain highly conserved domains known as FAT and FATC (8,9). Recent structural studies of *S. pombe*

Tel1 show two Tel1 molecules that interact through the kinase and FAT domain to form a dimer (Fig. 1A) (10).

Tel1 (ATM) and Mec1 (ATR) respond to different forms of DNA damage. While Mec1 is activated by single stranded DNA coated with the single-stranded binding factor RPA, Tel1 responds primarily to DSBs (11-13). However, they share an overlapping number of downstream phosphorylation targets and show partial redundancy in their checkpoint function (4). One of the initial targets of Tel1 in *S. cerevisiae* is histone H2A. Phosphorylation of H2A marks the chromatin surrounding the DNA lesion and is important for recruitment and retention of DNA repair proteins (14). Phosphorylated H2A is bound by the scaffold adaptor protein Rad9. The association of Rad9 with chromatin facilitates the recruitment of the effector kinase Rad53, the budding yeast functional homologue of mammalian Chk1 and Chk2 kinases (15). Phosphorylation of Rad53 by Tel1, followed by further autophosphorylation of Rad53 results in full activation of Rad53 (16). Rad53 has many downstream targets, some of which couple cell cycle arrest with damage repair (12,16,17).

Recruitment of Tel1 to sites of DNA damage is dependent on Xrs2 (human Nbs1) protein. Xrs2 is a subunit of the Mre11-Rad50-Xrs2 (MRX) complex (18,19). The MRX (human MRN) complex is involved in recognition and processing of DSBs. Mre11 and Rad50 are highly conserved and are found in all forms of life. Xrs2/Nbs1 is only present in eukaryotes and is not well conserved at the primary sequence level (20). MRX has several enzymatic and scaffolding properties and plays major roles in DNA break metabolism. It is a crucial player in all aspects of DSB processing: damage detection, cell cycle checkpoint initiation, and facilitating and catalyzing repair of the lesion (2,21,22). Mre11 belongs to the lambda phosphatase family of enzymes and has both endo and exonuclease activities (23,24). Studies of budding yeast Mre11 show that mutations ablating its nuclease activity cause severe meiotic defects, but result in only mild IR sensitivity, suggesting that the Mre11 nuclease activity is largely dispensable for DSB repair (25,26). Rad50 belongs to the ABC transporter family of ATPases, and shares structural features with Structural Maintenance of Chromosome (SMC) proteins (20,27,28). Its ATP binding domains are split and located at the N- and C-termini, separated by long coil-coiled domains (29,30) (Fig. 1B). Active ATPase sites are only formed when two Rad50 molecules dimerize in an ATP dependent manner (27). A conserved zinc-hook at the apex of the coil-coiled region, distal from the ATPase domains also mediates Rad50 dimerization (31). The ATPase domains of Rad50 along with the nuclease and DNA binding regions of Mre11 make up the catalytic core of the MRX complex (32,33). Upon ATP binding by Rad50, this catalytic core retains a closed conformation, whereas ATP hydrolysis releases the MRX complex from the DNA (27,34-37) (Fig. 1B).

Critical studies of the mammalian ATM and the MRN complex have resulted in a mechanistic framework for checkpoint initiation to DSBs (38). In an independent approach, extensive genetic studies of *S. cerevisiae* Tel1 and the MRX complex have given us a comprehensive understanding where and how these factors function in various DNA metabolic pathways, and which activities and/or domains are essential in each of these pathways (2,21). However, until now, biochemical studies with purified yeast proteins have been lacking. In this study, we present biochemical data that illuminate how DNA and MRX orchestrate the activation of Tel1 checkpoint kinase. We show that double-stranded DNA is indispensable for stimulation of Tel1 kinase by MRX. A DNA length with a minimum of 80 base pairs is required for robust activation. Furthermore, DNA wrapped up into a nucleosome is ineffective. Surprisingly, double-stranded DNA ends were not required for activation of Tel1 by MRX *in vitro,* even though on small DNA effectors a significant stimulatory function of DNA ends can be detected. Analysis of individual subunits and different heterodimeric pairs of MRX in the presence of DNA reveal that Rad50 is critical for activating Tel1. This stimulatory effect of Rad50 is absolutely dependent on its ATPase activity.

Results

DNA is required for MRX to fully stimulate Tel1

Previously, we described the overproduction and purification of *S. cerevisiae* Tel1 from yeast and described an initial structural analysis (6). When Tel1 was examined by electron microscopy, the main species was that of a dimer. Cryo-EM studies of human ATM and *S. pombe* Tel1 show that these orthologs are also homodimeric in structure (10,39).

In order to allow for a comprehensive biochemical analysis of the MRX complex in its stimulation of Tel1 kinase activity, we purified each subunit separately from yeast, as well as the heterodimeric Mre11-Xrs2 complex. However, these highly purified preparations, particularly the Mre11-Xrs2 preparation, consistently showed protein kinase

activity in the absence of Tel1 addition. In part, the contaminating kinase activity could be assigned to Tel1 itself, which copurified with these subunits. Because each subunit of the MRX complex interacts with Tel1 (see below), this finding was not unexpected. However, even when the MRX subunits were purified from a *tel1Δ* strain, detectable kinase activity remained. Mass-spectrometric analysis of the purified preparations identified Tda1 as the co-purifying kinase (data not shown). *TDA1* shows genetic interactions with topoisomerase 1, suggesting that it may play a role in DNA metabolism (40). A potential role of Tda1 in MRX-dependent DNA metabolic processes remains to be investigated. When we purified the MRX subunits and subassemblies from a *tel1Δ tda1Δ* strain of yeast, essentially no contaminating protein kinase activity was observed (Fig. 2A, lane 2), and these preparations were used in all our studies (Fig. 1C).

To study the protein kinase activity of Tel1, we used the downstream effector kinase Rad53, which is a physiological Tel1 substrate (12). The catalytic inactive form Rad53kd was used, so that all observable protein phosphorylation was Tel1-dependent. In addition, the general PIKK substrate PHAS-I was used in several experiments (41), in order to query whether MRX stimulation of Tel1 kinase activity was specific for Rad53 as a substrate or a more general property.

Fig. 1A summarizes the critical aspects of the assay, which show that Tel1 kinase activity is weakly stimulated by either DNA or MRX alone, but both DNA and MRX show strong synergism. This assay was followed up with comprehensive time-course analyses of each of the conditions. The weak activity of Tel1 alone (0.065 phosphates transferred to Rad53 per min per Tel1 monomer) was stimulated about 2-3 fold in the presence of linear 2 kb plasmid DNA (Fig. 2B,D). Without DNA, the MRX complex increased Tel1's basal activity also 2-3 fold (Fig. 2C,E). The presence of both DNA and MRX in the reaction resulted in a synergistic, 20-30 fold increase in Rad53 phosphorylation (Fig. 2C,E). The synergistic stimulation of Tel1 by MRX and DNA is not specific to Rad53 as a substrate; it was also observed with PHAS-I, a commonly used substrate to probe the ATM/ATR family of kinases (Supplemental Fig. S1A). In these assays, we had preassembled the MRX complex at 0 ˚C for 1h prior to addition into the assay. To assess whether MRX pre-assembly is required, we either mixed the individually purified subunits of MRX at 0 ˚C for 1 hour, and added the pre-assembled complex into the assay or added them individually into the assay. In both cases, saturation was achieved at 10-20 nM MRX, with 5 nM Tel1, indicating that pre-assembly was not required (Supplemental Fig. S1B,C). Therefore, we routinely used 30 nM MRX unless indicated otherwise.

A titration of the kinase substrate PHAS-I in the Tel1 assay in the presence of MRX, either with or without DNA present, gave an approximately linear dose-response curve up to 20 μM PHAS-I, indicative of a weak association of this substrate to Tel1 (Supplemental Fig. S1D). Given these results, we cannot conclude whether DNA enhances the affinity of kinase substrates to MRX•Tel1, which would be a possible explanation for the observed synergism. Finally, Tel1 also phosphorylates the Xrs2 and Mre11 subunits of MRX (Fig. 2A), as it does inside the cell in response to DNA damage (18,42).

Nucleosome-free double stranded DNA is the preferred effector for Tel1/MRX

The homologous recombination repair pathway involves resection of double-stranded breaks by 5'-3' exonucleases to generate ssDNA 3'-ends that are coated by the single-strand DNA binding protein RPA (43). As resection proceeds and the 3'-overhangs increase in length, Tel1 activity is attenuated and the checkpoint response is switched to that of a Mec1-mediated response (26). Previous studies with human ATM and MRN showed that kilobase long dsDNA substrates were required in order to detect stimulation of ATM kinase activity (44). Here, the sensitivity of our *in vitro* kinase assay has enabled us to evaluate the roles of DNA strandedness, structure, and length as effector for Tel1. A single-stranded 80-mer oligonucleotide was inactive for stimulation, whether coated with RPA or not, whereas the double-stranded form showed significant activity (Fig. 3A). This is in direct contrast to Mec1, which shows optimal activity on RPA-coated ssDNA (45). These findings are consistent with the proposed model where stretches of RPA-coated ssDNA resulting from DNA end resection mediate the transition from a Tel1- to Mec1-dependent checkpoint response (46).

We next probed the DNA length requirement for stimulation. We compared double-stranded oligonucleotides in a size range of 20-80bp, 147bp, and a 2kb linear plasmid DNA (Fig. 3B,C). This analysis showed that up to a length of 60 bp, little to no stimulation was observed. The 147-mer dsDNA showed substantially higher activity than the 80-mer. A further increase in the effector DNA length to 2 kb showed another two-fold increase in maximal activity.

The activity data were plotted as a function of the concentration of dsDNA ends (Fig. 3B). Unexpectedly, the 2kb linear DNA showed half-maximal activation at merely 0.1 nM DNA ends. If only DNA ends would be active in the MRX•Tel1 assay, given that the assay contains 2.5 nM Tel1 dimers, half-maximal activation should occur at an end concentration of ≥1.25 nM DNA ends, depending on the affinity of MRX•Tel1 for ends. This titration experiment alone suggests that internal sites must be active for optimal stimulation of Tel1. The 147-mer dsDNA gave half-maximal activation at 0.2 nM ends and the 80-mer at 1.1 nM ends (Figure 3B). Therefore, only the half-maximal concentration of the 80-mer is consistent with the model that only DNA ends serve as effectors of MRX•Tel1.

The data were re-plotted as a function of the total nucleotide concentration (Fig. 3C). Half-maximal stimulation was reached at 45 nM, 16 nM, and 125 nM nucleotide concentration for the 80-mer, 147-mer, and 2 kb DNA, respectively. While the total of these data indicate that some variation in the strength of DNA effectors may occur, possibly because of sequence and/or DNA composition contexts, they also indicate that internal sites serve as effectors of MRX•Tel1. Consequently, the large number of potential internal binding sites on the 2 kb DNA contribute substantially to stimulation.

One possible model for Tel1 activity that maintains a requirement for DNA ends is one in which DNA ends are required for loading of MRX•Tel1, but that subsequently the complex can slide to internal regions along the dsDNA. This would allow the assembly of additional complexes that are all active for kinase activity. This model would explain why the half-maximal concentration of the 2 kb effector is over ten times lower than the concentration of MRX•Tel1 complexes. To test this model, we carried out an assay with the 2 kb plasmid either in the supercoiled, nicked or linear form (Fig. 4A). In control experiments, we showed that the supercoiled and the nicked DNA effectors remained intact during the course of the assay (data not shown). Mre11 is a known nuclease, however, Mre11 nuclease activity requires manganese while our studies have been carried out in magnesium-containing buffers (47,48).

Although the stimulation of Tel1 activity by MRX on linear DNA was slightly higher than on supercoiled or nicked DNA, the difference was of low statistical significance. Therefore, DNA ends are not essential for MRX-dependent Tel1 kinase activity. However, are ends stimulatory? The result shown in Fig. 4A would be expected if the contribution by the vast excess of internal sites masked the stimulatory contribution stemming from DNA ends. In order to reveal a possible contribution by DNA ends, we repeated this experiment with a much shorter DNA, 262 nt in length (Supplemental Fig. S2A). Indeed, with this small DNA, the linear form is more active than the circular form, even though the circular DNA shows robust activity at higher DNA concentrations (Fig. 4B). Collectively, these data indicate the significance of internal DNA binding sites for MRX-dependent activation of Tel1. In support of the internal entry model, proficient internal loading of MRX has been shown in single-molecule studies (49).

Thus far, our experiments have been carried out with naked DNA. We next determined whether nucleosomal DNA showed activity in our assay, but it did not. First, assembly of the DNA into a nucleosome caused inhibition of the MRX-independent but DNA-dependent activation of Tel1's basal kinase activity (Fig. 2A, Supplemental Fig. S2B). With the complete system, we observed at least a 100-fold difference in the ability of the naked 147-mer to activate Tel1 compared to the same DNA wrapped up into a nucleosome (Fig. 4C,D). The inhibitory effect of mononucleosomal DNA was recapitulated when PHAS-I was used instead of Rad53 as a substrate for Tel1 (Supplemental Fig. S2C). We carried out two additional control experiments. We showed that histone octamers themselves, i.e. not bound up in a nucleosome, did not cause inhibition of Tel1 (Supplemental Fig. S2D). Furthermore, we showed that the binding of DNA by general dsDNA binding proteins, such as HMGB-1, is also inhibitory albeit less absolutely than that by the nucleosome (Supplemental Fig S2E).

Rad50, but not Xrs2 or Mre11, is essential for DNA dependent activation of Tel1 by MRX

In order to determine which of the subunit(s) of the MRX complex are essential for Tel1 kinase activation, we measured Tel1 stimulation by each of the subunits alone and by the different heterodimeric complexes. These experiments were carried out in the presence of saturating concentrations of the 2 kb linear DNA effector. None of the single subunits alone stimulated Tel1 kinase (Supplemental Fig. S3A), suggesting that the mere physical association of these factors with Tel1 (see below) is insufficient for activation. The Mre11-Xrs2 pair was also unable to stimulate kinase activity (Fig. 5A, lane 6). In contrast, both the Rad50-Mre11 and Rad50-Xrs2 pairs showed substantial kinase activation (lanes 8,10). These data

indicate that while neither Mre11 or Xrs2 is required, the interaction of either subunit with Rad50 is a prerequisite for Rad50 to function in Tel1 activation. The activity of the complete MRX complex was 1.5-fold higher than that of the Rad50-Xrs2 pair. Two sets of observations exclude the possibility that the activity of the heterodimers is caused by cross-contamination of the Rad50-Mre11 assay with Xrs2 or the Rad50-Xrs2 subunit with Mre11. First, the Rad50-Mre11 assay lacks detectable phosphorylated Xrs2 and the Rad50-Xrs2 assay lacks detectable phosphorylated Mre11 (Fig. 5A, lanes 4 and 8, respectively). Second, the same robust activity of the Rad50-Xrs2 pair was observed when Rad50 was purified from a yeast *mre11Δ* mutant and Xrs2 from *E. coli*, eliminating the possibility of contamination with Mre11 (Supplemental Fig. S3B).

Rad50 belongs to the ABC transporter family of ATPases and shares structural similarities to Structural Maintenance of Chromosome proteins (38). The ATP-dependent activities of *S. cerevisiae* Rad50 are required for all of its functions in DNA repair as ATPase-dead mutants show a similar phenotype to *rad50Δ* mutants. DNA stimulates the ATPase activity of Rad50 alone, or of the MRX complex, and at least one study shows that ends are important for this stimulation (50). We also observed that the linear plasmid was significantly more stimulatory for the ATPase than the circular plasmid DNA (Supplemental Fig. S2F). As discussed below, ATP turnover is not important for MRX-dependent activation of Tel1, however ATP binding is. To test the ATP-binding requirement, we mutated the conserved Walker A-box lysine residue to either alanine or arginine, which has been shown to inactivate its ATPase activity (51). Neither mutant MRX complex showed detectable ATP binding (Fig. 5B). Furthermore, the mutant complexes were inactive for Tel1 stimulation (Fig 5C). We further tested whether the Rad50-K40A and -K40R mutant MRX complexes retained partial activity in stimulating Tel1 at higher concentrations of ATP. However, even at ATP concentrations as high as 0.5 mM, no significant stimulation by the mutant complexes was observed (Fig. 5D). Thus, the ATP-dependent activity of Rad50 is essential for the stimulatory role of MRX.

Each member of MRX individually interacts with Tel1

To further increase the knowledge of the system, we probed the physical interactions between each of the MRX subunits with Tel1. The C-terminal region of Xrs2 has been shown to physically associate with Tel1 and this association is required for localizing Tel1 to DSBs (18,19). To determine whether Mre11 and Rad50 also interact with Tel1, we performed a pull-down experiment with the individual subunits (Fig. 6A). GST-Tel1, or GST as a control, was incubated with each subunit together with glutathione beads. The beads were washed three times with buffer to remove non-specifically bound proteins and subjected to SDS-PAGE analysis. Proteins were visualized using silver staining (Fig. 6A). Tel1 was able to pull down each individual subunit, indicating that each subunit binds Tel1. Mre11 showed the most robust interaction with Tel1. As the Tel1-Rad50 interaction appeared rather weak, we repeated the pull-down experiment using a more sensitive Western analysis with anti-Rad50 antibodies (Fig. 6B, lane 5). This experiment positively established the interaction between Rad50 and Tel1. In addition, we probed Rad50 interactions with Mre11 and Xrs2 (Fig. 6B, lanes 3 and 4, respectively). As a positive control, we confirmed the known interaction of Rad50 with Mre11 (24). A previous study established interactions between human Rad50 and Nbs1 (52). Our data extend this interaction network to yeast Rad50 with Xrs2 (lane 4). These experiments establish that each of the subunits of MRX interact with each other and with Tel1.

Discussion

Prior to this biochemical analysis of the yeast MRX•Tel1 checkpoint complex, only the mammalian MRN•ATM complex had been studied in a purified protein system, in a series of insightful studies by Paull and coworkers (53). While a comparison of the yeast and mammalian systems show some broad similarities, they also reveal critical differences that may have decisive impact on the mechanism of action by these checkpoint complexes in the different organisms. Human ATM kinase activity is stimulated about 100-fold when both MRN and kilobase-long DNA are present, and there is an absolute requirement for dsDNA ends (44). There is also a requirement for Mn^{2+} rather than Mg^{2+}, however the nuclease activities of Mre11, which also depend on Mn^{2+}, are dispensable for kinase activation (54). ATM dimer to monomer transitions are mediated by phosphorylation and acetylation of specific residues (55,56). Based on mutational studies of ATM sites that are subject to post-translational modification, it has been proposed that the active form of ATM is that of a monomer (44,55). However, the orthologous mouse ATM mutants are without an *ataxia telangiectasia*

phenotype, suggesting that regulation of ATM activity in human and mouse may not be conserved (57). Importantly, the assembly state of active ATM or Tel1 when bound to DNA still remains to be established.

Our biochemical analysis has been carried out under near-physiological conditions with Mg^{2+} as cofactor. The 50-100-fold stimulation of Tel1 kinase activity when both MRX and DNA are present has allowed us to attach statistical significance to the observation that either MRX or DNA alone stimulates the kinase activity 2-3-fold (Fig. 2D,E). Our studies have been aided by the rigorous elimination of contaminating and cross-contaminating activities through the isolation of the checkpoint proteins from appropriate yeast deletion strains (see Results section). The dsDNA length requirement for activation was shorter for the yeast system with near-full activity achieved with a 147-mer DNA while robust ATM activation required much longer DNA, 0.7 kb for partial activity and 2 kb for full activity (44). The fundamental difference between the human and the yeast system, however, is that MRX•Tel1 does not require DNA ends for maximal activity (Fig. 4A), whereas human MRN•ATM is absolutely dependent on DNA ends. The stimulation by DNA ends can only be observed on small DNAs (Fig. 4B).

In principle, this surprising result is not incompatible with the known dsDNA break checkpoint activity of MRX•Tel1. Kinase activation is completely inhibited on nucleosomal DNA (Fig. 4C,D). This result predicts that spontaneous activation of Tel1 kinase would not occur on undamaged, fully chromatinized chromosomes. However, extensive nucleosome disassembly has been documented at dsDNA breaks in yeast and in other organisms (58,59). The resulting naked DNA is more than 0.5 kb in length yeast, which is sufficient for robust MRX•Tel1 loading. This model of Tel1 activation at dsDNA breaks through its exclusion from normal chromatin is shown in Fig. 6C. The model does not exclude the possibility of other accessory factors further enhancing binding at dsDNA ends, but in our biochemical assay there is no prerequisite for such factors.

Structural and biochemical studies based on archaeal and bacterial Mre11-Rad50 complexes (60), as well as biochemical and genetic studies of eukaryotic MRX(N) complexes have led to a model where ATP binding by Rad50 promotes DNA binding and Tel1 kinase activation (50,61). ATP hydrolysis on the other hand releases the complex from DNA (Figure 1A). Consistent with this model, Rad50 ATP-binding mutants show no activation of Tel1 activity (Fig. 5C). As expected, our analysis of the individual subunits of MRX showed that Rad50 is essential for Tel1 activation in the presence of dsDNA (Fig. 5A). But it is not sufficient and either Mre11 or Xrs2 is also required. Possibly, because Rad50 alone shows very weak interactions with Tel1 (Fig. 6A), the additional interactions mediated by either Mre11 or Xrs2 strengthen complex formation with Tel1, leading to robust kinase activation. In yeast, all three subunits of MRX are essential for Tel1-dependent phosphorylation of Rad53 in response to zeocin, a dsDNA break-inducing agent, although Xrs2 is dispensable for several other functions of MRX provided nuclear localization of Mre11-Rad50 is ensured (62).

When comparing the activation mechanism of $Tel1^{ATM}$ to that of the related PIKKs $Mec1^{ATR}$ and DNA-PK, it is interesting to note that Mec1 can be activated by an activator protein alone such as $Dpb11^{TopBP1}$, or even by a peptide derived from an activator protein (63), whereas DNA-PK activation can be accomplished by DNA binding alone (64). In contrast, Tel1 requires both DNA and MRX, with Rad50 also requiring proficient ATP-binding capacity. A comprehensive description of the Tel1 activation mechanism will have to take into consideration that DNA and MRX individually stimulate Tel1 kinase activity 2-3 fold, but that both factors together show a profound synergism. Our studies show that Tel1 alone binds DNA proficiently and saturably in the absence of MRX (Fig. 2D), and Tel1 binds MRX proficiently in the absence of DNA (Fig. 6A,B). Therefore, increases in binding affinities are unlikely explanations for the observed hyperactivity by the ternary complex. It is probable that DNA-induced conformational changes within the MRX complex is the driving force for Tel1 kinase activation. Whether kinase activation is a consequence of MRX- and DNA-mediated monomerization of Tel1, or whether other MRX- and DNA-induced conformational rearrangements of Tel1 result in its activation, is currently not known and an important question for further investigation.

Experimental Procedures

Yeast strains, DNA, and proteins. The strains used were BJ2168 (*MAT**a** leu2-3,112 pep4-3 prb1-1122 prc1-407 trp1-289 ura3-52*), PY265 (*MAT**a** can1 his3 leu2 trp1 ura3 pep4Δ::HIS3 nam7Δ::KanMX4*), PY335 (*MAT**a** his3 leu2 trp1 ura3 pep4Δ::HIS3 tel1Δ::KanMX4 tda1Δ::NAT1*), and BY4741-Mre11

(*MAT**a** his3Δ1 leu2Δ0 met15Δ0 ura3Δ0 mre11Δ::KanMX4*).

The oligonucleotides used are listed in supplemental material.

Tel1 was overexpressed in yeast strain PY265 from the galactose-inducible plasmid pBL602, and purified as described previously (6). The protein was purified containing a N-terminal glutathione-S-transferase (GST) domain fusion. The GST domain was retained for the protein interaction studies in Fig. 6A, but was cleaved off followed by heparin-agarose purification as described (6), for all other experiments. Rad50 was overexpressed in BJ2168 or BY4741-Mre11 from the galactose-inducible plasmid pPM321, and purified as described previously (65). Rad50 mutants were made in this plasmid and purified similarly.

Plasmid pBL535 (pRS424-GAL [2 μM ori, *TRP1*] ZZ-3C-*XRS2, MRE11*) has the IgG binding StrepA-ZZ tag fused to the N-terminus of Xrs2, separated by a Prescission protease cleavage site, and Mre11 divergently expressed from the galactose-inducible *GAL1-10* promoter. The IgG-tagged Mre11-Xrs2 dimer was overexpressed in yeast strain PY335 from pBL535. After growth and galactose induction, cells were harvested and resuspended in ½ volume of 3xHep_{200} buffer (Hep_{200} = 30 mM HEPES, pH 7.8, 10% glycerol, 200 mM NaCl, 150 mM ammonium sulfate, 2 mM DTT, 0.1% Tween 20, 1 mM EDTA, 0.5 mM EGTA, 5 μM pepstatin A, 5 μM leupeptin, 1 mM $NaHSO_3$) and frozen in liquid nitrogen as popcorn as described (66). The frozen cells were lysed by blending in dry ice in, treated with polyamin P, centrifuged, the supernatant treated with ammonium sulfate, and centrifuged as described (66).The ammonium sulfate pellet was resuspended in buffer HEP_0 (as HEP_{200} but no NaCl), and incubated with IgG-sepharose beads (GE Healthcare, 1 ml per 100 g of frozen popcorn cells) for 4 hours at 4 ˚C. The beads were washed with 50 column volumes of HEP_{300} supplemented with 0.02% E10C12 detergent. The beads were rotated gently overnight at 4 ˚C with 1 ml HEP_{300} supplemented with Prescission protease to cleave the ZZ-tag. The Mre11-Xrs2 dimer was further purified over a 1 ml heparin-agarose column. The protein was loaded in HEP_{300} buffer, the column was washed with 50 ml HEP_{300}, and the protein eluted with HEP_{700} buffer.

Plasmid pBL532 (pRS424-GAL [2 μM ori, *TRP1*] GST-3C-*MRE11*) has GST fusion at the N-terminus of Mre11, separated by a Prescission protease cleavage site, placed under control of the galactose-inducible *GAL1-10* promoter. Expression of Mre11 in yeast strain PY335 and purification are exactly as described for Mre11-Xrs2. Xrs2 was overexpressed in E. coli BL21-DE3-Star (Invitrogen) from plasmid pBL533 (pGEX-6P1-GST-3C-Xrs2). Cells were grown and induced at 37 ˚C using standard procedures. The cells were harvested and resuspended in and equal volume of 2x buffer HEP_{200} (including 5 μM bestatin and 1 μM E64, both form Sigma-Aldrich), subjected to a freeze-thaw cycle, incubated with 0.2 mg/ml lysozyme for 30 min on ice, and lysed by sonication. Polyamin P (40 μl of a 10% solution per ml of lysate) was added, and the lysate was cleared at 27,000xg for 20 min. Solid ammonium sulfate (0.3 g per ml of cleared lysate) was added with stirring, and after 30 min, the precipitate was collected at 27,000xg for 30 min, resuspended in 10 ml (per liter of induction culture) of the same buffer. After binding for 4 h to 1 ml of glutathione-sepharose, the beads were washed with 50 ml of buffer, followed by elution with 30 mM reduced glutathione in HEP_{200} (but at pH 8.1). The eluted Xrs2 was further purified over a 1 ml heparin agarose column as described above.

The MRX complex was formed by incubating equimolar amounts of Rad50 and Mre11-Xrs2, or the individual subunits at 0 ˚C for one hour.

Tel1 kinase assay

The 10 μl standard assay contained 25 mM HEPES-NaOH pH 7.6, 80 mM NaCl, 7 mM Mg-acetate, 100 μg/ml BSA, 1 mM DTT, 50 μM ATP, 0.05 μCi [γ-P32]-ATP, 200 nM GST-Rad53-kd, 30 nM MRX, 5 nM linear 2kb DNA (pUC19-Δ2, a 1973 bp plasmid derived from pUC19, cut with *Bam*HI). Reactions were started with 5 nM Tel1 (monomer concentration) at 30 ˚C for 15 min, stopped with 4 ml of 2.5xSDS-PAGE loading dye, boiled, and separated on 7 % SDS-PAGE gels. The gels were dried and exposed to a phosphor screen (GE Healthcare). Variations are indicated in the legends to figures. pUC19-Δ2 was nicked with the BbvC1 nickase (NE-Biolabs) for the experiment in Fig. 4A. Quantification of the data was carried out using ImageQuant software. Data were analyzed and plotted using KaleidaGraph software, which was also used to model the data in Fig. 3B,C and 5D to the Michaelis-Menten equation

GST-pulldown experiments and ATP-binding studies

Purified MRX subunits (500 ng) were incubated with GST-tagged Tel1 (2 μg) in the

presence of 50 µl glutathione-sepharose beads in a total volume of 200 µl $HEP2_{00}$ buffer (without protease inhibitors). After four hours of incubation at 4 ˚C with rotation, the beads were subjected to three 0.5 ml washes with HEP_{200} to remove non-specifically bound proteins. The beads were loaded in a spin-column and briefly centrifuged to remove residual buffer, suspended in 50 µl SDS-PAGE loading buffer, boiled, spun, and the supernatant analyzed by 7% SDS-PAGE. Visualization was by silver staining. Alternatively, the proteins were transferred to a PVDF membrane and further processed for Western analysis with anti-scRad50 antibodies (Thermo-Fisher) using standard procedures.

Nitrocellulose filter binding experiments were performed as described (67), using 500 nM MRX in kinase buffer and 50 µM [γ-P32]-ATP in a 20 µl assay. After incubation at 0 ˚C for 30 min, the mixture was passed through a nitrocellulose membrane with gentle suction, and washed with 2x0.5 ml buffer. The dried filters were subjected to Cerenkov scintillation counting.

Acknowledgments: The authors thank Bonita Yoder for strain construction, Carrie Stith for general support with all aspects of this work, and Roberto Galletto for the Xrs2 overexpression plasmid.

Conflicts of interest: The authors declare that they have no conflicts of interest with the contents of this article.

Author contributions

SK cloned and purified Tel1. SH and PMB designed the experiments and wrote the paper. SH carried out the biochemical studies. All authors contributed to the final version of the paper.

References

1. Lavin, M. F., and Shiloh, Y. (1997) The genetic defect in ataxia-telangiectasia. *Annu Rev Immunol* **15**, 177-202
2. Oh, J., and Symington, L. S. (2018) Role of the Mre11 Complex in Preserving Genome Integrity. *Genes (Basel)* **9**
3. Abraham, R. T. (2001) Cell cycle checkpoint signaling through the ATM and ATR kinases. *Genes Dev* **15**, 2177-2196
4. Mallory, J. C., and Petes, T. D. (2000) Protein kinase activity of Tel1p and Mec1p, two Saccharomyces cerevisiae proteins related to the human ATM protein kinase. *Proc Natl Acad Sci U S A* **97**, 13749-13754
5. Perry, J., and Kleckner, N. (2003) The ATRs, ATMs, and TORs are giant HEAT repeat proteins. *Cell* **112**, 151-155
6. Sawicka, M., Wanrooij, P. H., Darbari, V. C., Tannous, E., Hailemariam, S., Bose, D., Makarova, A. V., Burgers, P. M., and Zhang, X. (2016) The Dimeric Architecture of Checkpoint Kinases Mec1ATR and Tel1ATM Reveal a Common Structural Organization. *J Biol Chem* **291**, 13436-13447
7. Shiloh, Y. (2003) ATM and related protein kinases: safeguarding genome integrity. *Nat Rev Cancer* **3**, 155-168
8. Bosotti, R., Isacchi, A., and Sonnhammer, E. L. (2000) FAT: a novel domain in PIK-related kinases. *Trends Biochem Sci* **25**, 225-227
9. Ogi, H., Goto, G. H., Ghosh, A., Zencir, S., Henry, E., and Sugimoto, K. (2015) Requirement of the FATC domain of protein kinase Tel1 for localization to DNA ends and target protein recognition. *Mol Biol Cell* **26**, 3480-3488
10. Wang, X., Chu, H., Lv, M., Zhang, Z., Qiu, S., Liu, H., Shen, X., Wang, W., and Cai, G. (2016) Structure of the intact ATM/Tel1 kinase. *Nat Commun* **7**, 11655
11. Sanchez, Y., Desany, B. A., Jones, W. J., Liu, Q., Wang, B., and Elledge, S. J. (1996) Regulation of RAD53 by the ATM-like kinases MEC1 and TEL1 in yeast cell cycle checkpoint pathways. *Science* **271**, 357-360
12. Usui, T., Ogawa, H., and Petrini, J. H. (2001) A DNA damage response pathway controlled by Tel1 and the Mre11 complex. *Mol Cell* **7**, 1255-1266
13. Zou, L., and Elledge, S. J. (2003) Sensing DNA damage through ATRIP recognition of RPA-ssDNA complexes. *Science* **300**, 1542-1548
14. Downs, J. A., Lowndes, N. F., and Jackson, S. P. (2000) A role for Saccharomyces cerevisiae histone H2A in DNA repair. *Nature* **408**, 1001-1004
15. Hammet, A., Magill, C., Heierhorst, J., and Jackson, S. P. (2007) Rad9 BRCT domain interaction with phosphorylated H2AX regulates the G1 checkpoint in budding yeast. *EMBO Rep* **8**, 851-857
16. Usui, T., Foster, S. S., and Petrini, J. H. (2009) Maintenance of the DNA-damage checkpoint requires DNA-damage-induced mediator protein oligomerization. *Mol Cell* **33**, 147-159
17. Lee, S. J., Schwartz, M. F., Duong, J. K., and Stern, D. F. (2003) Rad53 phosphorylation site clusters are important for Rad53 regulation and signaling. *Mol Cell Biol* **23**, 6300-6314
18. Nakada, D., Matsumoto, K., and Sugimoto, K. (2003) ATM-related Tel1 associates with double-strand breaks through an Xrs2-dependent mechanism. *Genes Dev* **17**, 1957-1962
19. You, Z., Chahwan, C., Bailis, J., Hunter, T., and Russell, P. (2005) ATM activation and its recruitment to damaged DNA require binding to the C terminus of Nbs1. *Mol Cell Biol* **25**, 5363-5379
20. Aravind, L., Walker, D. R., and Koonin, E. V. (1999) Conserved domains in DNA repair proteins and evolution of repair systems. *Nucleic Acids Res* **27**, 1223-1242
21. Adelman, C. A., and Petrini, J. H. (2009) Division of labor: DNA repair and the cell cycle specific functions of the Mre11 complex. *Cell Cycle* **8**, 1510-1514
22. Lamarche, B. J., Orazio, N. I., and Weitzman, M. D. (2010) The MRN complex in double-strand break repair and telomere maintenance. *FEBS Lett* **584**, 3682-3695

23. Paull, T. T., and Gellert, M. (1998) The 3' to 5' exonuclease activity of Mre 11 facilitates repair of DNA double-strand breaks. *Mol Cell* **1**, 969-979
24. Usui, T., Ohta, T., Oshiumi, H., Tomizawa, J., Ogawa, H., and Ogawa, T. (1998) Complex formation and functional versatility of Mre11 of budding yeast in recombination. *Cell* **95**, 705-716
25. Furuse, M., Nagase, Y., Tsubouchi, H., Murakami-Murofushi, K., Shibata, T., and Ohta, K. (1998) Distinct roles of two separable in vitro activities of yeast Mre11 in mitotic and meiotic recombination. *Embo j* **17**, 6412-6425
26. Symington, L. S., and Gautier, J. (2011) Double-strand break end resection and repair pathway choice. *Annu Rev Genet* **45**, 247-271
27. Hopfner, K. P., Karcher, A., Shin, D. S., Craig, L., Arthur, L. M., Carney, J. P., and Tainer, J. A. (2000) Structural biology of Rad50 ATPase: ATP-driven conformational control in DNA double-strand break repair and the ABC-ATPase superfamily. *Cell* **101**, 789-800
28. Raymond, W. E., and Kleckner, N. (1993) RAD50 protein of S.cerevisiae exhibits ATP-dependent DNA binding. *Nucleic Acids Res* **21**, 3851-3856
29. Melby, T. E., Ciampaglio, C. N., Briscoe, G., and Erickson, H. P. (1998) The symmetrical structure of structural maintenance of chromosomes (SMC) and MukB proteins: long, antiparallel coiled coils, folded at a flexible hinge. *J Cell Biol* **142**, 1595-1604
30. Walker, J. E., Saraste, M., Runswick, M. J., and Gay, N. J. (1982) Distantly related sequences in the alpha- and beta-subunits of ATP synthase, myosin, kinases and other ATP-requiring enzymes and a common nucleotide binding fold. *Embo j* **1**, 945-951
31. Hopfner, K. P., Craig, L., Moncalian, G., Zinkel, R. A., Usui, T., Owen, B. A., Karcher, A., Henderson, B., Bodmer, J. L., McMurray, C. T., Carney, J. P., Petrini, J. H., and Tainer, J. A. (2002) The Rad50 zinc-hook is a structure joining Mre11 complexes in DNA recombination and repair. *Nature* **418**, 562-566
32. Lammens, K., Bemeleit, D. J., Mockel, C., Clausing, E., Schele, A., Hartung, S., Schiller, C. B., Lucas, M., Angermuller, C., Soding, J., Strasser, K., and Hopfner, K. P. (2011) The Mre11:Rad50 structure shows an ATP-dependent molecular clamp in DNA double-strand break repair. *Cell* **145**, 54-66
33. Mockel, C., Lammens, K., Schele, A., and Hopfner, K. P. (2012) ATP driven structural changes of the bacterial Mre11:Rad50 catalytic head complex. *Nucleic Acids Res* **40**, 914-927
34. Anderson, D. E., Trujillo, K. M., Sung, P., and Erickson, H. P. (2001) Structure of the Rad50 x Mre11 DNA repair complex from Saccharomyces cerevisiae by electron microscopy. *J Biol Chem* **276**, 37027-37033
35. de Jager, M., van Noort, J., van Gent, D. C., Dekker, C., Kanaar, R., and Wyman, C. (2001) Human Rad50/Mre11 is a flexible complex that can tether DNA ends. *Mol Cell* **8**, 1129-1135
36. Hopfner, K. P., Karcher, A., Craig, L., Woo, T. T., Carney, J. P., and Tainer, J. A. (2001) Structural biochemistry and interaction architecture of the DNA double-strand break repair Mre11 nuclease and Rad50-ATPase. *Cell* **105**, 473-485
37. Moreno-Herrero, F., de Jager, M., Dekker, N. H., Kanaar, R., Wyman, C., and Dekker, C. (2005) Mesoscale conformational changes in the DNA-repair complex Rad50/Mre11/Nbs1 upon binding DNA. *Nature* **437**, 440-443
38. Paull, T. T. (2018) 20 Years of Mre11 Biology: No End in Sight. *Mol Cell* **71**, 419-427
39. Lau, W. C., Li, Y., Liu, Z., Gao, Y., Zhang, Q., and Huen, M. S. (2016) Structure of the human dimeric ATM kinase. *Cell Cycle* **15**, 1117-1124
40. Reid, R. J., Gonzalez-Barrera, S., Sunjevaric, I., Alvaro, D., Ciccone, S., Wagner, M., and Rothstein, R. (2011) Selective ploidy ablation, a high-throughput plasmid transfer protocol, identifies new genes affecting topoisomerase I-induced DNA damage. *Genome Res* **21**, 477-486
41. Brunn, G. J., Hudson, C. C., Sekulic, A., Williams, J. M., Hosoi, H., Houghton, P. J., Lawrence, J. C., Jr., and Abraham, R. T. (1997) Phosphorylation of the translational repressor PHAS-I by the mammalian target of rapamycin. *Science* **277**, 99-101

42. Baroni, E., Viscardi, V., Cartagena-Lirola, H., Lucchini, G., and Longhese, M. P. (2004) The functions of budding yeast Sae2 in the DNA damage response require Mec1- and Tel1-dependent phosphorylation. *Mol Cell Biol* **24**, 4151-4165
43. Mimitou, E. P., and Symington, L. S. (2009) DNA end resection: many nucleases make light work. *DNA Repair (Amst)* **8**, 983-995
44. Lee, J. H., and Paull, T. T. (2005) ATM activation by DNA double-strand breaks through the Mre11-Rad50-Nbs1 complex. *Science* **308**, 551-554
45. Majka, J., Niedziela-Majka, A., and Burgers, P. M. (2006) The checkpoint clamp activates Mec1 kinase during initiation of the DNA damage checkpoint. *Mol Cell* **24**, 891-901
46. Shiotani, B., and Zou, L. (2009) Single-stranded DNA orchestrates an ATM-to-ATR switch at DNA breaks. *Mol Cell* **33**, 547-558
47. Reginato, G., Cannavo, E., and Cejka, P. (2017) Physiological protein blocks direct the Mre11-Rad50-Xrs2 and Sae2 nuclease complex to initiate DNA end resection. *Genes Dev* **31**, 2325-2330
48. Trujillo, K. M., Yuan, S. S., Lee, E. Y., and Sung, P. (1998) Nuclease activities in a complex of human recombination and DNA repair factors Rad50, Mre11, and p95. *J Biol Chem* **273**, 21447-21450
49. Myler, L. R., Gallardo, I. F., Soniat, M. M., Deshpande, R. A., Gonzalez, X. B., Kim, Y., Paull, T. T., and Finkelstein, I. J. (2017) Single-Molecule Imaging Reveals How Mre11-Rad50-Nbs1 Initiates DNA Break Repair. *Mol Cell* **67**, 891-898.e894
50. Deshpande, R. A., Lee, J. H., and Paull, T. T. (2017) Rad50 ATPase activity is regulated by DNA ends and requires coordination of both active sites. *Nucleic Acids Res* **45**, 5255-5268
51. Chen, L., Trujillo, K. M., Van Komen, S., Roh, D. H., Krejci, L., Lewis, L. K., Resnick, M. A., Sung, P., and Tomkinson, A. E. (2005) Effect of amino acid substitutions in the rad50 ATP binding domain on DNA double strand break repair in yeast. *J Biol Chem* **280**, 2620-2627
52. van der Linden, E., Sanchez, H., Kinoshita, E., Kanaar, R., and Wyman, C. (2009) RAD50 and NBS1 form a stable complex functional in DNA binding and tethering. *Nucleic Acids Res* **37**, 1580-1588
53. Paull, T. T. (2015) Mechanisms of ATM Activation. *Annu Rev Biochem* **84**, 711-738
54. Lee, J. H., Mand, M. R., Deshpande, R. A., Kinoshita, E., Yang, S. H., Wyman, C., and Paull, T. T. (2013) Ataxia telangiectasia-mutated (ATM) kinase activity is regulated by ATP-driven conformational changes in the Mre11/Rad50/Nbs1 (MRN) complex. *J Biol Chem* **288**, 12840-12851
55. Bakkenist, C. J., and Kastan, M. B. (2003) DNA damage activates ATM through intermolecular autophosphorylation and dimer dissociation. *Nature* **421**, 499-506
56. Sun, Y., Jiang, X., Chen, S., Fernandes, N., and Price, B. D. (2005) A role for the Tip60 histone acetyltransferase in the acetylation and activation of ATM. *Proc Natl Acad Sci U S A* **102**, 13182-13187
57. Pellegrini, M., Celeste, A., Difilippantonio, S., Guo, R., Wang, W., Feigenbaum, L., and Nussenzweig, A. (2006) Autophosphorylation at serine 1987 is dispensable for murine Atm activation in vivo. *Nature* **443**, 222-225
58. Osley, M. A., and Shen, X. (2006) Altering nucleosomes during DNA double-strand break repair in yeast. *Trends Genet* **22**, 671-677
59. Tsukuda, T., Fleming, A. B., Nickoloff, J. A., and Osley, M. A. (2005) Chromatin remodelling at a DNA double-strand break site in Saccharomyces cerevisiae. *Nature* **438**, 379-383
60. Stracker, T. H., and Petrini, J. H. (2011) The MRE11 complex: starting from the ends. *Nat Rev Mol Cell Biol* **12**, 90-103
61. Cassani, C., Vertemara, J., Bassani, M., Marsella, A., Tisi, R., Zampella, G., and Longhese, M. P. (2019) The ATP-bound conformation of the Mre11-Rad50 complex is essential for Tel1/ATM activation. *Nucleic Acids Res*
62. Oh, J., Al-Zain, A., Cannavo, E., Cejka, P., and Symington, L. S. (2016) Xrs2 Dependent and Independent Functions of the Mre11-Rad50 Complex. *Mol Cell* **64**, 405-415

63. Wanrooij, P. H., Tannous, E., Kumar, S., Navadgi-Patil, V. M., and Burgers, P. M. (2016) Probing the Mec1ATR Checkpoint Activation Mechanism with Small Peptides. *J Biol Chem* **291**, 393-401
64. Poltoratsky, V. P., Shi, X., York, J. D., Lieber, M. R., and Carter, T. H. (1995) Human DNA-activated protein kinase (DNA-PK) is homologous to phosphatidylinositol kinases. *J Immunol* **155**, 4529-4533
65. Trujillo, K. M., and Sung, P. (2001) DNA structure-specific nuclease activities in the Saccharomyces cerevisiae Rad50*Mre11 complex. *J Biol Chem* **276**, 35458-35464
66. Bylund, G. O., Majka, J., and Burgers, P. M. (2006) Overproduction and purification of RFC-related clamp loaders and PCNA-related clamps from Saccharomyces cerevisiae. *Methods Enzymol* **409**, 1-11
67. Gomes, X. V., Schmidt, S. L., and Burgers, P. M. (2001) ATP utilization by yeast replication factor C. II. Multiple stepwise ATP binding events are required to load proliferating cell nuclear antigen onto primed DNA. *J. Biol. Chem.* **276**, 34776-34783

Footnotes

This work was supported in part by a grant from the National Institutes of Health (GM118129 to P.B.) and a NSF Graduate Research Fellowship (2014157291 to S.H.)

The abbreviations used are: DSB, double-stranded DNA break; PIKK, phosphatidylinositol 3-kinase-related protein kinase; ssDNA, single-stranded DNA; dsDNA, double-stranded DNA; MRX, Mre11-Rad50-Xrs2 complex

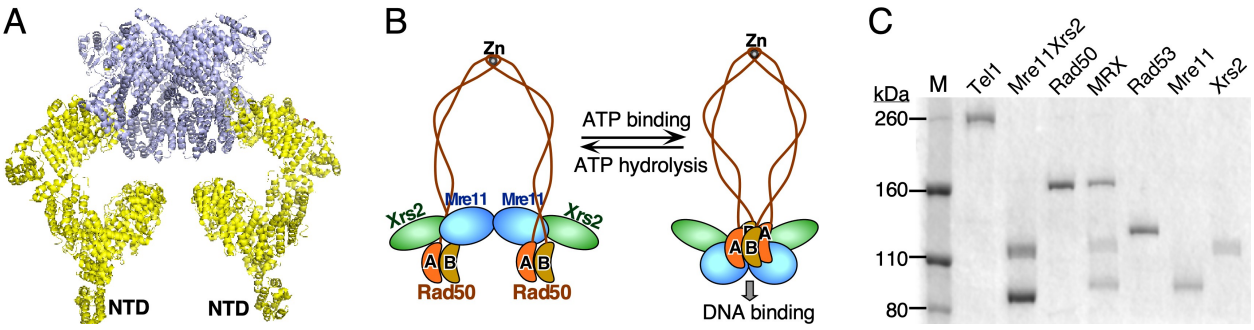

FIGURE 1. **Tel1 kinase and the MRX complex.** *A*, Tel1 and ATM kinases exist as dimers. The structure shown is that of human ATM (PDB ID:4JSV): yellow, HEAT repeats; blue, kinase and kinase-associated domains. *B*, Schematics of the MRX complex in the presence and absence of ATP. The model is based on structural analysis of archaeal MR complexes. ATP binding by Rad50 transforms MRX from an open to closed conformation (see text for details). *C*, 7% SDS-PAGE analysis of purified Tel1, MRX and MRX subunits, and Rad53-kd. Staining was with coomassie blue.

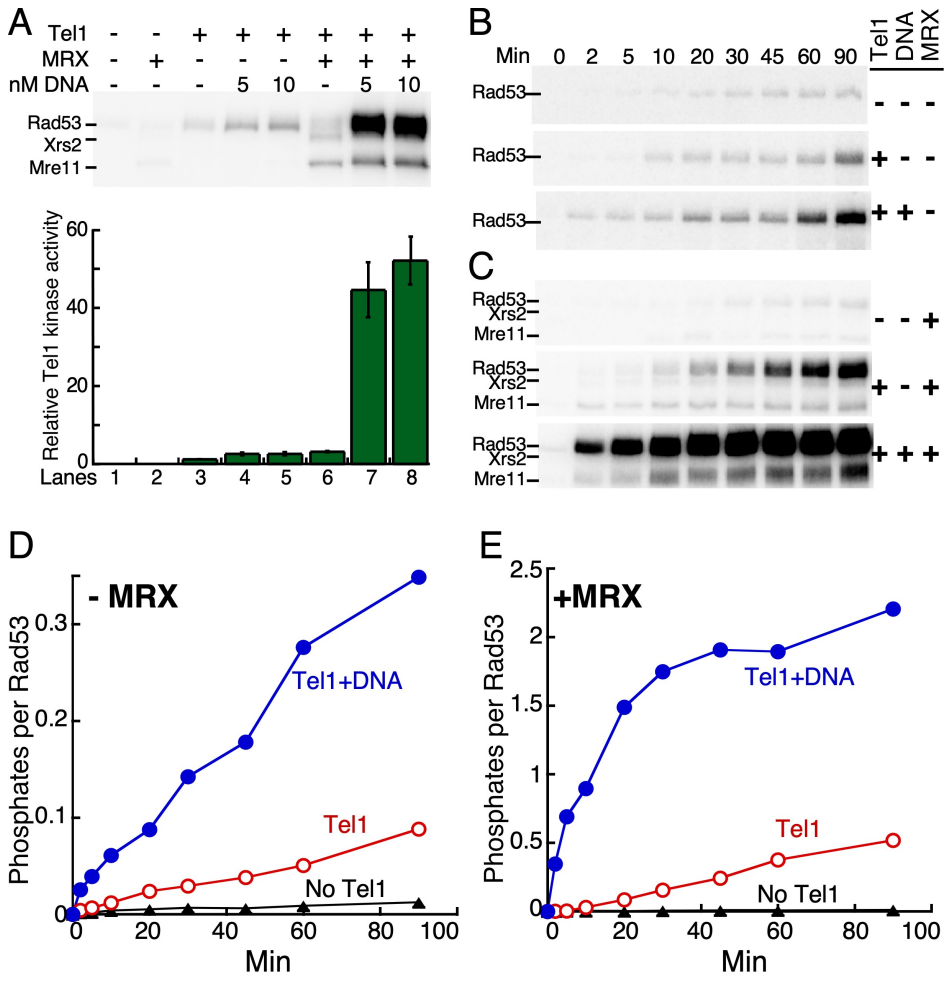

FIGURE 2. **MRX and DNA synergistically activate Tel1 kinase.** *A*, standard kinase reactions contained 200 nM Rad53-kd and 50 μM [γ-^{32}P]-ATP in kinase buffer with or without 30 nM MRX and the indicated concentration of 2 kb linear DNA. Kinase reactions were initiated with 5 nM Tel1 (lanes 1 and 2 are negative controls). Reactions were stopped after 15 min at 30 ˚C and analyzed by 7% SDS-PAGE, followed by phosphorimaging. A representative experiment is shown at top. Bottom, phosphorylation of Rad53 was quantified and plotted as fold increase of Tel1 kinase activity with lane 3 set at 1. Averages and standard errors are derived from three independent experiments. *B*, *C,* time course analyses of Rad53 phosphorylation under standard conditions with 5 nM Tel1, 5 nM linear 2 kb DNA and 30 nM MRX where indicated. *D*, quantification of the data in *B*. *E*, quantification of the data in *C*. Note the different Y-axis scales in *D* and *E*. A representative of two independent experiments is shown. In panels A, B and C, the migration of GST-Rad53-kd (118 kDa), Xrs2 (96 kDa), and Mre11 (77 kDa) is as shown.

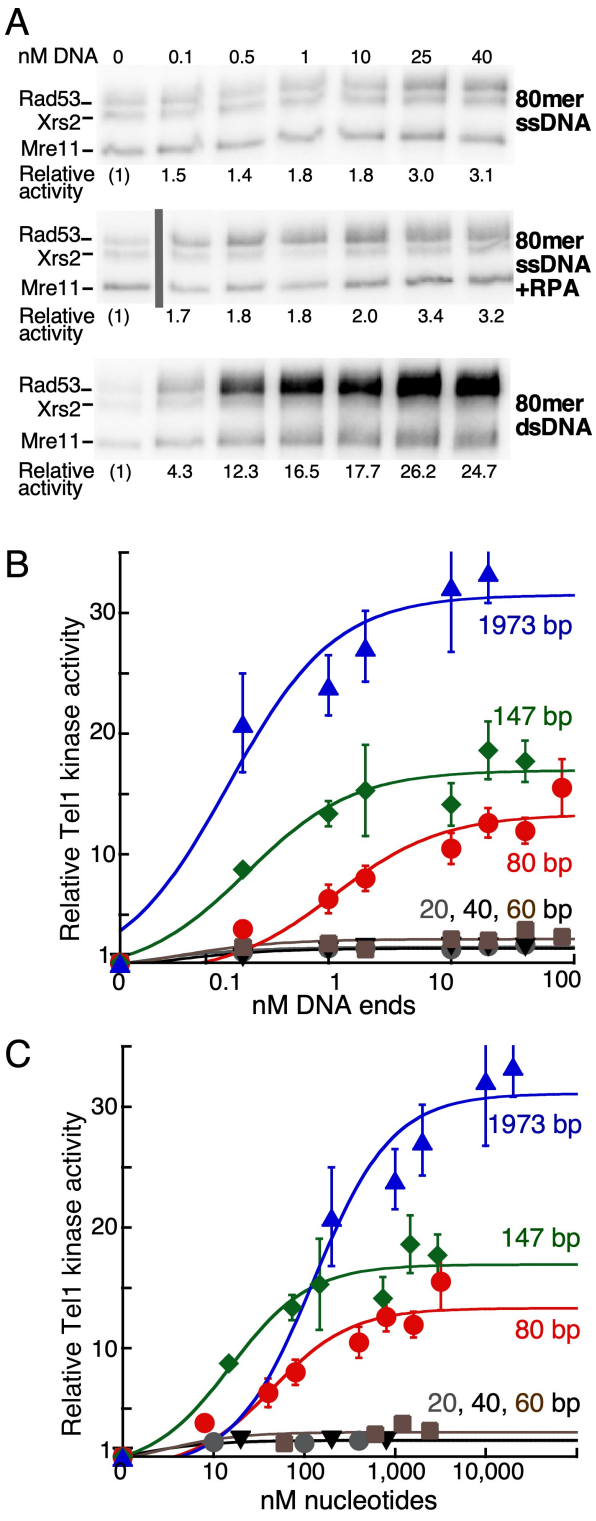

FIGURE 3. **MRX•Tel1 exhibits a preference for long double-stranded DNA.** *A*, standard kinase reactions contained 5 nM Tel1, 30 nM MRX, 200 nM Rad53, and the indicated concentrations of 80-mer ssDNA with or without RPA, or 80-mer dsDNA. The amount of RPA required to coat ssDNA was calculated for each DNA concentration with a single RPA trimer coating 30 nt. Relative Tel1 activity was calculated by setting the reaction without DNA to 1 (lane 1). The first lane in the ssDNA/RPA experiment comes from a different gel in the same experiment. The grey bar indicates the discontinuity. The migration of GST-Rad53-kd (118 kDa), Xrs2 (96 kDa), and Mre11 (77 kDa) is as shown. *B*, standard kinase reactions contained 5 nM Tel1, 30 nM MRX, 200 nM Rad53, and increasing concentrations of linear dsDNA molecules with the indicated lengths. Data were plotted as a function of DNA end concentrations in a log plot. Relative Tel1 kinase activity was calculated by setting the reaction without DNA to 1. Averages and standard errors are derived from four independent experiments. *C*, the same data were plotted as a function of total DNA as nucleotide concentrations.

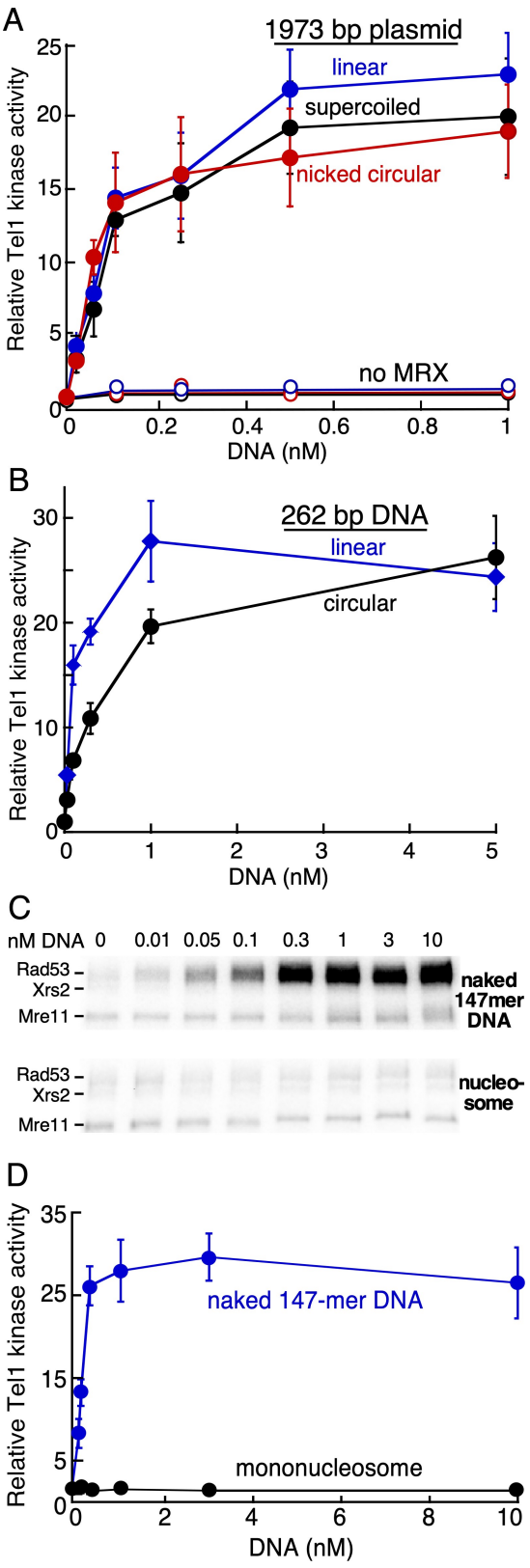

FIGURE 4. **Requirement for nucleosome-free DNA, but not DNA ends for Tel1 activation.** *A*, kinase reactions contained 5 nM Tel1, 30 nM MRX, 200 nM Rad53, and increasing concentrations of 2 kb DNA with the structures indicated. Relative Tel1 kinase activity was calculated by setting the reaction without DNA to 1. Averages and standard errors are derived from five independent experiments. The "no MRX" control titrations are shown for each DNA substrate. *B*, kinase reactions contained 5 nM Tel1, 30 nM MRX, 200 nM Rad53, and increasing concentrations of either linear or circular 262 bp DNA. Relative Tel1 kinase activity was calculated by setting the reaction without DNA to 1. Averages and standard errors are derived from three independent experiments. *C*, standard kinase reactions contained 5 nM Tel1, 30 nM MRX, 200 nM Rad53, and increasing concentrations of either 147 bp naked DNA, or the nucleosome assembled on the same DNA. A representative experiment is shown. The migration of GST-Rad53-kd (118 kDa), Xrs2 (96 kDa), and Mre11 (77 kDa) is as shown. *D*, Quantification of four independent experiments with standard errors shown.

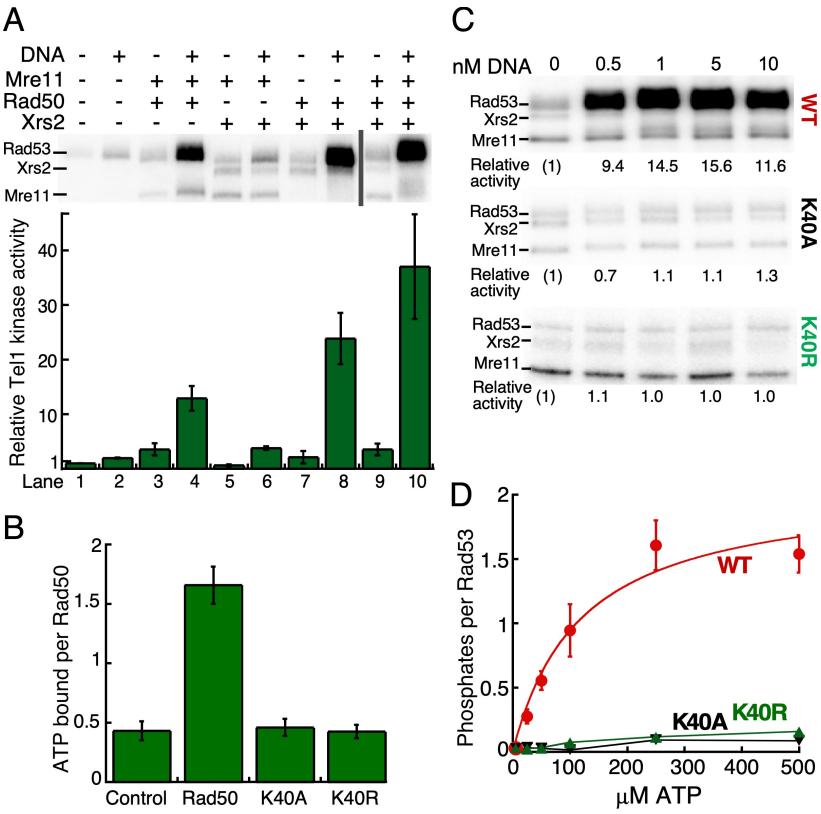

FIGURE 5. **Rad50 ATP binding is required for Tel1 activation.** *A*, standard kinase reaction with 5 nM Tel1, 200 nM Rad53, and 30 nM MR, MX, RX or MRX, with or without 5 nM linear 2 kb DNA. Top, representative of three independent experiments. The right two lanes are derived from a different gel in the same experiment (both gels are shown in supplemental Fig. S3A). The grey bar indicates the discontinuity. Bottom, quantification and standard errors. Relative Tel1 kinase activity was calculated by setting Tel1 alone (lane 1) to 1. *B*, nitrocellulose filter binding assays of the binding of 50 μM [γ-^{32}P]-ATP to 500 nM wild-type or mutant MRX. Control, no MRX (details in Experimental procedures). Quantification of four independent experiments with standard errors is shown. *C*, kinase assays were carried out using 5 nM Tel1, 200 nM Rad53, 30 nM MRX, MR(K40A)X, or MR(K40R)X, and increasing concentrations of 80 mer dsDNA. A representative of two experiments is shown. *D*, standard kinase reaction with 5 nM Tel1, 200 nM Rad53, and 30 nM MRX, MR(K40A)X, or MR(K40R)X, 5 nM linear 2 kb DNA, and increasing concentrations of [γ-^{32}P]-ATP. Quantification of three independent experiments with standard errors is shown. In panels A and C, the migration of GST-Rad53-kd (118 kDa), Xrs2 (96 kDa), and Mre11 (77 kDa) is as shown.

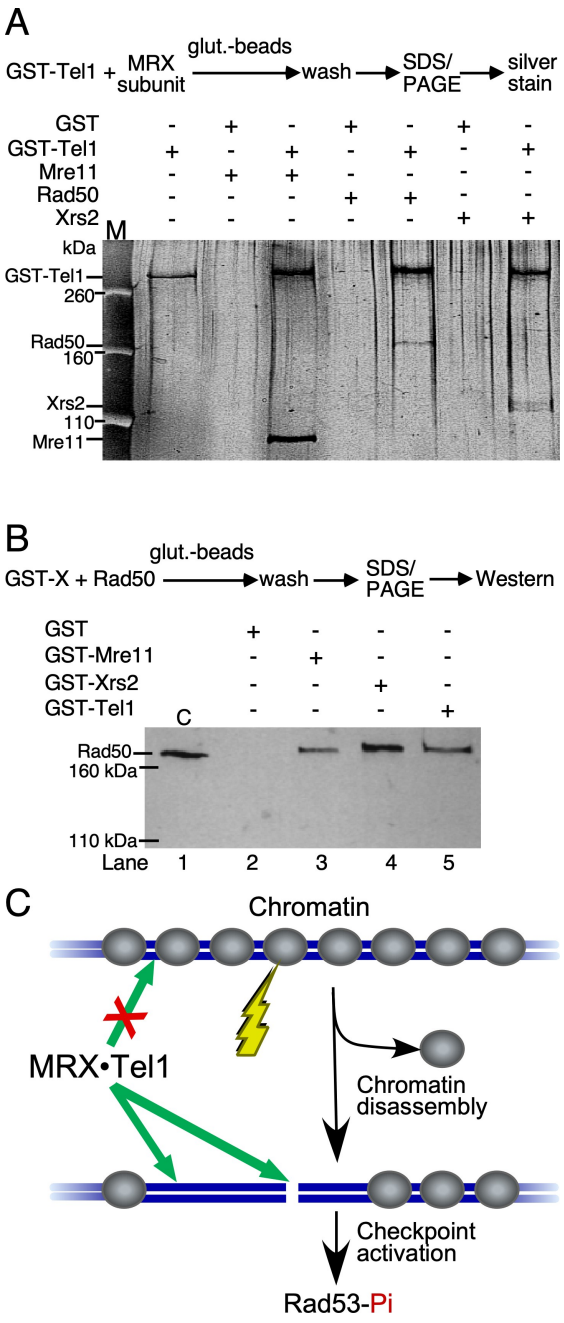

FIGURE 6. **MRX•Tel1 interaction network.** *A*, purified MRX subunits were incubated with GST-tagged Tel1 in the presence of glutathione-sepharose beads. The beads were washed and bound proteins analyzed by 7% SDS-PAGE, followed by silvers staining (experimental procedures). GST was used as a negative control for each subunit, as indicated. A representative of three independent experiments is shown. *B*, purified Rad50 subunit was incubated with either GST-tagged Mre11, Xrs2, or Tel1. Bound Rad50 was analyzed by western blotting with anti-Rad50 antibody. Lane 2, negative control; binding of Rad50 to GST. *C*, Model for MRX•Tel1 recruitment to non-nucleosomal DNA (see text for details).

Activation of Tel1^{ATM} kinase requires Rad50 ATPase and long nucleosome-free DNA, but no DNA ends

Sarem Hailemariam, Sandeep Kumar and Peter M Burgers

J. Biol. Chem. published online May 9, 2019

Access the most updated version of this article at doi: 10.1074/jbc.RA119.008410

Supporting information to:

Activation of Tel1^{ATM} kinase requires Rad50 ATPase and long nucleosome-free DNA, but no DNA ends

Sarem Hailemariam[1], Sandeep Kumar[1,2], and Peter M. Burgers[1]*

[1]Department of Biochemistry and Molecular Biophysics, Washington University School of Medicine, Saint Louis, Missouri, USA, [2]current address: Intellia Therapeutics, Cambridge, MA 02139.

*Corresponding author: TEL (314) 362-3772; FAX (314) 362-7183; burgers@wustl.edu

---

DNA substrates used:

20mer: 5'-TTGATAAGAGGTCATTTTT
40mer: 5'-TTGATAAGAGGTCATTTTTGCGGATGGCTTAGAGCTTAAT
60mer: 5'-ACATGTTGAGCTACAGCACCAGATTCAGCAATTAAGCTCTAAGCCATCCGCAAAAATGAC
80mer: 5'-TTGATAAGAGGTCATTTTTGCGGATGGCTTAGAGCTTAATTGCTGAATCTGGTGCTGTAG
CTCAACATGTTTTAAATATG
147mer: 5'-ATCGAGAATCCCGGTGCCGAGGCCGCTCAATTGGTCGTAGACAGCTCTAGCACCGCTTA
AACGCACGTACGCGCTGTCCCCCGCGTTTTAACCGCCAAGGGGATTACTCCCTAGTCTCCAGG
CACGTGTCAGATATATACATCCGAT

Oligonucleotides were hybridized to their complementary sequences in a 1:1 ratio to form blunt-end dsDNAs. The sequence of the 80-mer shown was used as ssDNA in the experiment shown in Fig. 3A. The 147-mer sequence is the Widom 601 sequence (1), and was purchased from EpiCypher, as was the mononucleosome assembled on the same sequence, and used in Fig. 4B,C.

1. Lowary, P.T., and Widom, J. (1998). New DNA sequence rules for high affinity binding to histone octamer and sequence-directed nucleosome positioning. J Mol Biol *276*, 19-42.

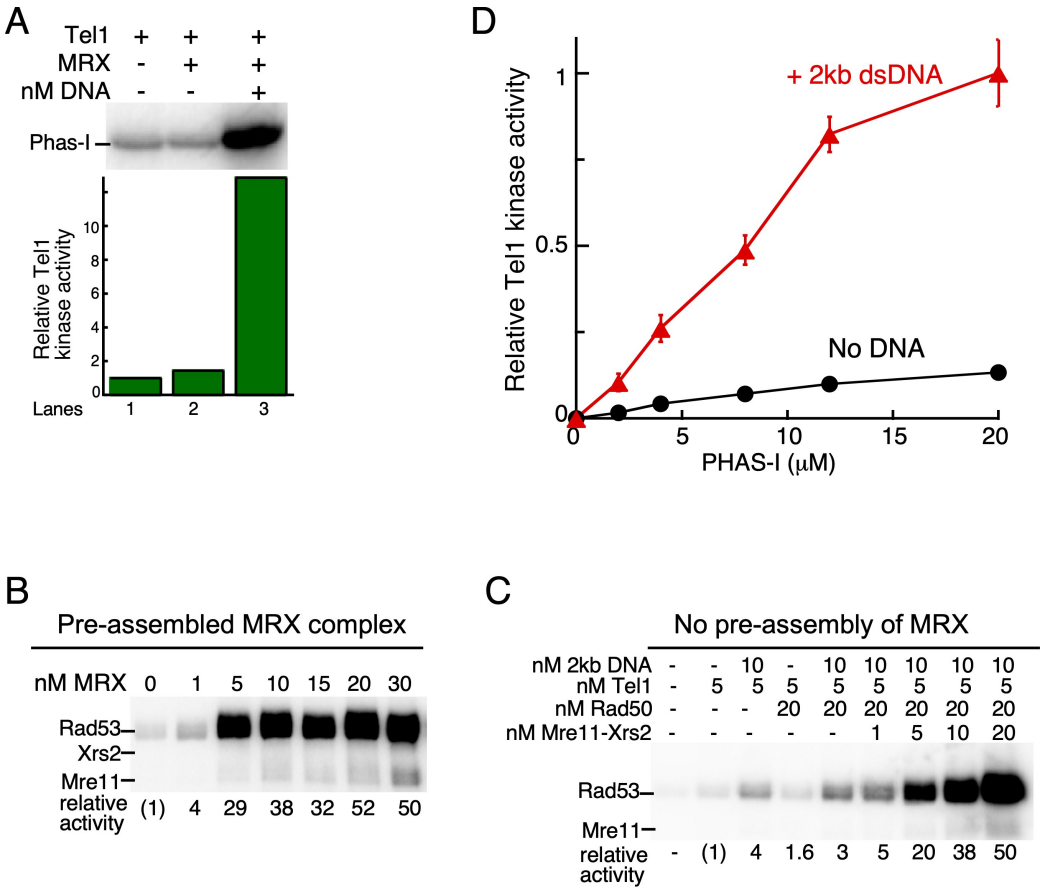

FIGURE S1. **Tel1 activation by MRX and DNA.** *A*, standard kinase reactions contained 2 μM PHAS-I and 50 μM [γ-^{32}P]-ATP in kinase buffer with or without 30 nM MRX and 5 nM 2 kb linear DNA. Kinase reactions were initiated with 5 nM Tel1. Reactions analyzed by 15% SDS-PAGE, followed by phosphorimaging. A representative experiment is shown at top. Bottom, phosphorylation of PHAS-I was quantified and plotted as fold increase of Tel1 kinase activity with lane 1 set at 1. The migration of PHAS-I (15 kDa) is as shown. *B,* standard kinase reactions contained 5 nM Tel1, 10 nM 2kb linear DNA, 200 nM Rad53, and the indicated concentrations of MRX. The MRX used in this experiment was pre-assembled by incubating 300 nM Rad50 with 300 nM Mre11-Xrs2 at 0 ˚C for one hour, prior to dilution into the assay. Rad53 phosphorylation was quantified by setting Tel1 alone reaction (lane 1) to 1. *C*, kinase reactions contained 5 nM Tel1, 10 nM 2kb linear DNA, 200 nM Rad53, 20 nM Rad50. The indicated concentrations of Mre11-Xrs2 was added into the assay at 0 ˚C and the assay incubated at 30 ˚C for 15 min. Rad53 phosphorylation was quantified by setting Tel1 alone reaction (lane 2) to 1. *D,* standard kinase reactions contained 5 nM Tel1, 30 nM MRX, and increasing concentrations of PHAS-I in the presence or absence of 5 nM 2kb linear DNA. In panels B and C the migration of GST-Rad53-kd (118 kDa), Xrs2 (96 kDa), and Mre11 (77 kDa) is as shown.

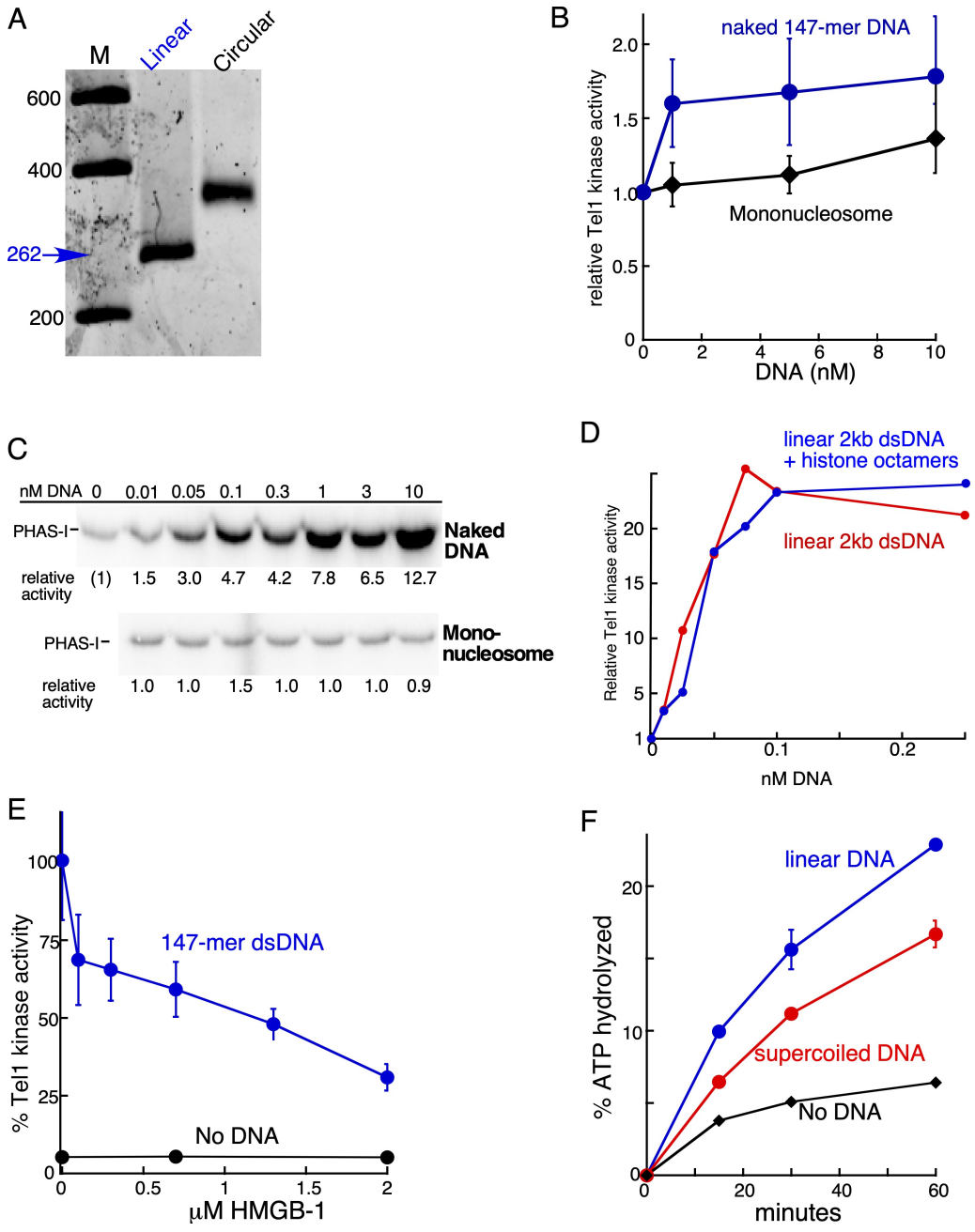

FIGURE S2. **Nucleosome-free DNA, but not DNA ends, is required for Tel1 activation.** *A, preparation of 262-mer circular DNA.* A 262-mer DNA fragment was cut out of a 3 kb plasmid by *Sal*1 and *Xho*1 digestion, and purified by differential PEG_{8000} precipitation in 0.5 M NaCl. The 5-9% w/w cut was >90% pure. It was ligated in a 1 ml ligation reaction containing 20 mM Tris-HCl 7.6, 100 mM Na-acetate, 10 mM Mg-acetate, 1 mM ATP, 1 mM spermidine, 1.5 μg/ml ethidium bromide, 50 nM 262-mer fragment, and 4,000 units of T4 ligase, for 24 h at 13 ˚C. The optimal concentration of ethidium bromide to obtain circularization was previously determined in a test assay with concentrations varying between 0.2-10 μg/ml. The DNA was recovered by ethanol precipitation, and the circular DNA was purified on a 3% preparative Metaphor gel. The

linear DNA was purified on the same gel to remove contaminating plasmid DNA. A comparison of the linear and circular preparations is shown on a 3% Metaphor gel, which was stained with GelRed. *B, Tel1 alone is not stimulated by nucleosomal DNA.* Standard kinase reactions without MRX contained 5 nM Tel1, and increasing concentrations of either 147 bp naked DNA, or the nucleosome assembled on the same DNA. Phosphorylation of Rad53-kd was quantified as fold increase of Tel1 kinase activity, with no DNA set to 1. *C, nucleosomal DNA does not stimulate Tel1 in the MRX-dependent assay using PHAS-I as substrate.* Standard kinase reactions lacking contained 5 nM Tel1, 30 nM MRX, 2 μM PHAS-I instead of Rad53-kd, and increasing concentrations of either 147 bp naked DNA, or the nucleosome assembled on the same DNA. Phosphorylation of PHAS-I was quantified as fold increase of Tel1 kinase activity with lane 1 (on naked DNA gel) set at 1. The migration of PHAS-I (15 kDa) is as shown. *D, free histone octamers do not inhibit Tel1 kinase.* Standard kinase reactions contained 5 nM Tel1, 30 nM MRX, 200 nM Rad53, and increasing concentrations of 2 kb linear DNA with or without increasing concentrations of histone octamers. The concentration of histone octamers required to coat DNA was calculated for each DNA concentration with a single octamer wrapping 147 bp. Relative Tel1 activity was calculated by setting the reaction without DNA to 1. *E, DNA coating by HMGB-1 inhibits Tel1.* Standard kinase reactions contained 5 nM Tel1, 30 nM MRX, 200 nM Rad53-kd, either no DNA or 1 nM 147-mer dsDNA, as indicated, and increasing concentrations of HMGB-1. *F, ATPase activity of MRX is stimulated preferentially by linear DNA.* Standard ATPase reactions contained 50 μM [γ-^{32}P]-ATP, 100 nM MRX, and 1 nM of the indicated 2 kb DNA. Radioactive ATP and ADP were separated by PEI-Cellulose TLC and quantified as described (1).

1. Chen, L., Trujillo, K. M., Van Komen, S., Roh, D. H., Krejci, L., Lewis, L. K., Resnick, M. A., Sung, P., and Tomkinson, A. E. (2005) Effect of amino acid substitutions in the rad50 ATP binding domain on DNA double strand break repair in yeast. *J Biol Chem* **280**, 2620-2627

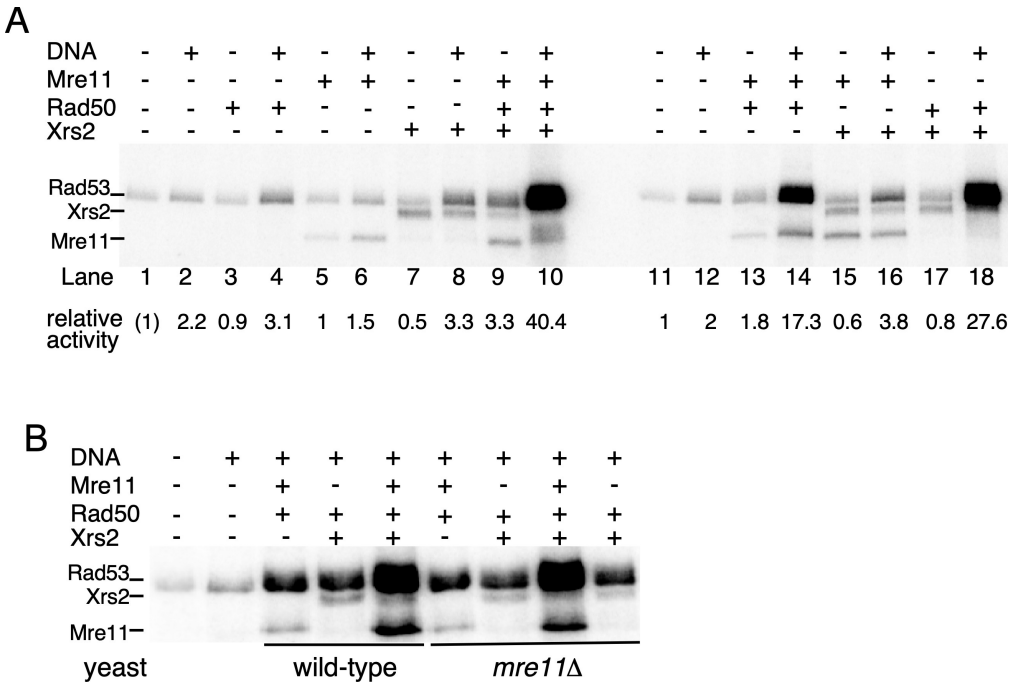

FIGURE S3. *A*, **Single subunits of MRX do not show a substantial activation of Tel1 kinase**. *A*, standard kinase reaction with 5 nM Tel1, 200 nM Rad53, and 30 nM Mre11, Rad50, or Xrs2, with or without 5 nM linear 2 kb DNA (left panel, lanes 1-8). The right panel (lanes 9-18) is the same data presented in FIGURE 5A. Lanes 9 and 10 of the left panel are presented as lanes 9 and 10 in Fig. 5A. Relative Tel1 kinase activity was calculated by setting Tel1 alone (lane 1) to 1. *B*, standard kinase reaction with 5 nM Tel1, 200 nM Rad53, and 30 nM MR, RX or MRX, with 5 nM linear 2 kb DNA. The Rad50 protein used in lanes 3-5 is purified from a wild-type yeast strain while the Rad50 used in the last four lanes is from a yeast *mre11Δ* strain. In all panels, the migration of GST-Rad53-kd (118 kDa), Xrs2 (96 kDa), and Mre11 (77 kDa) is as shown.

Chapter III

Opposing roles of Rad50 ATPase and Rif2 in the activation of Tel1^{ATM} kinase

Sarem Hailemariam[1], Paolo De Bona[1], Marcel Hohl[2], John Petrini[2], Roberto Galletto[1], and Peter Burgers[1]

[1]Department of Biochemistry and Molecular Biophysics, Washington University in St. Louis; St. Louis, MO 63110; [2]Molecular Biology Program, Memorial Sloan-Kettering Cancer Center, Molecular Biology Program, New York, NY 10021

*Corresponding author: TEL (314) 362-3772; FAX (314) 362-7183; burgers@wustl.edu

Abstract

Telomeres are nucleoprotein complexes that define ends of linear chromosomes. In mammalian cells, a multi-subunit protein complex called shelterin protects telomeres from being recognized as intrachromosomal DNA breaks, thereby preventing a checkpoint response. In *Saccharomyces cerevisiae*, the telomere regulator Rif2 (Rap1-interacting-factor 2), is a key protein involved in suppressing the Tel1 checkpoint response at long telomeres. Conversely, Rif2 occupancy at short telomeres is low, allowing the recruitment and activation of Tel1 by the Mre11-Rad50-Xrs2 (MRX) complex. Tel1 activity results in telomerase activation. In order to understand the role of Rif2 in inhibiting MRX-dependent activation of Tel1, we employed an *in vitro* kinase assay using purified proteins. Using this approach we recently showed that DNA and Rad50, along with either Mre11 or Xrs2, are required for activation of Tel1 kinase. Our studies show that Rif2 directly inhibits MRX-dependent activation of Tel1 kinase. Rif2 attenuates MRX-mediated activation of Tel1 by discharging the ATP-bound form of Rad50, which is important for all MRX-dependent activities in the cell. This conclusion is further strengthened by studies of a Rad50 allosteric ATPase mutant that maps outside of the conserved ATP binding pocket.

Introduction

Telomeres are DNA-protein complexes that define the physical ends of linear eukaryotic chromosomes. Telomeric DNA is composed of short, tandem G-rich repeats that extend for thousands of bases at the 3'-ends of chromosomes. Proper establishment and maintenance of telomeres is essential for genome stability and cell survival (Gomes et al., 2010; Wellinger and Zakian, 2012). Telomeres progressively shorten as cells divide. Telomere shortening is counteracted by telomerase, a reverse transcriptase that synthesizes the G-rich telomeric repeats *de novo* (Greider and Blackburn, 1985). Both yeast cells and primary mammalian cells that are unable to maintain telomeres, progress into senescence, which is mediated by a DNA damage-signaling pathway (d'Adda di Fagagna et al., 2003). Telomere-induced senescence underlies a plethora of human genetic disorders that share short telomere as a common molecular defect (Armanios and Blackburn, 2012). On the other hand, in humans, the inappropriate elongation of telomere leads to cancer predisposition and aids in the survival of cancer cells (Kim et al., 1994).

In addition to telomerase, telomere DNA repeats are bound by a set of proteins that assemble into a protective capping structure (Palm and de Lange, 2008; Wright et al., 1992). This DNA-protein structure serves two important functions. First, it protects chromosome ends from nucleolytic degradation and from being recognized as double-stranded DNA breaks (DSBs). Improper recognition of chromosome ends as DSBs would elicit a DNA-damage checkpoint and promote repair, which at telomeres could result in telomeric fusions. Second, shelterin regulates telomere length by controlling access of telomerase and its activity (Bianchi and Shore, 2008; Smogorzewska and de Lange, 2004). In *Saccharomyces cerevisiae*, this capping complex is composed of many proteins which include the Rap1-Rif1-Rif2 complex and the Cdc13-Stn1-Ten1 (CST) complex. The Rap1-Rif1-Rif2 protein complex associates with the double-stranded TG(1-3) repeat and is a pivotal player in telomere homeostasis (Hardy et al., 1992; Longtine et al., 1989; Wotton and Shore, 1997). The CST complex forms RPA-like trimeric complex that binds to the single-stranded 3' overhang and prevents its nucleolytic degradation(Gao et al., 2007; Grandin et al., 1997). In addition to these major telomere-associated proteins, there are other enzymes that mediate both end protection and telomere length control. Among these are Tel1 checkpoint kinase, the ortholog of human ATM, and the MRX complex composed of Mre11, Rad50, and Xrs2(Ritchie and Petes, 2000). The human ortholog of Xrs2 is Nbs1, and therefore, the human complex is abbreviated as MRN(Carney et al., 1998).

The Rad50 subunit binds ATP, and has weak ATPase activity that is stimulated a few fold in the presence of dsDNA. Disabling ATP binding to Rad50 is associated with a phenotype similar to that of the *rad50D* mutant(Chen et al., 2005).

The double-stranded telomeric region of *S. cerevisiae* contains an array of high affinity Rap1 binding sites. Consistent with its essential role in telomere homeostasis, telomeric $TG_{(1-3)}$ repeat containing DNA substrates exhibit the highest affinity binding sites for Rap1(Gilson et al., 1993; Longtine et al., 1989). Rap1 also recruits Rif1 and Rif2 to telomeres. Both of these protein bind to the C-terminal domain of Rap1 and this interaction is required for their recruitment (Hardy et al., 1992; Levy and Blackburn, 2004; Marcand et al., 1997; Wotton and Shore, 1997). Deletion of Rif1 and Rif2 leads to telomere elongation and deletion of both has an additive effect. Strains that express a Rap1 variant lacking the C-terminal domain confer a telomere phenotype similar to *rif1Δ rif2Δ* double deletion(Wotton and Shore, 1997). Based on these genetic observations, a protein-counting model has been proposed to describe how these factors coordinate to negatively regulate telomere length (**Fig. 1A**)(Marcand et al., 1997). The model suggests that long telomeres, by virtue of their size, are able to support the binding of multiple Rap1-Rif1-Rif2 complexes. This large number of Rap1-Rif1-Rif2 molecules leads to an increased repressive effect on telomere elongation. On the other hand, short telomeres bind fewer of these repressive complexes are consequently are more frequently elongated (Marcand et al., 1997). Tethering Rif1 and Rif2 to telomeres by other means than binding to Rap1 also limits telomere elongation. This suggests that Rif1 and Rif2, and not Rap1 are responsible for the repressive effect(Levy and Blackburn, 2004). The preferential extension of short telomeres coupled with the restrained elongation of long telomeres maintains telomere length homeostasis.

The protein kinase Tel1 coordinates checkpoint activation in response to DSBs(Mallory and Petes, 2000). Tel1's recruitment to DSBs and the subsequent activation of its protein kinase activity is dependent on MRX(Nakada et al., 2003). This central three-subunit complex consists of Mre11 nuclease, Rad50 ATPase, and the auxiliary subunit Xrs2, the ortholog of human NBS1 (Oh and Symington, 2018; Paull, 2018). In addition to its role in DNA break repair, Tel1 is also involved in telomere length regulation(Ritchie and Petes, 2000). Tel1 specifically associates with short telomeres and *tel1D* mutants show a defect in telomerase-mediated telomere elongation(Chang et al., 2007; Hector et al., 2007; Sabourin et al., 2007; Viscardi et al., 2007). Although the exact mechanism of Tel1-mediated telomere length regulation is unknown, its

kinase activity is essential because cells expressing kinase-dead Tel1 show similar telomere length defects as *tel1*Δ cells(Greenwell et al., 1995; Mallory and Petes, 2000). Tel1 binding to telomeres has been shown to depend on the C-terminal domain of the Xrs2 subunit of MRX(Nakada et al., 2003). Deletion of any of the subunits of MRX, or destructive mutation of the ATP-binding site in Rad50 results in telomere shortening similar to that observed in a *tel1D* mutant, indicating that Tel1, MRX, and Rad50 ATPase positively regulate telomere length in the same pathway(Hector et al., 2007; Park et al., 2017; Ritchie and Petes, 2000).

The mechanism by which Rif2 controls telomere length remains elusive. Recent studies have suggested that Rif2 attenuates the functions of Tel1 and MRX at telomeres (Cassani et al., 2016; Hirano et al., 2009). Rif2 interacts with Xrs2 in the same region as Tel1 does, prompting the model that Rif2 counteracts MRX-dependent recruitment of Tel1 to telomeres by simple competition (Hirano et al., 2009). Here, we have studied the role of Rif2 in the MRX -dependent activation of Tel1 in a reconstituted biochemical system. Our data show that Rif2 directly inhibits MRX-dependent stimulation of Tel. *In vitro*, this inhibition does not depend on the interaction of Rif2 with Rap1 or with Xrs2. Rather; Rif2 acts directly on Rad50 by discharging its activated ATP-bound state, thereby making the MRX complex incompetent for Tel1 activation.

Results and Discussion

Rif2 inhibits MRX-dependent activation of Tel1 kinase

We have employed an *in vitro* assay using purified proteins to examine the potential role that Rif2 plays in regulating the activities of Tel1 and MRX. Tel1's physiological substrate is Rad53, the effector kinase in the cell cycle checkpoint pathway (Usui et al., 2001). Phosphorylation of Rad53 was used as a direct readout of Tel1 kinase activity. We previously showed that individually, MRX or DNA caused a 2-3 fold stimulation of Tel1 kinase activity, however, when both are present, a synergistic stimulation of Tel1 kinase was observed (Hailemariam et al., 2019) (**Fig. 1B**). This strong stimulation is independent of DNA sequence: both random DNA (Nat) and telomeric repeat DNA (Telo) showed a similar response.

To test whether Rif2 has a function in the MRX-dependent activation of Tel1, we titrated Rif2 into the complete assay, containing both MRX and DNA (**Fig. 1C**). Rif2 inhibited Tel1

kinase in this assay, as shown by reduced Rad53 phosphorylation. The inhibitory role of Rif2 in the DNA-MRX-Tel1 assay is not dependent on a telomeric DNA repeat sequence, because a similar inhibition was observed when a non-telomeric DNA sequence (Nat) was used (**Fig. 1C,D)**. The Rif2-mediated inhibition is independent of its known telomere-recruiting partner, Rap1 (**Fig. S1A**). This result is consistent with the genetic observation that Rap1's requirement for telomere length control can be bypassed by artificially tethering Rif2 to telomeres(Levy and Blackburn, 2004). Taken together, these observations support the model that was based on genetic data, that Rif2 attenuates the functions of Tel1 and MRX at telomeres. In a control experiment, we determined that the Rif2 mediated inhibition is not specific to Tel1's physiological phosphorylation target Rad53. A heterologous substrate, human PHAS-I also showed severely reduced phosphorylation by Tel1 in this assay when Rif2 was added (**Fig. S1B**).

The protein kinase activity of Tel1 is required for all Tel1-mediated transactions, including telomere regulation *in vivo* (Greenwell et al., 1995; Mallory and Petes, 2000). However, the inhibitory activity of Rif2 does not proceed through Tel1 directly. Rif2 inhibited neither the basal Tel1 kinase activity (not shown) nor the DNA-stimulated Tel1 kinase activity (**Fig. S1C**). These data suggest that Rif2 inhibition may proceed through MRX.

The Xrs2 subunit of MRX is dispensable for Rif2's inhibitory activity in vitro

Tel1 is recruited to telomeres and double-stranded DNA breaks through its association with the C-terminus of Xrs2 (Nakada et al., 2003). A C-terminal truncation of Xrs2 (human NBS1) attenuates MRX function without affecting the stability of the MRX complex in budding, fission yeast, and in human cells (Difilippantonio et al., 2007; Nakada et al., 2003; You et al., 2005). Moreover, Rif2 interacts with Xrs2 within the same C-terminal region as Tel1. This has led to the proposal of a model by which Rif2 may exert its inhibitory role by abrogating the binding of Tel1 to Xrs2, and thereby to MRX (Hirano et al., 2009). One prediction of the model is that inhibition is dependent on Xrs2.

In a recent study, we showed that Rad50 is the critical subunit of MRX for full activation of Tel1 (Hailemariam et al., 2019). In addition to DNA and Rad50, either Mre11 or Xrs2 but not both, is also required. Thus, both the Mre11-Rad50 and Rad50-Xrs2 pairs, but not the Mre11-Xrs2 dimer, function efficiently *in vitro* (Hailemariam et al., 2019). We tested whether Rif2 inhibited the activation of Tel1 by the different dimeric pairs of MRX. With an identical

efficiency, Rif2 inhibited Tel1 activation by MRX and by RX, but also by MR lacking Xrs2 (**Fig. 2A,B**). These data suggest that Rif2 enforces its inhibition through the Rad50 subunit, which is the common subunit in all complexes. The observation of a functional relationship between Rad50 and Rif2 prompted us to test for their physical interaction. GST-tagged Rif2 was able to pull down Rad50 with an efficiency comparable to that of the positive control Mre11, a known interactor of Rad50 (Usui et al., 1998) (**Fig. 2C**, compare lane 1 with 3).

The N-terminal region of Rif2 is essential for its regulatory role

To gain a better understanding of how Rif2 attenuates the MRX-dependent activation of Tel1, we sought to identify the region of Rif2 responsible for its inhibitory role. The extreme N-terminal region of Rif2 has been implicated in its telomere length regulatory function *in vivo* (Kaizer et al., 2015; Shi et al., 2013). This region is predicted to be largely unstructured and lies outside of the Orc4-homology domain (Shi et al., 2013). Specifically, the Rif2-F8A mutation completely abrogated Rif2's functionality in yeast (Kaizer et al., 2015). This point mutant confers a similar telomere phenotype to that of a *rif2D* mutant. We tested the F8A variant of Rif2 in our *in vitro* system. Rif2-F8A showed no inhibition of the MRX-dependent activation of Tel1 (**Fig. 3A,B**). Additionally, the Rif2-F8S mutant also showed no inhibition *in vitro*, consistent with genetic observations (**Fig. S3A**) (Kaizer et al., 2015). We carried out several control experiments to test the integrity of the F8A mutant. First, Rif2 shows a weak DNA binding activity; this activity is unaltered in the mutant (**Fig. S3B**). Second, the interaction between Rad50 and Rif2 is not affected by the F8A mutation (**Fig. 2C**). Furthermore, both the Rad50-Rif2 and Rad50-Rif2F8A interactions are unaffected by the presence of Mg-ATP in the assay (**Fig. S2**). Therefore, the interaction between Rif2 and Rad50 alone is not sufficient to mediate inhibition.

We next queried whether the entire Rif2 protein is required for inhibition. In yeast, the artificial tethering of Rif2(1-170) to telomeres *via* Tet-operator sites restored the regulatory function to a *rif2D* mutant (Hirano et al., 2009). In an independent study, fusion of Rif2(1-60) to Rap1, which ensures telomere localization by artificial means, similarly restored telomere length control to the *rif2D* mutant (Kaizer et al., 2015). In our *in vitro* assay, the GST-Rif2(1-170) truncation showed comparable inhibition to full-length GST-Rif2 **(Fig. 3C**, lanes 4,5), whereas the GST-Rif2(1-60) truncation showed low but measurable inhibition (50%, lane 6). The weaker

inhibitory activity of Rif2(1-60) compared to Rif2(1-170) and full-length Rif2 is consistent with the decreased interaction between Rif2(1-60) with Rad50 (**Fig. 2C**, compare lane 8 with 6,7). The extreme N-terminal location of the essential Phe might suggest that its mode of action requires insertion of the N-terminal peptide into a hydrophobic cavity. However, in control experiments, we show that the presence of the N-terminal GST-domain did not interfere with the function of Rif2 (Fig. 3C, **Fig. S3C,D**).

Finally, we tested whether the inhibitory function of Rif2 requires both MRX and DNA, even though the DNA-stimulated Tel1 kinase activity is not inhibited by Rif2 (**Fig. S1B**). One proposed model for the regulatory role of Rif2 is that Rif2 changes the DNA end-tethering properties of MRX (Cassani et al., 2016). This model can be tested because MRX stimulates the kinase activity of Tel1 2-3 fold in the absence of DNA (**Fig. 1B**) (Hailemariam et al., 2019). Rif2 or Rif2-F8A were added to standard Tel1 kinase reactions containing MRX but no DNA. Rif2 inhibited the MRX-dependent stimulation of Tel1 while the mutant was ineffective (Fig. 3D). Interestingly, the Tel1-catalyzed phosphorylation of Mre11 and Xrs2 is not affected by Rif2. This result is consistent with our previous observation that the phosphorylation of these two subunits is largely constitutive, i.e. is not stimulated by the presence of DNA (Hailemariam et al., 2019).

Rif2 stimulates the ATPase activity of MRX

We have recently shown that Rad50, along with DNA, is absolutely required for MRX to fully activate Tel1 (Hailemariam et al., 2019). Rad50 protein exists as a dimer and shares structural and functional similarities to proteins belonging to structural maintenance of chromosomes (SMC) family. Mutations that disrupt zinc hook mediated dimerization of Rad50 lead to defects in DNA repair (Hopfner et al., 2002). However, Rif2-WT does not function through the disruption of Rad50 dimer. We observed no difference in migration on a native acrylamide gel between Rad50 dimer and Rad50 dimer incubated with Rif2 (**Fig.S4A**). Several studies have shown that the ATP-dependent activities of Rad50 are required for all of its functions in checkpoint activation and DNA repair, as ATP-binding mutants are phenotypically similar to *rad50D* (Chen et al., 2005; Hailemariam et al., 2019). This knowledge raises the possibility that Rif2 acts by modulating the ATPase activity of MRX and in fact, in one study, Rif2 was shown to stimulate the ATPase activity of MRX by about two-fold (Cassani et al.,

2016). Our own assessment of the role of Rif2 on the MRX ATPase activity recapitulates this observation and extends it. Rif2 stimulated the ATPase activity of MRX either in the absence (**Fig. S4C**) or the presence of DNA (**Fig. 4A**). In contrast, Rif2-F8A showed no detectable stimulation of the MRX ATPase (**Fig. 4A, Fig. S4C**). Considering that none of the other activities of Rif2 is altered in the F8A mutant (DNA binding, interaction with Rad50), the most straightforward conclusion from these data is that the increase in the ATPase of MRX is associated with loss of Tel1-specific MRX activity.

To understand how Rif2 interferes with the MRX-mediated activation of Tel1 through the Rad50 ATPase, we used an allosteric ATPase mutant of Rad50. Rad50(ΔCC48) has two point mutations (S685R, Y688R) and lacks an additional 104 amino acids of the coiled-coiled domain near the zinc hook motif (**Fig. 1B**) (Hohl et al., 2015; Hohl et al., 2011; Park et al., 2017; Wiltzius et al., 2005). The *rad50-DCC48* mutant is defective for Tel1-mediated checkpoint signaling in response to DNA double-stranded breaks. In addition, the mutant has shortened telomeres (Park et al., 2017). In biochemical studies, the mutant MR(ΔCC48)X complex lacks ATPase activity. The effect of these mutations are allosteric in nature, because they are distal from the ATPase domains (Fig 1B). In support of an allosteric mechanism, the mutant MRX complex still binds ATP like wild-type (**Fig. 4B**). Studies by others have shown that ATP binding, and not its hydrolysis drives the activation of $Tel1^{ATM}$ kinase in the complex with DNA and MRX(N) (Cassani et al., 2019; Deshpande et al., 2017). Therefore, since the mutant complex still binds ATP, the observation that it activates Tel1 like wild-type was to be expected (**Fig. 4C**, lanes 1 and 4). However, the observed inhibition by Rif2 is surprising, since MR(ΔCC-48)X shows little or no ATPase activity. Remarkably, we found that Rif2, but not Rif2-F8A, caused a potent stimulation of the mutant's ATPase activity (**Fig. 4D**). Like observed with wild-type MRX, the stimulation of ATPase activity in MR(ΔCC48)X does not require the presence of effector DNA(**Fig. S4B, D**).

A new model for Rif2 mediated regulation of Tel1 kinase

The Rad50(ΔCC48) mutant has given us an unique window into observing the regulatory function of Rif2. The ATPase of wild-type MRX is stimulated about two-fold by either DNA or Rif2, and when both are present, the activity is additive. In sharp contrast, the mutant complex shows marginal ATPase activity, which is not stimulated by DNA (**Fig. S4E, F**). However, its

ATPase is greatly stimulated by Rif2, regardless whether DNA is present. These data indicate that the structural changes that occur in MRX when the bound ATP hydrolyzes are principally different whether DNA or Rif2 is the effector molecule. However, the effects of Rif2 on Tel1's activity can also be observed in the absence of DNA for both wild-type MRX and MR(ΔCC48)X (**Fig. 3D, Fig. S4B**). One possible explanation is that the association of MRX with Tel1 is disrupted by Rif2, but not by Rif2-F8A. However, this was not observed (data not shown). Taking these observations together, it is plausible that MRX incorporates both ATP binding and ATP hydrolysis activities for signaling and Tel1 stimulation. Signature motif mutants of Rad50 that prevent formation of the ATP-bound 'closed' state but are defective in homology repair support this thinking (Frank et al., 2006). Further studies are required to decipher the exact role of ATP hydrolysis by MRX, and how MRX interacts with DNA in ATP-bound state.

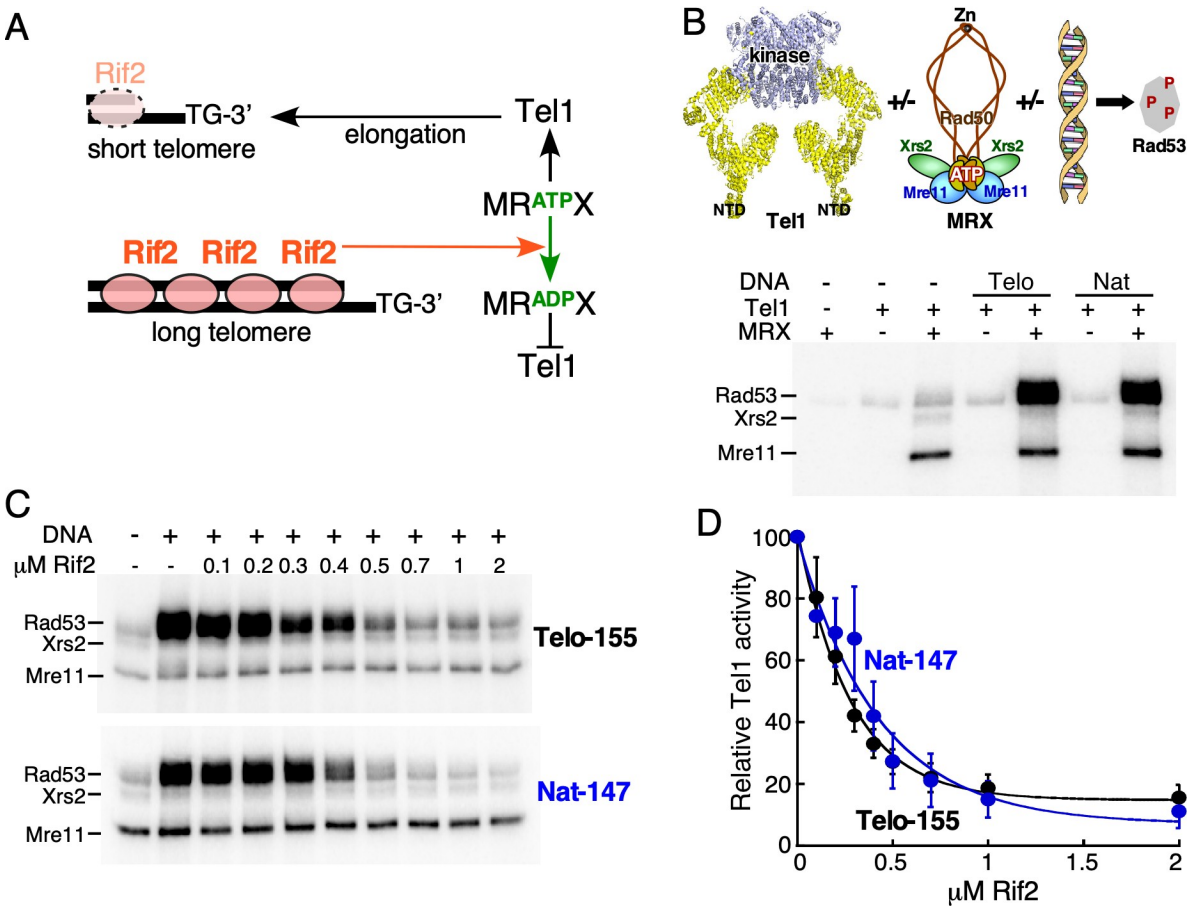

Figure 1. Rif2 inhibits MRX-dependent activation of Tel1 kinase.
A. Simplified model for the regulatory activity of Rif2. Note that localization of Rif2 to telomers requires interaction with Rap1 (not shown). B. Top, schematic representation of in vitro kinase assay using purified proteins. The mutations in Rad50(DCC48) are near the Zn binding site. Bottom, Standard kinase reactions (Materials and Methods) contained the indicated factors, and either 10nM Telo-155 or Nat-147 DNA where indicated. C. Standard kinase reaction with MRX, and either 10 nM Telo-155 or Nat-147 DNA, contained the indicated concentrations of Rif2. D, Quantification of four independent replicates of the assay shown in C. Relative Tel1 activity of the reaction without Rif2 was set to 100 (lane 2). Averages and standard errors are shown.

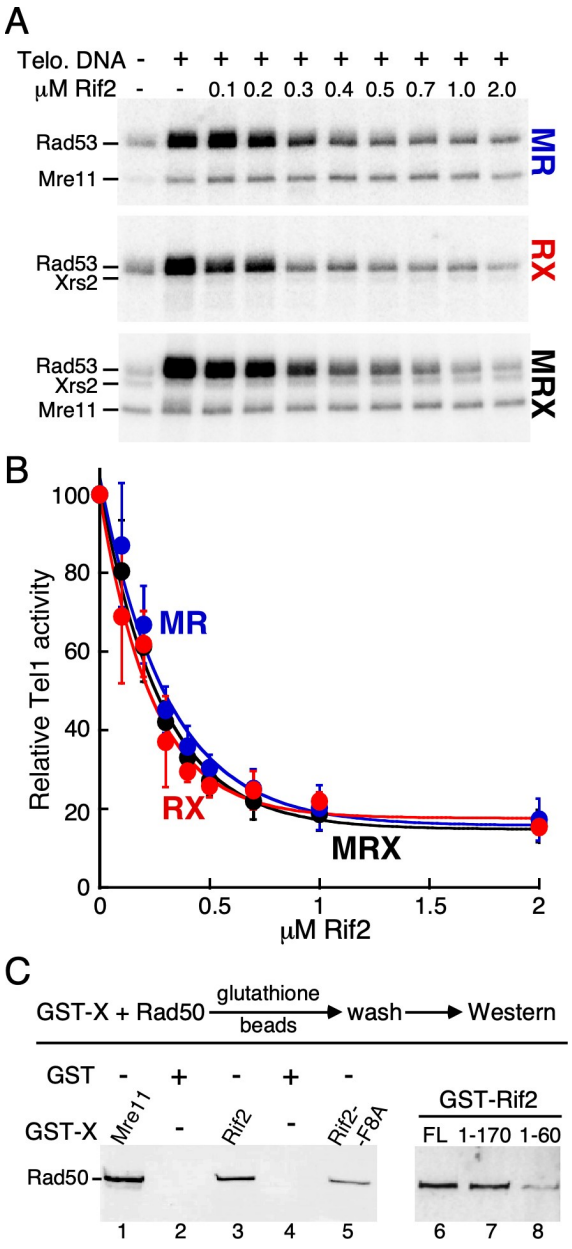

Figure 2. The Xrs2 subunit of MRX is dispensable for Rif2's inhibitory activity in vitro. *A*, standard kinase reaction with increasing concentrations of Rif2, and 30 nM of either MR, RX, or MRX complex. A representative experiment is shown. *B*, Quantification of three independent experiments with standard errors. The reaction without Rif2 (lane 2) was set to 100. *C*, Purified Rad50 subunit was incubated with either GST-tagged Mre11, Rif2-WT, Rif2-F8A, Rif2(1-170), or Rif2(1-60). The beads were washed and bound Rad50 was analyzed by 7% SDS-PAGE, followed by western blotting with anti-Rad50 antibody, exactly as described (Hailemariam et al., 2019). GST (lanes 2,4) was used as a negative control.

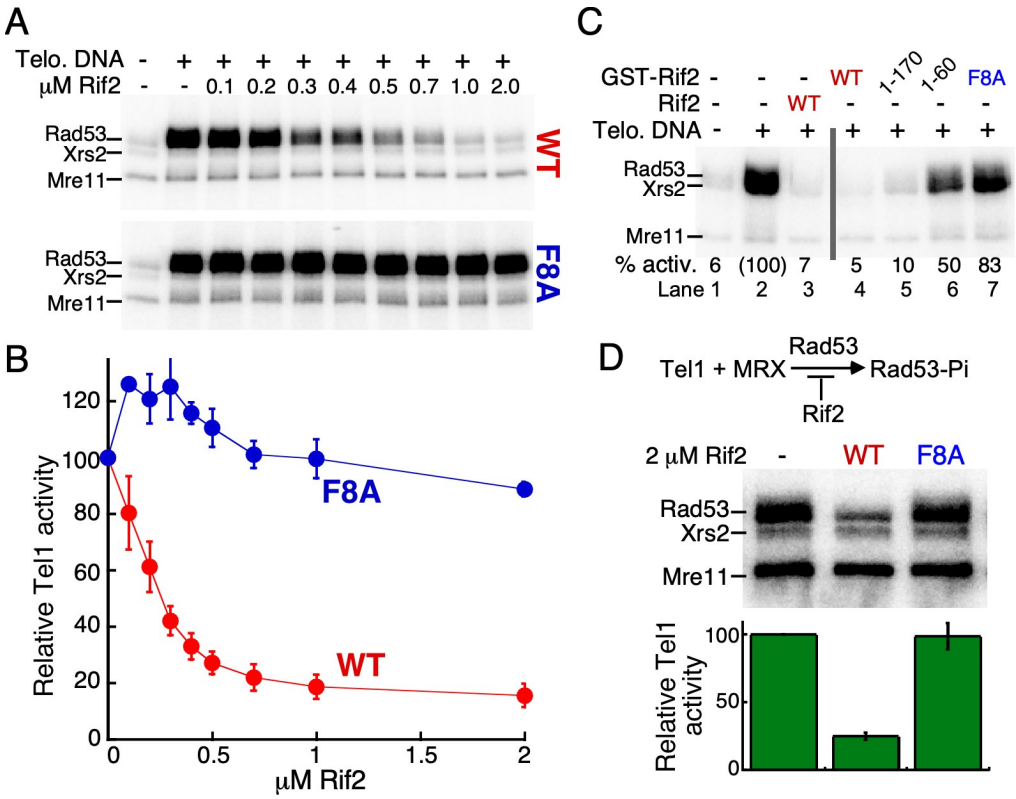

Figure 3. The N-terminal region of Rif2 is important for its inhibitory role.
A, standard kinase reaction with increasing concentrations of either Rif2-WT or Rif2-F8A. A representative experiment is shown. *B*, Quantification of three independent experiments with standard errors. Relative Tel1 activity of the reaction without Rif2 was set to 100 (lane 2). *C*, Standard kinase assays contained 2 mM of the indicated Rif2 or GST-Rif2 variants. *D,* Standard kinase assays were carried out without DNA and Rif2 as indicated. Reactions were incubated for 30 minutes. Bottom, averages and standard errors are derived from three independent experiments. The reaction without Rif2 (lane 1) was set to 100.

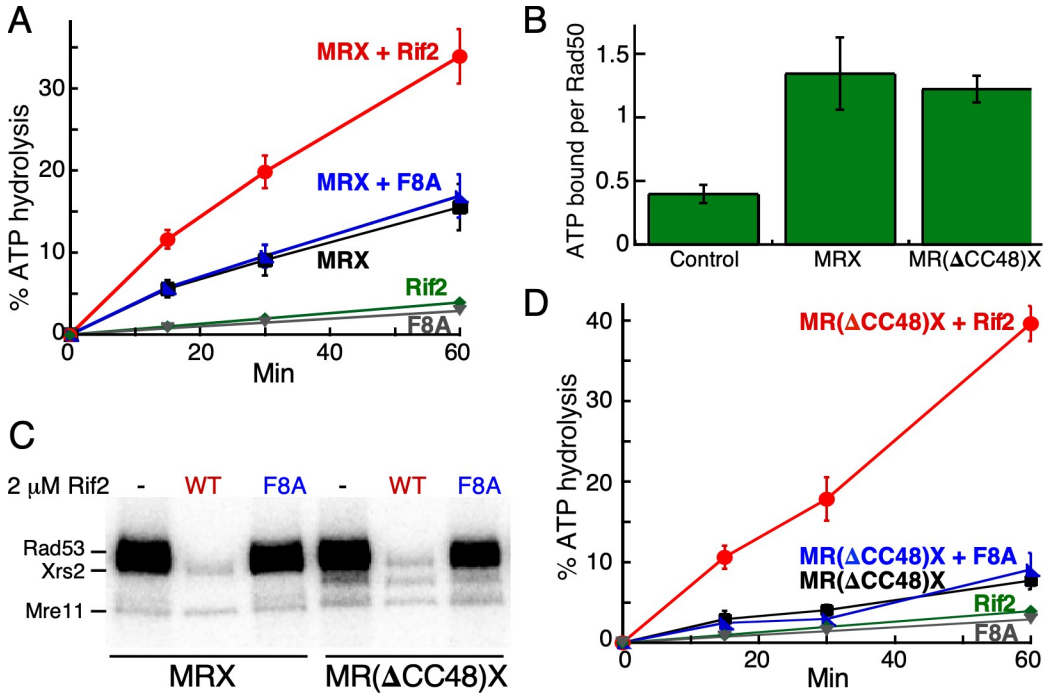

Figure 4. Rif2 stimulates the ATPase activity of MRX.
A, Standard ATPase assays with DNA and wild-type MRX contained either no Rif2 (black) 2 mM Rif2 (red) or Rif2-F8A (blue). Negative controls contained 2 mM Rif2 (green) or Rif2-F8A) (gray, but no MRX. B, nitrocellulose filter binding assays of [g-^{32}P]-ATP to wild-type or mutant MRX, as described (Hailemariam et al., 2019). Control, no MRX. Quantification of three independent experiments with standard errors is shown. C, Tel1 kinase assays with 30 nM MRX or M(Rad50*ΔCC-48)X and 2* μM Rif2 or Rif2-F8A as indicated. D, ATPase reactions as in A, but with M(Rad50ΔCC-48)X. The green Rif2 and gray Rif2-F8A curves, minus MRX, are from the same data set as shown in A.

References

Armanios, M., and Blackburn, E.H. (2012). The telomere syndromes. Nature reviews Genetics *13*, 693-704.

Bianchi, A., and Shore, D. (2008). How telomerase reaches its end: mechanism of telomerase regulation by the telomeric complex. Molecular cell *31*, 153-165.

Carney, J.P., Maser, R.S., Olivares, H., Davis, E.M., Le Beau, M., Yates, J.R., 3rd, Hays, L., Morgan, W.F., and Petrini, J.H. (1998). The hMre11/hRad50 protein complex and Nijmegen breakage syndrome: linkage of double-strand break repair to the cellular DNA damage response. Cell *93*, 477-486.

Cassani, C., Gobbini, E., Wang, W., Niu, H., Clerici, M., Sung, P., and Longhese, M.P. (2016). Tel1 and Rif2 Regulate MRX Functions in End-Tethering and Repair of DNA Double-Strand Breaks. PLoS biology *14*, e1002387.

Cassani, C., Vertemara, J., Bassani, M., Marsella, A., Tisi, R., Zampella, G., and Longhese, M.P. (2019). The ATP-bound conformation of the Mre11-Rad50 complex is essential for Tel1/ATM activation. Nucleic Acids Res.

Chang, M., Arneric, M., and Lingner, J. (2007). Telomerase repeat addition processivity is increased at critically short telomeres in a Tel1-dependent manner in Saccharomyces cerevisiae. Genes & development *21*, 2485-2494.

Chen, L., Trujillo, K.M., Van Komen, S., Roh, D.H., Krejci, L., Lewis, L.K., Resnick, M.A., Sung, P., and Tomkinson, A.E. (2005). Effect of amino acid substitutions in the rad50 ATP binding domain on DNA double strand break repair in yeast. The Journal of biological chemistry *280*, 2620-2627.

d'Adda di Fagagna, F., Reaper, P.M., Clay-Farrace, L., Fiegler, H., Carr, P., Von Zglinicki, T., Saretzki, G., Carter, N.P., and Jackson, S.P. (2003). A DNA damage checkpoint response in telomere-initiated senescence. Nature *426*, 194-198.

Deshpande, R.A., Lee, J.H., and Paull, T.T. (2017). Rad50 ATPase activity is regulated by DNA ends and requires coordination of both active sites. Nucleic Acids Res *45*, 5255-5268.

Difilippantonio, S., Celeste, A., Kruhlak, M.J., Lee, Y., Difilippantonio, M.J., Feigenbaum, L., Jackson, S.P., McKinnon, P.J., and Nussenzweig, A. (2007). Distinct domains in Nbs1 regulate irradiation-induced checkpoints and apoptosis. The Journal of experimental medicine *204*, 1003-1011.

Frank, C.J., Hyde, M., and Greider, C.W. (2006). Regulation of telomere elongation by the cyclin-dependent kinase CDK1. Molecular cell *24*, 423-432.

Gao, H., Cervantes, R.B., Mandell, E.K., Otero, J.H., and Lundblad, V. (2007). RPA-like proteins mediate yeast telomere function. Nature structural & molecular biology *14*, 208-214.

Gilson, E., Roberge, M., Giraldo, R., Rhodes, D., and Gasser, S.M. (1993). Distortion of the DNA double helix by RAP1 at silencers and multiple telomeric binding sites. Journal of molecular biology *231*, 293-310.

Gomes, N.M., Shay, J.W., and Wright, W.E. (2010). Telomere biology in Metazoa. FEBS letters *584*, 3741-3751.

Grandin, N., Reed, S.I., and Charbonneau, M. (1997). Stn1, a new Saccharomyces cerevisiae protein, is implicated in telomere size regulation in association with Cdc13. Genes & development *11*, 512-527.

Greenwell, P.W., Kronmal, S.L., Porter, S.E., Gassenhuber, J., Obermaier, B., and Petes, T.D. (1995). TEL1, a gene involved in controlling telomere length in S. cerevisiae, is homologous to the human ataxia telangiectasia gene. Cell *82*, 823-829.
Greider, C.W., and Blackburn, E.H. (1985). Identification of a specific telomere terminal transferase activity in Tetrahymena extracts. Cell *43*, 405-413.
Hailemariam, S., Kumar, S., and Burgers, P.M. (2019). Activation of Tel1(ATM) kinase requires Rad50 ATPase and long nucleosome-free DNA but no DNA ends. The Journal of biological chemistry *294*, 10120-10130.
Hardy, C.F., Sussel, L., and Shore, D. (1992). A RAP1-interacting protein involved in transcriptional silencing and telomere length regulation. Genes & development *6*, 801-814.
Hector, R.E., Shtofman, R.L., Ray, A., Chen, B.R., Nyun, T., Berkner, K.L., and Runge, K.W. (2007). Tel1p preferentially associates with short telomeres to stimulate their elongation. Molecular cell *27*, 851-858.
Hirano, Y., Fukunaga, K., and Sugimoto, K. (2009). Rif1 and rif2 inhibit localization of tel1 to DNA ends. Molecular cell *33*, 312-322.
Hohl, M., Kochanczyk, T., Tous, C., Aguilera, A., Krezel, A., and Petrini, J.H. (2015). Interdependence of the rad50 hook and globular domain functions. Molecular cell *57*, 479-491.
Hohl, M., Kwon, Y., Galvan, S.M., Xue, X., Tous, C., Aguilera, A., Sung, P., and Petrini, J.H. (2011). The Rad50 coiled-coil domain is indispensable for Mre11 complex functions. Nature structural & molecular biology *18*, 1124-1131.
Hopfner, K.P., Craig, L., Moncalian, G., Zinkel, R.A., Usui, T., Owen, B.A., Karcher, A., Henderson, B., Bodmer, J.L., McMurray, C.T.*, et al.* (2002). The Rad50 zinc-hook is a structure joining Mre11 complexes in DNA recombination and repair. Nature *418*, 562-566.
Kaizer, H., Connelly, C.J., Bettridge, K., Viggiani, C., and Greider, C.W. (2015). Regulation of Telomere Length Requires a Conserved N-Terminal Domain of Rif2 in Saccharomyces cerevisiae. Genetics *201*, 573-586.
Kim, N.W., Piatyszek, M.A., Prowse, K.R., Harley, C.B., West, M.D., Ho, P.L., Coviello, G.M., Wright, W.E., Weinrich, S.L., and Shay, J.W. (1994). Specific association of human telomerase activity with immortal cells and cancer. Science (New York, NY) *266*, 2011-2015.
Levy, D.L., and Blackburn, E.H. (2004). Counting of Rif1p and Rif2p on Saccharomyces cerevisiae telomeres regulates telomere length. Molecular and cellular biology *24*, 10857-10867.
Longtine, M.S., Wilson, N.M., Petracek, M.E., and Berman, J. (1989). A yeast telomere binding activity binds to two related telomere sequence motifs and is indistinguishable from RAP1. Current genetics *16*, 225-239.
Mallory, J.C., and Petes, T.D. (2000). Protein kinase activity of Tel1p and Mec1p, two Saccharomyces cerevisiae proteins related to the human ATM protein kinase. Proceedings of the National Academy of Sciences of the United States of America *97*, 13749-13754.
Marcand, S., Gilson, E., and Shore, D. (1997). A protein-counting mechanism for telomere length regulation in yeast. Science (New York, NY) *275*, 986-990.
Nakada, D., Matsumoto, K., and Sugimoto, K. (2003). ATM-related Tel1 associates with double-strand breaks through an Xrs2-dependent mechanism. Genes & development *17*, 1957-1962.

Oh, J., and Symington, L.S. (2018). Role of the Mre11 Complex in Preserving Genome Integrity. Genes *9*.
Palm, W., and de Lange, T. (2008). How shelterin protects mammalian telomeres. Annual review of genetics *42*, 301-334.
Park, Y.B., Hohl, M., Padjasek, M., Jeong, E., Jin, K.S., Krezel, A., Petrini, J.H., and Cho, Y. (2017). Eukaryotic Rad50 functions as a rod-shaped dimer. Nature structural & molecular biology *24*, 248-257.
Paull, T.T. (2018). 20 Years of Mre11 Biology: No End in Sight. Molecular cell *71*, 419-427.
Ritchie, K.B., and Petes, T.D. (2000). The Mre11p/Rad50p/Xrs2p complex and the Tel1p function in a single pathway for telomere maintenance in yeast. Genetics *155*, 475-479.
Sabourin, M., Tuzon, C.T., and Zakian, V.A. (2007). Telomerase and Tel1p preferentially associate with short telomeres in S. cerevisiae. Molecular cell *27*, 550-561.
Shi, T., Bunker, R.D., Mattarocci, S., Ribeyre, C., Faty, M., Gut, H., Scrima, A., Rass, U., Rubin, S.M., Shore, D.*, et al.* (2013). Rif1 and Rif2 shape telomere function and architecture through multivalent Rap1 interactions. Cell *153*, 1340-1353.
Smogorzewska, A., and de Lange, T. (2004). Regulation of telomerase by telomeric proteins. Annual review of biochemistry *73*, 177-208.
Usui, T., Ogawa, H., and Petrini, J.H. (2001). A DNA damage response pathway controlled by Tel1 and the Mre11 complex. Molecular cell *7*, 1255-1266.
Usui, T., Ohta, T., Oshiumi, H., Tomizawa, J., Ogawa, H., and Ogawa, T. (1998). Complex formation and functional versatility of Mre11 of budding yeast in recombination. Cell *95*, 705-716.
Viscardi, V., Bonetti, D., Cartagena-Lirola, H., Lucchini, G., and Longhese, M.P. (2007). MRX-dependent DNA damage response to short telomeres. Molecular biology of the cell *18*, 3047-3058.
Wellinger, R.J., and Zakian, V.A. (2012). Everything you ever wanted to know about Saccharomyces cerevisiae telomeres: beginning to end. Genetics *191*, 1073-1105.
Wiltzius, J.J., Hohl, M., Fleming, J.C., and Petrini, J.H. (2005). The Rad50 hook domain is a critical determinant of Mre11 complex functions. Nature structural & molecular biology *12*, 403-407.
Wotton, D., and Shore, D. (1997). A novel Rap1p-interacting factor, Rif2p, cooperates with Rif1p to regulate telomere length in Saccharomyces cerevisiae. Genes & development *11*, 748-760.
Wright, J.H., Gottschling, D.E., and Zakian, V.A. (1992). Saccharomyces telomeres assume a non-nucleosomal chromatin structure. Genes & development *6*, 197-210.
You, Z., Chahwan, C., Bailis, J., Hunter, T., and Russell, P. (2005). ATM activation and its recruitment to damaged DNA require binding to the C terminus of Nbs1. Molecular and cellular biology *25*, 5363-5379.

Supplemental information to:

Opposing roles of Rad50 ATPase and Rif2 in the activation of Tel1^{ATM} kinase

Sarem Hailemariam[1], Paolo De Bona[1], Marcel Hohl[2], John Petrini[2], Roberto Galletto[1], and Peter Burgers[1]

[1]Department of Biochemistry and Molecular Biophysics, Washington University in St. Louis; St. Louis, MO 63110; [2]Molecular Biology Program, Memorial Sloan-Kettering Cancer Center, Molecular Biology Program, New York, NY 10021

*Corresponding author: TEL (314) 362-3772; FAX (314) 362-7183; burgers@wustl.edu

Running title: Rif2 inactivates the ATP form of MRX

DNA Substrates

The DNA substrates used were a linearized 2 kb DNA (by BamHI), derived from plasmid pUC19, a 147-mer natural DNA sequence (Nat), derived from the Widom 601 sequence(1). The 155-mer yeast telomeric repeat sequence (Telo) was derived from the left arm of Chromosome 4. The TG(1-3) repeats (Telo) account for 155 base pairs. Terminal AflII restriction sites were used for cloning in pUC19 and subsequent cleavage.

Protein Expression and purification

Tel1, MRX and MRX subcomplexes, and Rad53-kd were purified as described (2). The MR(DCC48)X mutant complex was purified as described(3). Rap full-length and Rap1 (1-622) were purified as described (4).

The Rif2 wild-type gene was cloned in pGEX-6p-1 vector at EcoRI/XhoI restriction sites and overexpressed in Rosetta2(DE3)-pLysS as described for Rap1 (4). GST-Rif2 overexpression cells were lysed by sonication in lysis buffer (50 mM sodium phosphate buffer (pH7.3), 400 mM sodium chloride, 10% glycerol, 1 mM EDTA, 1mM DTT and 0.1 mM PMSF). Cells debris was spun down, and 0.2% polyethyleneimine was added to the supernatant. After centrifugation the supernatant was incubated overnight with glutathione-Sepharose 4 Fast Flow resin (GE Healthcare). The resin was then extensively washed with lysis buffer and lysis buffer containing 1M sodium chloride. GST-Rif2 was finally eluted with 25 mM reduced glutathione in lysis buffer and dialyzed overnight against heparin buffer (25 mM Tris buffer (pH7.4), 150 mM NaCl, 10% glycerol, 1 mM EDTA and 1 mM DTT). The dialyzed protein was loaded on a Poros 50 HE

Heparin column (Life Technologies, Inc.) and eluted with heparin buffer containing 300 mM NaCl. Rif2 wild-type was purified using the same protocol, except that PreScission Protease was added during dialysis against heparin buffer. Rif2F8A and Rif2F8S were generated by standard site-specific mutagenesis using the Rif2 gene cloned in the pGEX6p-1 vector as template. Rif2F8A, GST-Rif2F8A, Rif2F8S and GST-Rif2F8S were expressed and purified using the procedure reported above for the Rif2 wild-type constructs. The Rif 2 truncation construct (1-170 and 1-60) were expressed and purified similarly, except that the GST-tag was kept on the purified truncated proteins. All Rif2 proteins were dialyzed against storage buffer (20 mM HEPES (pH 7.4), 400 mM NaCl, 40% (v/v) glycerol, 0.5 mM EDTA and 1 mM DTT) and stored at -80 ^{0}C.

Tel1 kinase assay

The standard 10 ml assay contained 25 mM HEPES-NaOH pH 7.6, 80 mM NaCl, 7 mM Mg-acetate, 100 μg/ml BSA, 1 mM DTT, 50 mM ATP, 0.05 mCi [g-^{32}P]-ATP, 200 nM GST-Rad53-kd, 30 nM MRX, and 10 nM Telo. DNA. Reactions were initiated with 5 nM Tel1 at 30 ˚C for 15 min, stopped with 4 ml of 2.5xSDS-PAGE loading dye, boiled, and separated on 7 % SDS-PAGE gels. Gels were dried and exposed to a phosphor screen (GE Healthcare). Deviations from the standard assay are indicated in the legends to figures. Data were analyzed with ImageQuant software and plotted using KaleidaGraph software.

ATPase assay

Standard 20 ml ATPase reactions contained 50 μM [a-^{32}P]-ATP, 100 nM MRX, and 10 nM of linearized pUC19 DNA in buffer containing 25 mM HEPES-NaOH pH 7.6, 80 mM NaCl, 7 mM Mg-acetate, and 1 mM DTT. At indicated times at 30 ˚C, 5 ml aliquots were quenched in 1.5ul of 150 mM EDTA/1% SDS. Radioactive ATP and ADP were separated by PEI-Cellulose TLC and quantified as described in (2).

GST-pulldown and ATP-binding experiments

Pulldown experiments in Figure 2C and Figure S2, and ATP binding in Figure 4B were performed exactly as described in (2).

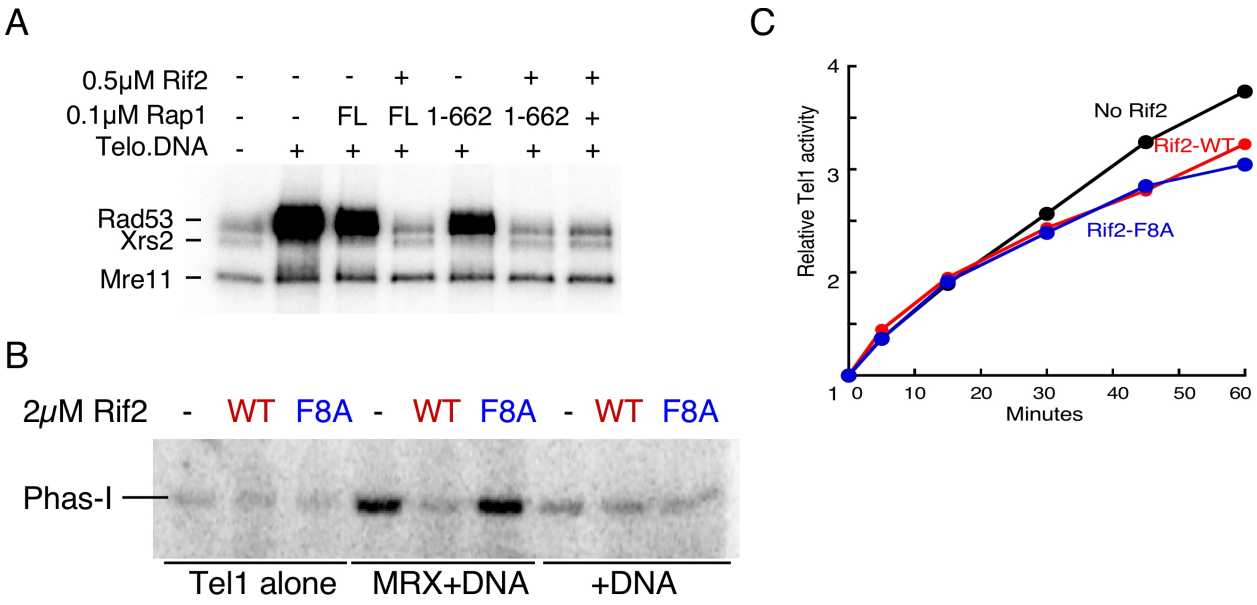

Figure S1. Related to Figure 1. *A, Rif2 inhibition is independent of Rap1*. Standard kinase assays were carried out the indicated concentrations of Rif2, and either full-length Rap1 (1-827) or Rap1 (1-662). *B, Rif2-mediated inhibition is not substrate dependent*. 1μM Phas-I was used instead of Rad53 in a standard kinase reaction. *C, Rif2 does not inhibit the catalytic activity of Tel1*. Kinase reactions contained 10 nM Telo-155 DNA, and 2μM Rif2-WT or Rif2-F8A where indicated, but no MRX. Tel1 activity is given in arbitrary units.

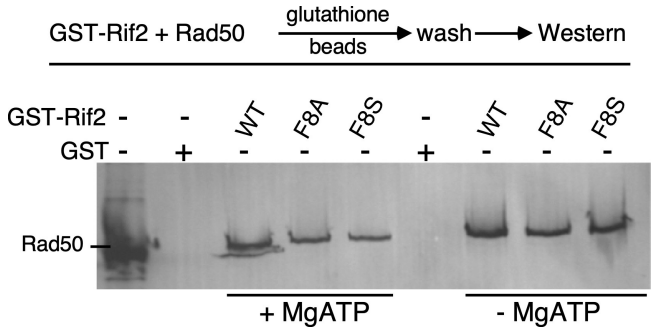

Figure S2. Related to Figure 2. *Association of Rif2-WT or Rif2-F8A with Rad50 is unaltered by the presence of Mg-ATP.* GST-tagged Rif2-WT, Rif2-F8A, and Rif2-F8S were incubated with purified Rad50 in the presence or absence of 50μM ATP and 7mM Mg-acetate. The beads were washed and bound Rad50 was analyzed by SDS-PAGE, followed by western blotting with anti-Rad50 antibody. GST negative control as indicated in lanes 2 and 6. This experiment also shows pull-down of a Rif2-F8S mutant, which showed the same properties as the F8A mutant, but has not been studied in detail.

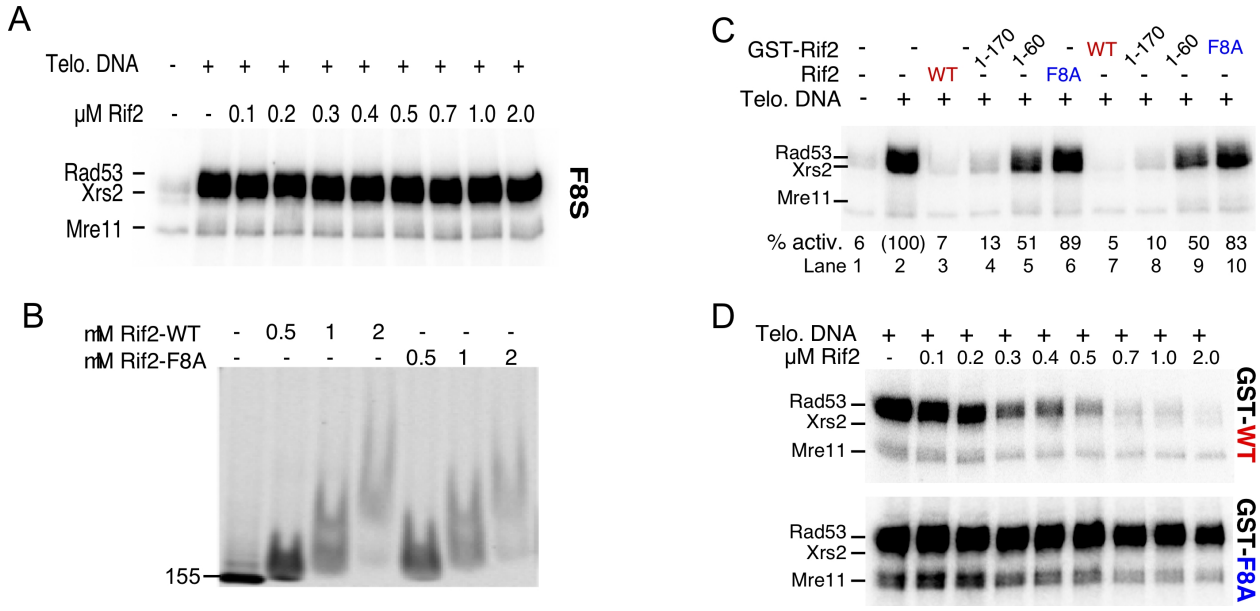

Figure S3. Related to Figure 3. *A, Rif2-F8S does not inhibit MRX-dependent activation of Tel1*. Standard kinase reactions contained the indicated concentrations of Rif2-F8S. *B, DNA binding activity is not affected by F8A mutation.* 10nM Telo-155 was incubated with the indicated concentrations of Rif2-WT or Rif2-F8A in binding buffer (50 mM Tris-HCl pH 7.4, 50 mM NaCl, 5 mM $MgCl_2$, 5% glycerol and 1 mM DTT). Protein-DNA complexes were resolved on a 1.5 % agarose gel in 0.5X TBE at 4 ^{o}C at 150V for 4 hours. The gel was stained using GelRed and the image was collected using a Typhoon phosphoimager. *C,* This is the complete gel of the data shown in Fig. 3C, with lanes 4-6 cropped out. *D, The N-terminal GST-tag does not interfere with the function of Rif2.* Standard kinase reactions contained the indicated concentrations of GST-Rif2 or GST-F8A. Compare this assay to the assay in Fig 1C, without GST tag.

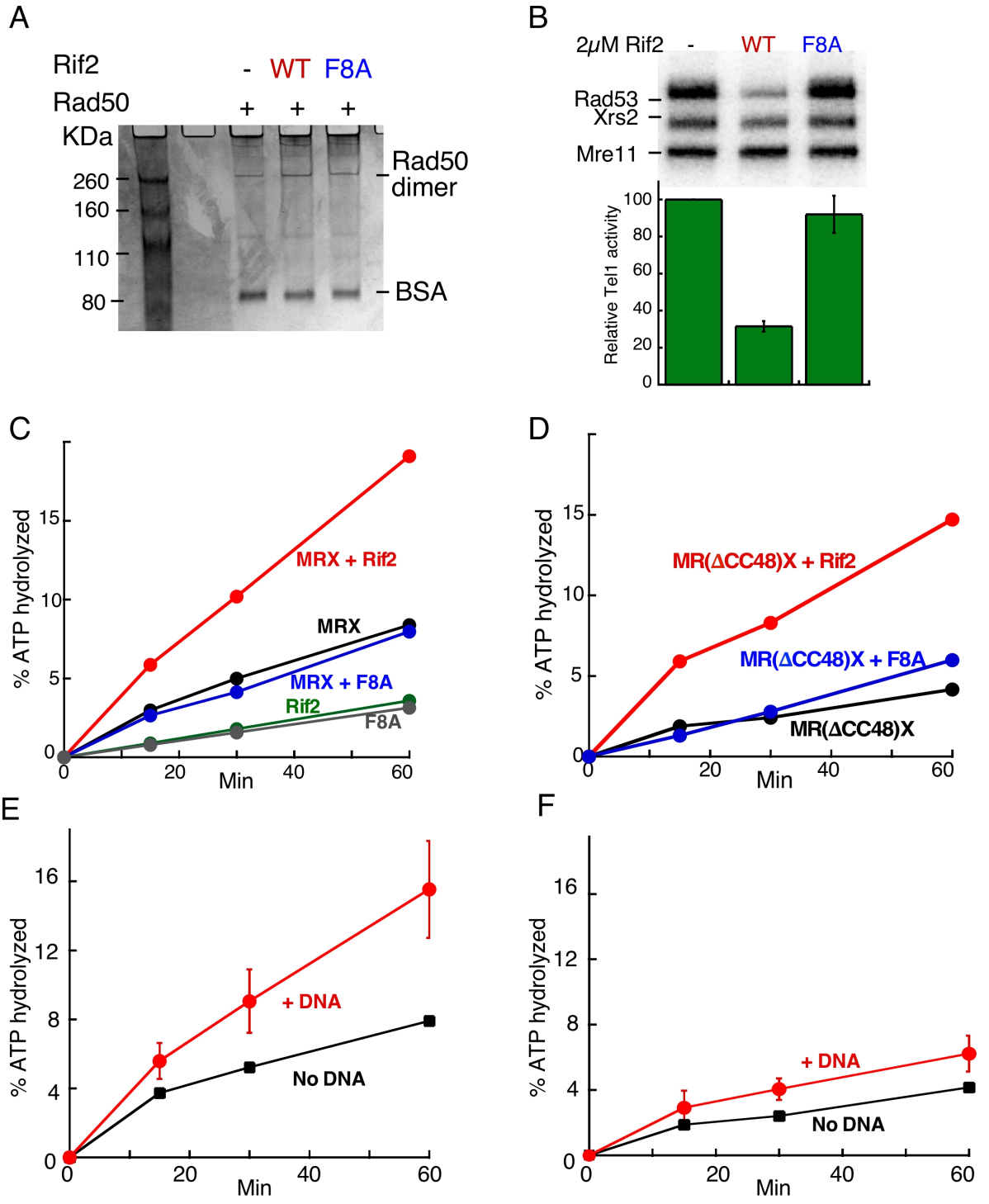

Figure S4. Related to Figure 4. *A, Rif2 does not disrupt the dimerization of Rad50 dimer.* 30nM Rad50 was incubated with 2μM Rif2-WT or Rif2-F8A under standard kinase assay conditions before loading on a native acrylamide gel. Silver staining was used to visualize results. *B, Rif2-WT inhibits DNA independent stimulation of Tel1 by M(Rad50ΔCC48)X.* Standard kinase assays were carried out without DNA and Rif2 as indicated. Reactions were incubated for 30 minutes. Bottom, averages and standard errors are derived from three independent experiments. The reaction without Rif2

(lane 1) was set to 100. *C, Rif2-WT stimulates the ATPase activity of MRX in the absence of DNA.* ATPase reactions contained MRX with either no Rif2 (black), 2μM Rif2-WT (red) or Rif2-F8A (blue), but no DNA. Negative controls were Rif2 (green) and Rif2-F8A (gray) without MRX and without DNA. *D,* as in C, but with M(Rad50ΔCC48)X. *E, DNA stimulates the ATPase activity of wild-type MRX.* Standard ATPase assays with wild-type MRX in the presence (red) or absence (black) of DNA. *F,* as in E, but with M(Rad50ΔCC48)X.

Supplemental References

1. Lowary, P. T., and Widom, J. (1998) New DNA sequence rules for high affinity binding to histone octamer and sequence-directed nucleosome positioning. *Journal of molecular biology* **276**, 19-42
2. Hailemariam, S., Kumar, S., and Burgers, P. M. (2019) Activation of Tel1(ATM) kinase requires Rad50 ATPase and long nucleosome-free DNA but no DNA ends. *The Journal of biological chemistry* **294**, 10120-10130
3. Park, Y. B., Hohl, M., Padjasek, M., Jeong, E., Jin, K. S., Krezel, A., Petrini, J. H., and Cho, Y. (2017) Eukaryotic Rad50 functions as a rod-shaped dimer. *Nature structural & molecular biology* **24**, 248-257
4. Feldmann, E. A., and Galletto, R. (2014) The DNA-binding domain of yeast Rap1 interacts with double-stranded DNA in multiple binding modes. *Biochemistry* **53**, 7471-7483

Chapter IV

Future direction

Future direction

The second chapter of this thesis discusses the coordinated regulation of Tel1 kinase by the MRX complex and double-stranded DNA. Although both of these DNA repair protein factors have been the focus of extensive genetic studies, our work offer new biochemical insight and in turn generate questions that need to be addressed. Experiments assessing the effect of DNA on the basal activity of Te1l reveal that DNA stimulates its catalytic activity 2-3 fold. These data indicate that Tel1 binds DNA efficiently in the absence of MRX. The dsDNA length requirement for stimulation of the basal activity of Tel1 is longer than that of MRX. The 80mer dsDNA substrate, which gives a significant activation of Tel1 in the presence of MRX, has no effect on its own on Tel1 basal activity (unpublished data). The linear 2kb DNA results in 2-3 fold increase in the basal activity of Tel1, suggesting Tel1 might require a larger footprint of DNA. It is also intriguing that MRX alone result in a similar stimulation of Tel1 kinase. One important question with respect to these observations is what is the oligomeric assembly of active Tel1 when it's bound either to DNA or the MRX complex. How is this assembly state different when the ternary complex with Tel1-MRX-DNA is formed? In order to address these questions and gain structural insight, we have initiated collaboration with the laboratory of Xiaodong Zhang at the Imperial College of London. Cryo-EM has been an instrumental approach in providing structural information on members of PI3 family of kinases, including both Te1l and Mec1 kinases. Although these reported reconstructions have revealed a highly conserved PI3 architecture, additional information is needed to understand how interamolecular and intermolecular interactions regulate Te1l catalytic activity (Sawicka et al., 2016; Wang et al., 2016; Xin et al., 2019) .

As discussed in Chapter II, Tel1 has a low basal kinase activity. Insights gained from Cry-EM studies of both *S. cerevisiae* and *S. pombe* have attributed this low basal activity due to an intrinsic Tel1 conformation where the activation loop is immobilized by the PRD and FATC domains, inhibiting substrate binding by encircling the substrate-binding groove (Wang et al., 2016; Xin et al., 2019). These observations suggest that Tel1 exists in an autoinhibitory state and binding to both MRX and DNA could be required for total relief of such inhibition. Several hyper-activating mutations within Tel1 have been genetically characterized and were shown to compensate for the hypersensitivity to genotoxic stress and checkpoint defects of Mec1-deficient cells. These hyper-activating mutations are condensed around and within the substrate-binding groove of Tel1 (Baldo et al., 2008). Many of these mutations are also similar to known and cancer-associated mutations in mTOR, and are presumed to alter substrate binding (Yang et al., 2017). We are in the process of biochemically characterizing these hyperactive Tel1 mutants to assess whether their hyperactivity stems from increased substrate binding and/or increased DNA binding. Biochemical data on these mutants will complement the structural data and would provide further clarity on the mechanism of activation of Te1l kinase.

Studies in *S. pombe* have shown the C-terminal region of Xrs2/Nbs1 binds to the N-terminal HEAT repeats within Tel1 (You et al., 2005). Our studies show Mre11 and Rad50 subunits interact with Tel1 independent of Xrs2, indicating an extensive Tel1-MRX interaction interface. The interaction between Tel1 and Rad50 is rather weak and it's likely that the additional interaction provided by Mre11 and Xrs2 is important for full activation of Tel1. Whether simultaneous binding by subunits of MRX to Tel1 is required for Tel1 activation remains to be investigated. Whether Mre11 and Rad50 interacting motifs within Tel1 are near the Xrs2 binding domain is also an open question.

In addition to being part of Tel1 activating complex, Mre11 and Xrs2 are also phosphorylation targets of Tel1. Unlike Rad53 the phosphorylation of Mre11 and Xrs2 is not stimulated by DNA, suggesting their phosphorylation is constitutive. *In vivo* phosphorylation of Mre11 and Xrs2/Nbs1 has been reported in mammalian, yeast, and *Xenopus* extracts (D'Amours and Jackson, 2001; Di Virgilio et al., 2009; Usui et al., 2001). The functional importance of phosphorylation of Mre11 and Xrs2 either in checkpoint activation or DNA repair in yeast is still unclear as the reported data are not in agreement (D'Amours and Jackson, 2001; Mallory et al., 2003). Our preliminary studies show only about 20% of Mre11 is phosphorylated under saturating conditions. This observation combined with the constitutive phosphorylation of Mre11suggest that hyper-phosphorylation of Mre11 could be detrimental for Tel1 activation. Hence, careful biochemical studies are required to address what the function implication of Tel1-mediated phosphorylation of Mre11 is, and also how Tel1 activity is altered when this phosphorylation is abrogated.

The third chapter discusses the role of Rif2 on MRX-dependent activation of Tel1. There have been numerous genetic data suggesting Rif2 acts through the MRX-Tel1 pathway to regulate telomere length. Our data provide the first biochemical evidence that Rif2 directly inhibits MRX-mediated stimulation of Tel1. This inhibition proceeds through the Rad50 subunit, and more particularly through the modulation of its ATPase activity. The inhibitory role of Rif2 does not rely on DNA as Rif2 interferes with DNA-independent activation of Tel1 by MRX. However, it is still possible that Rif2 attenuates MRX-Tel1 activity by altering the DNA binding properties of MRX. Testing this possibility would provide a clearer mechanistic framework of Rif2 function. Structural and mutational studies have identified Arginine residues in Rad50 that mediate the transitions from open to closed confirmation (Deshpande et al., 2014; Williams et

al., 2011). The presence of such residues suggests that Rad50 ATP binding cavities can be controlled by small molecules or peptides. It also raises the question of whether Rif2 acts as a switch. The observation that peptides designed after the first 30 amino acids do not result in MRX-Tel1 inhibition would argue against this possibility (data not shown). Rad50 coiled-coil domains also have a direct impact on Rad50 ATPase. Results from MR(ΔCC48)X indicate that the 104 amino acids may not be important for Rad50-Rif2 interaction. Mapping the region within Rad50 that is important for Rif2 interaction would give additional insight into how Rif2 exerts its ATPase stimulatory role.

ATP-dependent activities of Rad50 are essential for all MRX functions in DNA repair and signaling (Chen et al., 2005). The observation that both DNA and Rif2 individually stimulate the ATPase activity of Rad50 raises the possibility that the elevated ATP hydrolysis stemming from Rif2 could be functionally distinct from DNA-mediated hydrolysis. Structural and biochemical studies have suggested MRX has the ability to simultaneously control what appears to be opposing functions in DSB repair. Its role in DNA end birding and DNA end resection is a good example. Thus, it is possible that interacting partners such as Rif2 might modulate the ATP binding and/or ATP hydrolysis rates by MRX to administer pathway effects. In fact, Mre11 nuclease activity is required for *de novo* telomere addition, suggesting Rif2-induced MRX ATPase activity is conducive for telomere maintenance (Frank et al., 2006). However, this scenario does not rule out that MRX may engage both its ATP binding and ATP hydrolysis activities to stimulate Tel1 and that the two state model of open and closed conformation is too simplistic.

Reference:

Baldo, V., Testoni, V., Lucchini, G., and Longhese, M.P. (2008). Dominant TEL1-hy mutations compensate for Mec1 lack of functions in the DNA damage response. Molecular and cellular biology *28*, 358-375.

Chen, L., Trujillo, K.M., Van Komen, S., Roh, D.H., Krejci, L., Lewis, L.K., Resnick, M.A., Sung, P., and Tomkinson, A.E. (2005). Effect of amino acid substitutions in the rad50 ATP binding domain on DNA double strand break repair in yeast. The Journal of biological chemistry *280*, 2620-2627.

D'Amours, D., and Jackson, S.P. (2001). The yeast Xrs2 complex functions in S phase checkpoint regulation. Genes & development *15*, 2238-2249.

Deshpande, R.A., Williams, G.J., Limbo, O., Williams, R.S., Kuhnlein, J., Lee, J.H., Classen, S., Guenther, G., Russell, P., Tainer, J.A.*, et al.* (2014). ATP-driven Rad50 conformations regulate DNA tethering, end resection, and ATM checkpoint signaling. The EMBO journal *33*, 482-500.

Di Virgilio, M., Ying, C.Y., and Gautier, J. (2009). PIKK-dependent phosphorylation of Mre11 induces MRN complex inactivation by disassembly from chromatin. DNA repair *8*, 1311-1320.

Frank, C.J., Hyde, M., and Greider, C.W. (2006). Regulation of telomere elongation by the cyclin-dependent kinase CDK1. Molecular cell *24*, 423-432.

Mallory, J.C., Bashkirov, V.I., Trujillo, K.M., Solinger, J.A., Dominska, M., Sung, P., Heyer, W.D., and Petes, T.D. (2003). Amino acid changes in Xrs2p, Dun1p, and Rfa2p that remove the preferred targets of the ATM family of protein kinases do not affect DNA repair or telomere length in Saccharomyces cerevisiae. DNA repair *2*, 1041-1064.

Sawicka, M., Wanrooij, P.H., Darbari, V.C., Tannous, E., Hailemariam, S., Bose, D., Makarova, A.V., Burgers, P.M., and Zhang, X. (2016). The Dimeric Architecture of Checkpoint Kinases Mec1ATR and Tel1ATM Reveal a Common Structural Organization. The Journal of biological chemistry *291*, 13436-13447.

Usui, T., Ogawa, H., and Petrini, J.H. (2001). A DNA damage response pathway controlled by Tel1 and the Mre11 complex. Molecular cell *7*, 1255-1266.

Wang, X., Chu, H., Lv, M., Zhang, Z., Qiu, S., Liu, H., Shen, X., Wang, W., and Cai, G. (2016). Structure of the intact ATM/Tel1 kinase. Nature communications *7*, 11655.

Williams, G.J., Williams, R.S., Williams, J.S., Moncalian, G., Arvai, A.S., Limbo, O., Guenther, G., SilDas, S., Hammel, M., Russell, P.*, et al.* (2011). ABC ATPase signature helices in Rad50 link nucleotide state to Mre11 interface for DNA repair. Nature structural & molecular biology *18*, 423-431.

Xin, J., Xu, Z., Wang, X., Tian, Y., Zhang, Z., and Cai, G. (2019). Structural basis of allosteric regulation of Tel1/ATM kinase. Cell research.

Yang, H., Jiang, X., Li, B., Yang, H.J., Miller, M., Yang, A., Dhar, A., and Pavletich, N.P. (2017). Mechanisms of mTORC1 activation by RHEB and inhibition by PRAS40. Nature *552*, 368-373.

You, Z., Chahwan, C., Bailis, J., Hunter, T., and Russell, P. (2005). ATM activation and its recruitment to damaged DNA require binding to the C terminus of Nbs1. Molecular and cellular biology *25*, 5363-5379.

APPENDIX
Structural Organization of Te1l Kinase

PREFACE TO THE APPENDIX

The large size of Tel1 and other PI3K kinases has made structural studies difficult. The work described in Appendix A and B highlights our effort to gain structural insight into Tel1 kinase. This work is done in collaboration with laboratory of Xiaodong Zhang at the Imperial College of London. EM and Cryo-EM reconstitutions have revealed that Tel1 kinase exists as a dimer. The kinase and FATC domains are important to mediate an interaction between two Tel1 monomers. This work provided insight into how intrinsic conformation of Tel1 may contribute to its low basal kinase activity, suggesting Tel1 exists in an autoinhibitory state and binding to either MRX or DNA or both could be required for total relief of such inhibition. My contribution to this work was in purifying Tel1 kinase and editing the manuscripts.

THE JOURNAL OF BIOLOGICAL CHEMISTRY VOL. 291, NO. 26, pp. 13436–13447, June 24, 2016

The Dimeric Architecture of Checkpoint Kinases Mec1^{ATR} and Tel1^{ATM} Reveal a Common Structural Organization*

Received for publication, December 3, 2015, and in revised form, April 27, 2016 Published, JBC Papers in Press, April 28, 2016, DOI 10.1074/jbc.M115.708263

Marta Sawicka[‡1,2], Paulina H. Wanrooij[§1,3], Vidya C. Darbari[‡1], Elias Tannous[§], Sarem Hailemariam[§], Daniel Bose[‡4], Alena V. Makarova[§], Peter M. Burgers[§5], and Xiaodong Zhang[‡6]

From the [‡]Section of Structural Biology, Department of Medicine, Imperial College London, South Kensington, London SW7 2AZ, United Kingdom and the [§]Department of Biochemistry and Molecular Biophysics, Washington University School of Medicine, St. Louis, Missouri 63110

The phosphatidylinositol 3-kinase-related protein kinases are key regulators controlling a wide range of cellular events. The yeast Tel1 and Mec1·Ddc2 complex (ATM and ATR-ATRIP in humans) play pivotal roles in DNA replication, DNA damage signaling, and repair. Here, we present the first structural insight for dimers of Mec1·Ddc2 and Tel1 using single-particle electron microscopy. Both kinases reveal a head to head dimer with one major dimeric interface through the N-terminal HEAT (named after Huntingtin, elongation factor 3, protein phosphatase 2A, and yeast kinase TOR1) repeat. Their dimeric interface is significantly distinct from the interface of mTOR complex 1 dimer, which oligomerizes through two spatially separate interfaces. We also observe different structural organizations of kinase domains of Mec1 and Tel1. The kinase domains in the Mec1·Ddc2 dimer are located in close proximity to each other. However, in the Tel1 dimer they are fully separated, providing potential access of substrates to this kinase, even in its dimeric form.

Mec1 (yeast orthologue of mammalian ATR (ataxia telangiectasia- and Rad3-related)) and Tel1 (yeast orthologue of ATM (ataxia telangiectasia-mutated)) belong to the phosphatidylinositol 3-kinase-related protein kinase (PIKK)[7] family, the members of which control a plethora of cellular events including DNA damage response, DNA replication, growth control, and mRNA surveillance. Other members of the PIKK family include mammalian DNA-PKcs, mTOR (Tor1 and Tor2 in yeast), TRRAP, and SMG-1 (1, 2). PIKKs have a conserved domain architecture consisting of the FAT domain (named after the members, FRAP, ATM, and TRRAP), kinase domain, and FATC (FRAP, ATM, and TRRAP C terminus) domain at the C terminus, as well as HEAT repeats of variable lengths at the N terminus.

Because of the large size of these proteins, ranging from 2,368 amino acids for Mec1 to 4,128 amino acids for DNA-PKcs, these proteins are difficult to be purified in large quantities, thus hindering biochemical and structural analysis. There are a number of low resolution electron microscopy reconstructions available. These include a monomeric ATM with and without DNA bound at 30 Å resolution (3), dimeric ATM at 26 Å (4), DNA-PKcs with and without DNA bound, as well as DNA-bound DNA-PKcs·Ku70·Ku80 complex, all at ~30 Å (5, 6), DNA-PKcs at 13 and 7 Å (7, 8), SMG-1 in complex with SMG-9 at 24 Å (9), SMG-1·UPF complexes (SMG-1·SMG-8·SMG-9 complex with UPF1 or UPF2) at a range of 17–22 Å (10, 11), mTOR complex 1 structure at 26 Å (12), and TOR complex 2 structure at 26 Å (13). The crystal structure of DNA-PKcs at 6.6 Å (14) provided the first medium resolution structural information on a full-length PIKK. Although not all regions are resolved, the structure reveals the large array of HEAT repeats arranged in a circular fashion, enclosing a large channel. Very recently, the crystal structure of the C-terminal domain of mTOR, containing the conserved FAT, kinase, and FATC regions was determined at 3.2 Å followed by the cryo-electron microscopy structure of the human mTOR complex 1 (mTORC1) at 5.9 Å revealing the dimeric organization of these domains (15, 16). Although the PIKKs feature a conserved amino acid sequence of the common domains, the known structures of monomers and dimers do not explain the precise domain organizations in a three-dimensional space for the various PIKKs. Furthermore, certain PIKKs such as ATM are believed to be active as monomers (17), whereas the mTOR structures reveal active dimers (13, 16).

In budding yeasts, Mec1 and Tel1 are apical enzymes in DNA damage checkpoint pathways. They detect DNA damage and temporarily halt cell cycle progression while elevating and activating DNA repair proteins (18–21). Mec1 and Tel1 phosphorylate numerous target proteins involved in cell cycle, DNA repair, and replication including Rad53, Chk1, Ddc1-Rad17-Mec3 (9-1-1 checkpoint clamp), RPA (replication protein A), and Rad51 (22–26). Furthermore, Mec1 and Tel1 also play important roles in telomere maintenance (27, 28). Current

* This work was supported by Wellcome Trust Senior Investigator Award WT/098412/Z/12/Z (to X. Z.) and National Institutes of Health Grant GM083970 (to P. M. B.). The authors declare that they have no conflicts of interest with the contents of this article. The content is solely the responsibility of the authors and does not necessarily represent the official views of the National Institutes of Health.

[1] These authors contributed equally to this work.
[2] Supported by a Biotechnology and Biological Sciences Research Council doctoral studentship.
[3] Supported by the Emil Aaltonen Foundation and the Swedish Cultural Foundation in Finland. Present address: Dept. of Medical Biochemistry and Biophysics, Umeå University, SE-901 87 Umeå, Sweden.
[4] Present address: Perelman School of Medicine, University of Pennsylvania, Philadelphia, PA 19104.
[5] To whom correspondence may be addressed. Tel.: 314-362--3872; E-mail: burgers@biochem.wustl.edu.
[6] To whom correspondence may be addressed. Tel.: 44-207-594-3151; E-mail: xiaodong.zhang@imperial.ac.uk.
[7] The abbreviations used are: PIKK, phosphatidylinositol 3-kinase-related protein kinase; mTOR, mammalian target of rapamycin; CA, class average(s); RP, reprojection(s); FSC, Fourier shell correlation coefficient.

models suggest that Tel1 is recruited to double-stranded DNA ends, whereas Mec1 is recruited to RPA-coated single-stranded DNA, generated either by end resection during the DNA double-strand break repair or during replication fork reversal (25, 29). Mec1 and Tel1 show all the domains characteristic of PIKKs, including a PIKK regulatory domain at the C terminus, but lack a distinct FKBP12-rapamycin binding domain acting as a recruitment module (30). The PIKK regulatory domain is sandwiched between the kinase and FATC domains and is an essential regulatory element in ATR and ATM (31). The FATC domain is very well conserved and absolutely essential for kinase activity (31). It has been proposed to be the site for protein interactions and localization to damage sites (31). Tel1 contains an additional conserved N-terminal motif called TAN (Tel1/ATM N-terminal motif) that is important for telomere length maintenance and checkpoint signaling (32).

Similar to ATR, which forms a constitutive complex with its partner ATRIP, Mec1 also forms an integral complex with Ddc2 (also called Lcd1 or Pie1) (33–35). This interaction is coordinated by the C terminus of Ddc2 and the N terminus of Mec1 (35, 36). The N-terminal domain of Ddc2 has a coiled-coil domain important for oligomerization (37, 38) followed by a region involved in interactions with checkpoint activators like Dpb11 (mammalian TopBP1) (31, 39). The N-terminal domain of Ddc2 also features an acidic stretch that recognizes RPA, thereby recruiting ATR-ATRIP$^{Mec1\cdot Ddc2}$ complexes to single-stranded DNA (40). Remarkably, ATRIP^{Ddc2} interaction partners like TopBP1^{Dpb11} and RPA also interact with the kinase domain of ATR^{Mec1} via contacts with the PIKK regulatory domain or FATC regions (31, 41). A structure of Mec1·Ddc2 is thus required to understand how Mec1 and Ddc2 can coordinate various interactions important for Mec1 function.

The activation of Mec1·Ddc2$^{ATR\text{-}ATRIP}$ complex and Tel1^{ATM} is tightly regulated. Post-translational modifications such as acetylation in ATM (42) and autophosphorylation in ATM and ATR (17, 43) are shown to play important roles in activation. Activator proteins have been identified to substantially enhance mammalian PIKKs kinase activities such as TopBP1 for ATR-ATRIP and the Mre11·Rad50·Nbs1 complex for ATM (31, 44). Yeast Mec1·Ddc2 has a number of cell cycle-dependent activators, with the 9-1-1 clamp activating Mec1·Ddc2 in the G_1 phase, Dpb11 together with the 9-1-1 clamp in the G_2 phase, whereas Dna2, Dpb11, and the 9-1-1 clamp act in the S phase (45–48). Conserved hydrophobic residues in unstructured tails of the activator proteins are involved in bringing about the activation in Mec1·Ddc2 (49).

The precise activation mechanism is still unclear for both ATR^{Mec1} and ATM^{Tel1}, especially regarding whether oligomerization plays a role in activation. For ATR-ATRIP, oligomerization of the ATRIP subunits is essential for activation (37, 38). However, ATM is proposed to undergo a dimer to monomer transition as a part of the activation mechanism. ATM also exists as active dimers on activation during oxidative stress; however, the dimers are formed by a disulfide bridge between the C-terminal FATC domains (50). Activation of both ATR and ATM is initiated by autophosphorylation, which has been proposed to happen in *trans* and hence might require the close association of both kinase domains (17, 43).

In this work, we provide the first structural information for dimers of Mec1·Ddc2 and Tel1 obtained using electron microscopy. These structures reveal the conformation of Mec1·Ddc2 and Tel1 in their preactivated states. Both Mec1·Ddc2 and Tel1 structures show a head to head dimer coordinated by the N-terminal HEAT repeats. Individual monomers of both Mec1 and Tel1 show a characteristic arm region formed by the N-terminal HEAT repeats and a head region formed by the FAT-kinase-FATC domains. A comparison of the Mec1·Ddc2 dimer with the Tel1 dimer shows a large difference in the distance between the head domains within the dimer, which are fully separated in Tel1 but in close proximity in the Mec1·Ddc2 complex.

Experimental Procedures

Protein Expression and Purification—The Mec1·Ddc2 complex was expressed and purified as previously described (51) with some modifications. The Mec1·Ddc2 complex tagged with an IgG binding domain (ZZ) was overexpressed in yeast from pBL904, and cells were harvested and lysed using buffer HEP^{300} (50 mM HEPES-KOH, pH 7.8, 300 mM KCl, 10% glycerol, 1 mM EDTA, 0.1% Tween 20, 0.02% $C_{12}E_{10}$, 3 mM DTT, 5 mM reduced glutathione, 10 mM $NaHSO_3$, 10 μM pepstatin A, 2 mM benzamidine, 10 μM leupeptin, 1 mM PMSF, 5 mM $NaPP_i$, 10 mM β-glycerophosphate, 1 mM α-naphtylic acid, 5 mM NaF; superscript designates 300 mM NaCl). The cell lysate was adjusted to a pH of 7.4 and a conductivity corresponding to that of 200 mM KCl buffer and was clarified by ultracentrifugation at 35,000 rpm for 1 h in a 45 Ti rotor (Beckman Coulter). The supernatant was incubated with IgG beads (IgG-Sepharose 6 Fast Flow; GE Healthcare) for 3 h and subjected to four consecutive washes with buffer HEP^{250}, HEP^{300}, HEP^{300} supplemented with 10 mM magnesium acetate and 1 mM ATP, and HEP^{400}. Mec1·Ddc2 was cleaved with HRV 3C protease and eluted.

The GST-tagged Tel1 was overexpressed in yeast from pBL602 and purified as previously described (51) with some modifications. Cells were harvested and lysed in buffer HEP^{300} (60 mM HEPES-KOH, pH 7.8, 40 mM potassium phosphate, pH 7.8, 10% glycerol, 300 mM KCl, 150 mM ammonium sulfate, 2 mM DTT, 0.1% Tween 20, 0.01% Nonidet P-40, 1 mM EDTA, 0.5 mM EGTA, 10 mM β-glycerophosphate, 1 mM α-naphtylic acid, 5 μM pepstatin A, 5 μM leupeptin, 3 mM $NaHSO_3$, and 2 mM benzamidine). Ammonium sulfate precipitated protein was resuspended in buffer HEP^0 and incubated with glutathione *S*-Sepharose beads for 3 h and subjected to four consecutive washes with buffer HEP^{100}, HEP^{100} lacking the protease and phosphatase inhibitors hereinafter, HEP^{100} supplemented with 10 mM magnesium acetate and 1 mM ATP, and HEP^{100}. The GST-tagged Tel1 was cleaved by HRV 3C protease and further purified over a heparin column and eluted in HEP^{700}.

Gel Filtration Analysis—Mec1·Ddc2 was buffer-exchanged to 50 mM HEPES-KOH, pH 7.4, 200 mM KCl, 10% glycerol, 0.1% Tween 20, 0.01% Nonidet P-40, 1 mM EDTA, 1 mM EGTA, and 2 mM DTT using Amicon Ultra 0.5 columns (Merck Millipore) and run over a Superose 6 HR 10/30 gel filtration column (Pharmacia Biotech) at 0.3 ml/min. Tel1 was buffer-exchanged to 50 mM HEPES-KOH (pH 7.4), 200 mM KCl, 10% glycerol, 0.1% Tween 20, 0.02% $C_{12}E_{10}$, 1 mM EDTA, and 3 mM DTT and run over a Superose 6 Increase 5/150 GL gel filtration column (GE

Healthcare) at 0.1 ml/min. Elution was monitored at 280 nm, and peak fractions were separated on an 8% SDS-PAGE gel to verify protein identity. Migration of the Mec1·Ddc2 complex and Tel1 was compared with that of the gel filtration standards (catalog no. 151-1901; Bio-Rad) to estimate the size of the complex.

Mec1 Kinase Activity Assays—10 nM Mec1·Ddc2 was incubated with 100 nM GST-Rad53-kd in 10-μl reactions containing 25 mM HEPES (pH 7.6), 100 mM NaCl, 8 mM magnesium acetate, 100 μg/ml BSA, 1 mM DTT, 100 μM ATP, 0.5 μCi of [γ-^{32}P]ATP and 50 nM Dpb11, where indicated. Reactions were allowed to proceed for 10 min at 30 °C and stopped by addition of 4 μl of 5× SDS-PAGE loading dye. Samples were boiled for 5 min, separated on 8% SDS-PAGE gels, dried, and exposed to a phosphor screen (GE Healthcare).

Antibody Labeling of Mec1·Ddc2 and Tel1—16 nM Mec1·Ddc2 complex was labeled with 32 nM goat anti-Mec1 FATC, yS-20, polyclonal antibody (Santa Cruz Biotechnology) in 10-μl reactions containing 30 mM HEPES-KOH (pH 7.4), 150 mM NaCl, 2.5% glycerol, 0.25 mM EDTA, and 0.5 mM DTT. 20 nM Tel1 was labeled with the same anti-FATC antibody at 40 nM in 25-μl reactions containing 50 mM HEPES-KOH (pH 7.4), 220 mM NaCl, 2% glycerol, 1 mM EDTA, 0.5 mM EGTA, 1 mM DTT, 1 mM $MgCl_2$, 0.02% Tween 20, 0.002% Nonidet P-40. The anti-Mec1, yS-20, antibody has been raised against the highly conserved C-terminal region of Mec1 (84% similarity with the Tel1 C-terminal region). The reactions were incubated on ice for 30 min before putting the labeled samples onto EM grids.

Negative Stain Electron Microscopy Data Collection—2 μl of 70 nM Mec1·Ddc2 (30 mM HEPES, pH 7.4, 200 mM NaCl, 5% glycerol, 0.5 mM EDTA, 1 mM DTT), 2 μl of 20 nM Tel1 (50 mM HEPES, pH 7.4, 150 mM NaCl, 5% glycerol, 1 mM EDTA, 1 mM DTT), and antibody-labeled samples at concentrations described above were deposited for 1 min on glow-discharged continuous carbon grids (TAAB Laboratory Equipment). The excess of liquid was blotted, and a 2-μl drop of 2% (v/v) uranyl acetate was added to the grids for 2 min. The excess liquid was blotted and left to air dry. Mec1·Ddc2, Tel1, and the anti-Mec1-labeled complexes of Mec1·Ddc2 were imaged in a Philips CM200 electron microscope operating at 200 kV and equipped with a TVIPS slow scan 4k × 4k CCD camera. Micrographs were manually collected at a nominal magnification of 50,000 with a pixel size of 1.76 Å/pixel corresponding to an electron dose of 20 e/Å^2/s. All images were taken at a range of defocus from −2.5 to −3.5 μm. The antibody-labeled Tel1 sample was imaged in an FEI Tecnai F20 electron microscope operating at 200 kV and equipped with an FEI Falcon II CMOS direct electron detection camera. Micrographs were manually collected at a nominal magnification of 62,000 corresponding to a pixel size of 1.65 Å/pixel and an electron dose of 32 e/Å^2/s.

Single Particle Negative Stain Image Processing—10,586 Mec1·Ddc2 and 7,350 Tel1 particles were picked using an e2boxer.py program of EMAN2 (52, 53). Defocus and astigmatism parameters were estimated using CTFFIND3 (54). Mec1·Ddc2 and Tel1 data sets were used for *ab initio* reconstructions using a standard multivariate statistical analysis/multireference alignment routine in IMAGIC-V (55). Briefly, all particles were band pass-filtered with a 200 Å high pass cutoff and a 10 Å low pass cutoff and subjected to reference-free alignment. Class averages were generated using multivariate statistical analysis allowing selecting distinctive classes, which were used as an initial reference set for multireference alignment. Euler angles were manually assigned to three class averages along distinctive views. The assigned angles served as a set of angular references to determine Euler angles for all class averages and subsequently create an initial three-dimensional model. Reprojections generated from the new model were used as a reference set to align particles and assign their orientation in three dimensions. Once the overall features of the Mec1·Ddc2 and Tel1 map were stabilized, 2-fold symmetry (C2) was applied onwards. Further refinement for Mec1·Ddc2 was carried out in RELION-1.3 (56). Particles were subjected to reference-free two-dimensional classification and subsequently reduced to 7,235 particles after removing poor quality particles. Three-dimensional reconstruction was generated by refining the Mec1·Ddc2 dimer model obtained using IMAGIC-V. The final reconstruction was obtained from 5,633 Mec1·Ddc2 particles at a resolution of 22.5 Å using the gold standard FSC (0.143 criterion) (57). The Tel1 reconstruction was further refined using reprojections from the 2-fold symmetrized model generated with IMAGIC-V and performing particle alignments and projection matching in SPIDER (58). Aligned particles were subjected to the multivariate statistical analysis routine to generate class averages in IMAGIC-V. Angular assignments of the class averages generated from IMAGIC-V, and back projection for refining the structure was performed in SPIDER iteratively. The final reconstruction was obtained from the full data set at a resolution of 21 Å (FSC = 0.5 criterion). The model was further verified using RELION 1.3 with the final reconstruction filtered to 40 Å that converged to a 24 Å similar model in RELION 1.3 using the gold standard FSC (0.143 criterion).

Because of high heterogeneity of the antibody-labeled Mec1·Ddc2 and Tel1, individual particles with a clearly visible extra density were selected manually. 1,951 antibody-labeled Mec1·Ddc2 particles were band pass-filtered with 220 and 20 Å cutoffs and subjected to a reference-free alignment in IMAGIC-V. Centered particles were subjected to the MSA routine followed by two-dimensional classification. Two-dimensional class averages that show a clear extra density were selected and compared with reprojections generated from the unlabeled model. 844 antibody-labeled Tel1 particles were also band pass-filtered with 220 and 20 Å cutoffs. Visual inspection between the two-dimensional class averages of anti-FATC Mec1·Ddc2/individual images of anti-FATC Tel1 particles and reprojections along the same Euler angles identified a number of antibody-labeled particles that show an extra density corresponding to the anti-FATC antibody. Positions of the bound antibodies were identified using triangulation methods.

Electron Cryomicroscopy Data Collection—Tel1 was diluted in a buffer optimized for cryofreezing while preserving the protein stability and integrity. The final buffer included 50 mM HEPES-KOH (pH 7.4), 210 mM KCl, 1% glycerol, 0.02% Tween 20, 0.002% Nonidet P-40, 1 mM EDTA, 0.5 mM EGTA, 1 mM DTT, and 0.5 mM $MgCl_2$. Aliquots of 2 μl of Tel1 at a concentration of 20 nM were applied to glow-discharged holey carbon

grids (Quantifoil Cu R2/2, 300 mesh) coated with an additional thin layer of carbon. After 30 s of incubation in a humidity chamber at 4 °C and 100% relative humidity, the grids were blotted for 6 s and flash frozen in liquid ethane using an FEI Vitrobot Mark III. The grids were imaged in an FEI Tecnai F20 electron microscope operating at 200 kV and equipped with an FEI Falcon II CMOS direct electron detection camera. Micrographs were manually collected at a nominal magnification of 62,000 corresponding to a pixel size of 1.65 Å/pixel and an electron dose of 32 e/Å^2/s. Images were recorded at a defocus ranging from −1 to −4 μm.

Electron Cryomicroscopy Image Processing—All data were processed in RELION-1.4 (56). All the micrographs were corrected for CTF using CTFFIND3 (54). An initial data set of 20,519 particles, selected using both manual and autopicking routine in RELION, was extracted after binning the particles twice giving the pixel size of 3.3 Å/pixel. References for autopicking were generated using the initial ~1,200 manually picked particles and performing a two-dimensional classification routine. The data set was further improved by multiple rounds of two-dimensional classification to remove poor quality particles, resulting in a reduced data set of 17,226 particles. Three-dimensional classification was then employed to extract structurally homogenous data for three-dimensional structure refinement. The negative stain-EM structure filtered to 60 Å was used as a starting model. The final data set included 8,962 particles for refinement of the Tel1 structure. Iterative rounds of three-dimensional classification protocol were used for refinement as described in the RELION tutorials for extremely difficult cases. Careful monitoring was carried out to avoid possible overfitting, and all interpretations of the structure have been carried out keeping this in mind. The final resolution estimated by this refinement protocol according to resolution estimates used in Bayesian approach (59) was 14.1 Å. A final round of refinement was then carried out for local refinement in Refine3D routine of RELION. The final reconstruction converged to a resolution of 19.2 Å using the gold standard FSC (0.143 criterion).

Fitting of mTOR Crystal Structures and Map Segmentation—A 3.2 Å crystal structure of the C-terminal mTOR (Protein Data Bank code 4JSV) without the FKBP12-rapamycin binding domain (residues 2,021–2,118) was docked into the EM density corresponding to the kinase domain of Mec1 and Tel1. A 5.9 Å atomic structure of mTOR (Protein Data Bank code 5FLC) modeled into the cryo-EM map of mTORC1 (EMD-3213) was docked into the EM densities of the Mec1·Ddc2 complex and Tel1. Prior to fitting, the densities corresponding to Raptor and mLST8 subunits and the FKBP protein were removed. The Mec1·Ddc2 and Tel1 three-dimensional maps were then segmented in Chimera (60), and the domain boundary was based on the molecular fitting.

Results

Mec1·Ddc2 and Tel1 Exist as Higher Order Oligomers—Mec1·Ddc2 was previously shown to form a stable complex of 360 kDa using analytical ultracentrifugation (51). However, these studies were carried out at high salt conditions (0.4 M KCl) to prevent aggregation. In this study, the protein was purified to high homogeneity with improved buffer conditions (Fig. 1*A*), and all the experiments have been carried out in physiological salt concentrations (100–200 mM KCl). We analyzed Mec1·Ddc2 on a Superose 6 HR 10/30 size exclusion column, and interestingly, we found that the majority of Mec1·Ddc2 elutes with a retention time corresponding to a complex of ~700 kDa and is thus consistent with the molecular mass of the Mec1·Ddc2 dimer (720 kDa; Fig. 1*B*). Mec1 activity has been measured with *in vitro* kinase assays. The enhanced phosphorylation of Rad53 (with the active site mutated) and Rpa1 in the presence of Dpb11 was observed for the fraction containing the Mec1·Ddc2 dimer (Fig. 1*B*, *inset*). Therefore, we confirmed that Dpb11 could activate the oligomeric form of Mec1·Ddc2 used in our structural studies. Tel1 was purified to high homogeneity (Fig. 1*C*), analyzed on a Superose 6 Increase 5/150 GL size exclusion column, and eluted with a retention time corresponding to ~700 kDa, which is consistent with the molecular mass of a Tel1 dimer (640 kDa; Fig. 1*D*).

Three-dimensional Reconstruction of Mec1·Ddc2 Dimer—To investigate the structural organization of Mec1·Ddc2, we used single particle negative stained EM to generate the three-dimensional model of the complex. Negative stained EM was selected because of relatively low sample concentration and poor contrast in cryo-EM. We observed two populations of particles that differed significantly in their sizes. The majority (81%) was consistent with the size of Mec1·Ddc2 dimer of 720 kDa (Fig. 2*A*). Based on the eigenimage analysis in IMAGIC-V (55), dimeric images displayed a 2-fold symmetry. Using angular reconstitution methodology implemented in IMAGIC-V, we obtained an *ab initio* three-dimensional reconstruction of Mec1·Ddc2 dimer and iteratively refined the model imposing 2-fold symmetry. The quality of model was assessed by a side by side comparison of the two-dimensional class averages (CA) with their corresponding reprojections (RP) generated from the three-dimensional model (Fig. 2*B*). The final negative stain Mec1·Ddc2 dimer model (Fig. 2*C*) was obtained from 5,633 particles. The distribution of Euler angles of all particles used in generating the C2 structure (Fig. 2*D*) covers all angular space. The three-dimensional refinement of the model converged at 22.5 Å (Fig. 2*E*). The dimeric Mec1·Ddc2 reconstruction (Fig. 2*C*) is 175 Å tall, 215 Å wide, and 115 Å thick, resembling a pretzel with tubular density encircling multiple cavities. We can clearly distinguish two regions, which have been referred to as the head and arm domain in ATM, DNA-PKcs, and SMG-1 reconstructions (3, 5, 9). Here, the head domain occupies the upper globular density, whereas the arm domain forms an elongated and curved shape and consists of tubular density regions encircling a cavity (Fig. 2*C*, *left panel*). The model reveals multiple interaction sites within the arm and the head domains. The arm of one monomer is intertwined with the arm of another monomer. Weak contacts are also observed between the two opposite head domains, suggesting their auxiliary roles in dimer formation and stabilization.

Three-dimensional Reconstruction of Tel1—Tel1 samples were initially analyzed using negative stained EM to build an initial model (Fig. 3). Single particles revealed a distinct 2-fold symmetry indicating that Tel1 existed mainly as dimers in the protein preparations. The initial model was generated using a

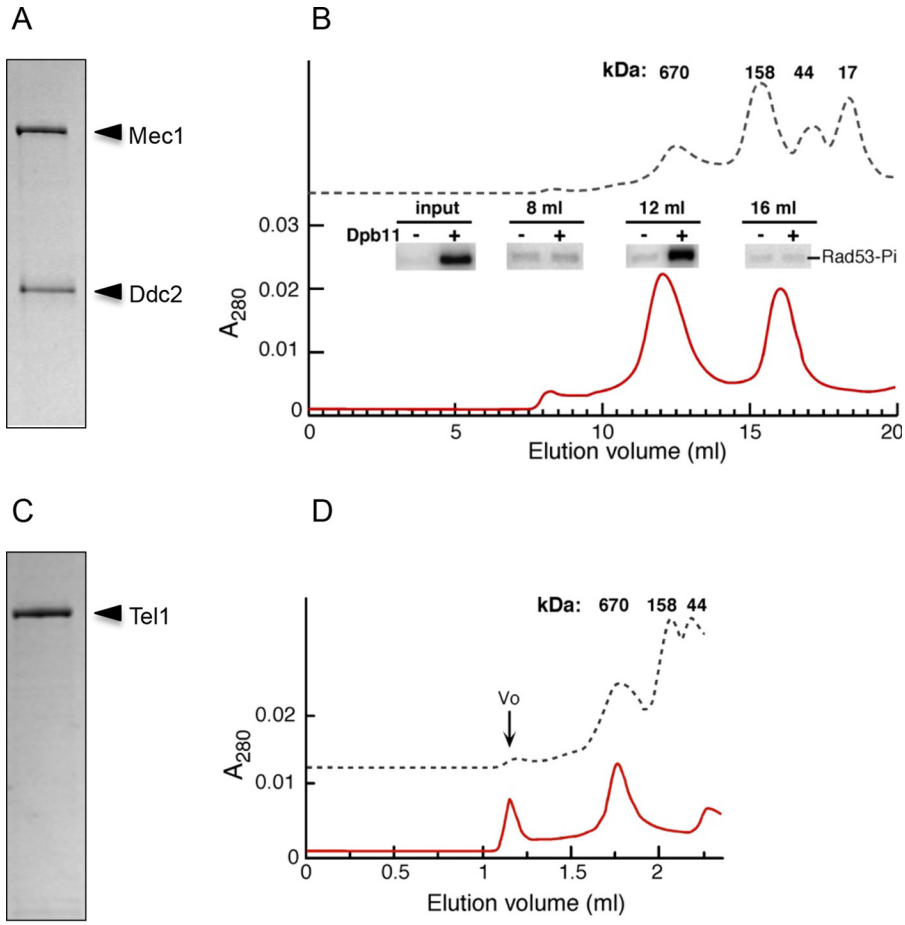

FIGURE 1. **Purification of Mec1·Ddc2 and Tel1.** *A*, SDS-PAGE of Mec1·Ddc2. *B*, gel filtration profile of Mec1·Ddc2 indicating that Mec1·Ddc2 exists as a dimer. The *inset* shows the kinase activity for specific fractions as indicated from the gel filtration profile. *C*, SDS-PAGE of Tel1. *D*, gel filtration profile of Tel1 indicating Tel1 exists as a dimer. V_0 represents the aggregated material.

data set of 7,350 particles using IMAGIC-V (55) and SPIDER (58). Reference-free alignments were carried during the initial stages of image processing, and subsequently angular reconstitution was utilized in building and refining the three-dimensional model. The quality of the model is assessed by the consistency between the CA and corresponding RP (Fig. 3*B*). The final negative stained three-dimensional model measures 185 Å tall, 230 Å wide, and 105 Å thick (Fig. 3*C*).

Tel1 was subsequently vitrified in a buffer that was compatible for cryo-freezing and stability of the protein to perform cryo-EM analysis (Fig. 4*A*). An initial data set of 20,519 particles was selected by a combination of manual and autopicking in RELION (56). Multiple rounds of two-dimensional classification were used to remove poor quality particles, resulting in a reduced data set of 17,226 particles. Three-dimensional classification was used to extract structurally homogenous data for three-dimensional structure refinements. The negative stained EM model filtered to 60 Å was used as the starting model. Extraction of particles from the best model led to the final data set of 8,962 particles that was used to refine the Tel1 structure using the three-dimensional classification protocol. A further local refinement resulted in a final model at a resolution of 19.2 Å using the gold standard FSC (0.143 criterion). The quality of the three-dimensional reconstruction generated in RELION was assessed by comparing the class averages calculated in IMAGIC-V with the reprojections along the same angles, assigned in IMAGIC-V using references generated from the three-dimensional model (Fig. 4*B*).

The cryo-EM Tel1 structure (Fig. 4*C*) overall resembles the negative stain reconstruction (Fig. 3*C*). However, it is taller (200 Å *versus* 185 Å) and narrower (215 Å *versus* 230 Å) when compared with the negatively stained model. This could be due to the stain procedure, which could cause flattening artifact. The Tel1 structure starkly resembles the overall Mec1·Ddc2 dimer architecture. Each monomer displays the characteristic domains of the PIKKs with the arm and the head region. However, the two head domains in Tel1 are fully separated by 35 Å in the narrowest region and enclose a cavity ~20 Å long and 125 Å wide. The Tel1 dimer structure displays no obvious steric hindrance for substrates to access the kinase domains.

Domain Assignment in Mec1·Ddc2 and Tel1—The three-dimensional reconstructions of both Mec1·Ddc2 and Tel1 display the head domain that is similar to head regions in other PIKK structures, where the FAT-kinase-FATC domains reside. We have used an antibody against the FATC domain to locate the FATC within Mec1·Ddc2 and Tel1 particle. Individual particles were carefully selected based on visual inspection. Only those representing the anti-FATC-labeled particle with additional density adjacent to it were selected. Subsequently we carried out the reference-free alignment and two-dimensional classifi-

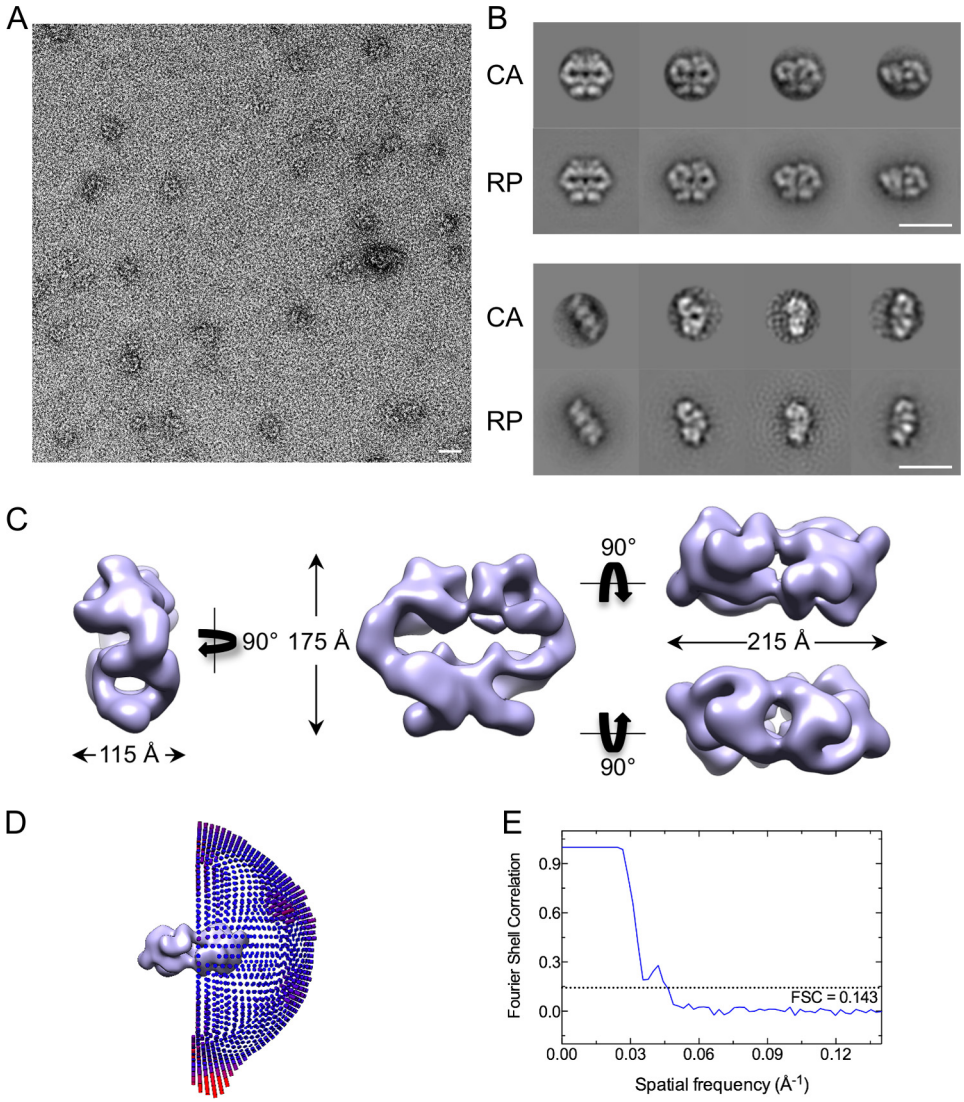

FIGURE 2. **Negative stain-EM three-dimensional reconstruction of Mec1·Ddc2 dimer.** *A*, a representative micrograph of negatively stained Mec1·Ddc2 particles. *B*, a comparison between two-dimensional CA and their corresponding RP generated from the negative stain three-dimensional model. *Scale bars* in *A* and *B* correspond to 200 Å. *C*, different views of the three-dimensional negative stain structure of Mec1·Ddc2 dimer. The *left panel* shows the side view, the *middle panel* shows the front view, and the *upper* and *lower right panels* show top and bottom views, respectively. *D*, Euler angle distribution of all particles used in refinement of the C2 symmetrized three-dimensional model. *E*, Fourier shell correlation curve used to calculate the model resolution of 22.5 Å according to the gold standard FSC (0.143 criterion).

cation. Comparisons of the class averages with the reprojections generated from the Mec1·Ddc2 reconstruction located an extra density that corresponds to the anti-FATC antibody (Fig. 5*A*). For antibody-labeled Tel1 data, because of the preferential orientation and the low antibody labeling efficiency, there were insufficient data for reliable two-dimensional classification. However, because of the distinct front view, it is unambiguous that the anti-FATC antibody is located within the globular head domain (Fig. 5*B*). Thus the FATC domains in both Tel1 and Mec1·Ddc2 are located within the globular domain.

Fitting the crystal structure of the C-terminal mTOR (15) and the FAT-kinase-FATC domain of mTORC1 (16) into our EM models of Mec1·Ddc2 and Tel1 (Fig. 6, *B* and *C*) further supports that the cradle-shaped density of the head region consist of the FAT, kinase domain, and the FATC domain. Based on our molecular fitting, we could also suggest the possible location of the catalytic and activation loop within the cleft of the Mec1 and Tel1 kinase domain as shown for mTOR (Fig. 6*D*). The elongated tubular arm domains agree with the shape and the dimensions of the HEAT repeats, which dominate both the N-terminal domains of Tel1 and Mec1, as well as the majority of Ddc2. Upon fitting all domains of the full-length mTOR into the Mec1·Ddc2 model, we have observed an unassigned density extending from the N-terminal HEAT repeats of Mec1. This density also forms an elongated and tubular arm, indicating that it is a natural extension of the N-terminal Mec1 and therefore might correspond to the Ddc2 subunit. These tubular arm domains intertwine and form the dimer interface.

Comparison of Mec1·Ddc2 and Tel1—Mec1·Ddc2 and Tel1 structures display a similar dimer arrangement with the dimer interface formed by the N-terminal HEAT repeats of Tel1 and Mec1, as well as Ddc2 in Mec1·Ddc2 (Fig. 6). The overall dimensions of these two models are also comparable. However, the clear tubular density encircling a cavity in the arm region of

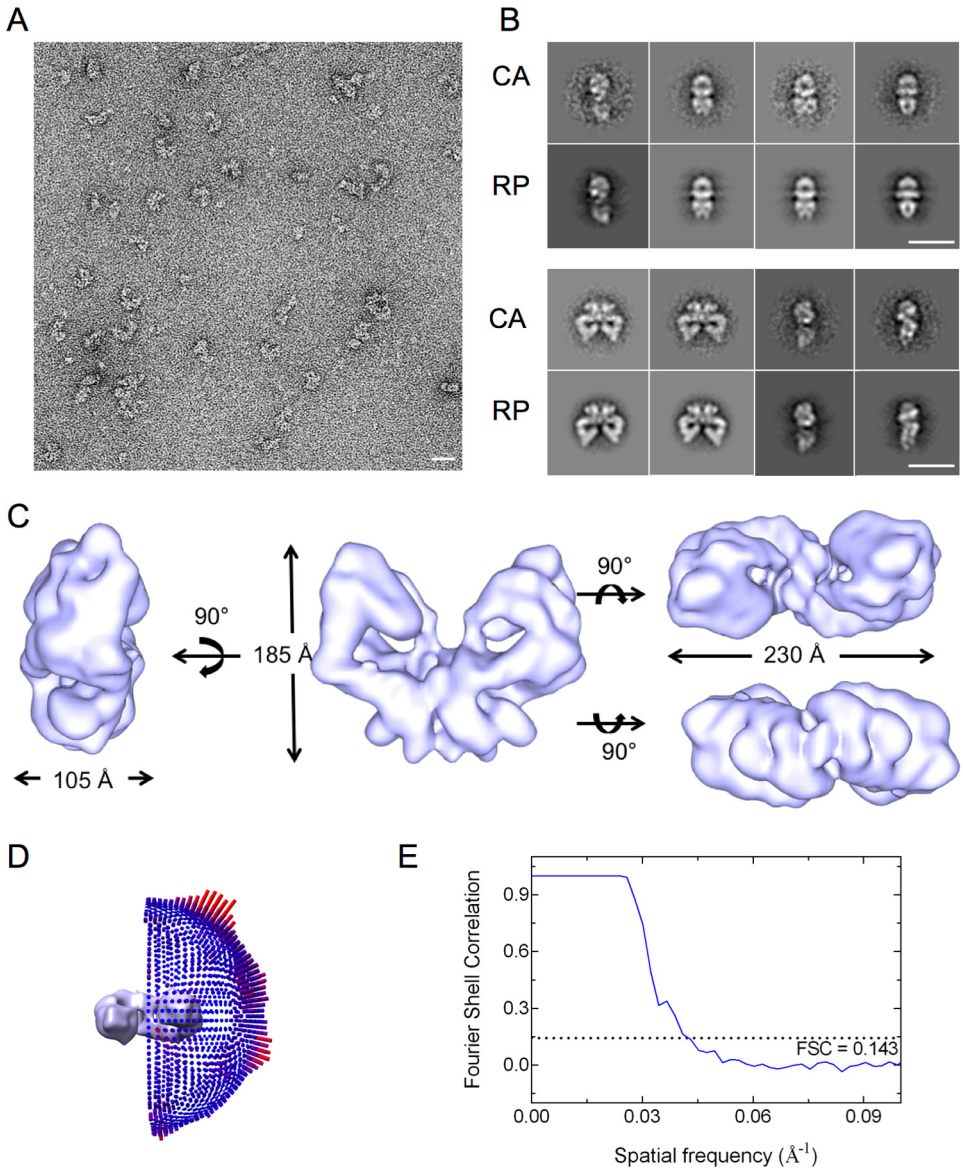

FIGURE 3. **Negative stain-EM three-dimensional reconstruction of Tel1 dimer.** *A*, a representative micrograph of negatively stained Tel1 particles. *B*, a comparison between two-dimensional CA and their corresponding RP generated from the negative stain three-dimensional model. *Scale bars* in *A* and *B* correspond to 200 Å. *C*, different views of the three-dimensional structure of Tel1 dimer. The *left panel* shows the side view, the *middle panel* shows the front view, and the *upper* and *lower right panels* show top and bottom views, respectively. *D*, Euler angle distribution of all particles used in refinement of the C2 symmetrized three-dimensional model. *E*, Fourier shell correlation curve used to calculate the model resolution.

the Mec1·Ddc2 reconstruction is missing in Tel1 (Figs. 2*C* and 3*C*). Monomeric Mec1·Ddc2 has a molecular mass of 360 kDa compared with 320 kDa of Tel1 (Fig. 6*A*); thus, it is likely that one of the tubular densities in the Mec1·Ddc2 reconstruction (Figs. 2*C*, *left panel*, and 6*B*, *front view*) accounts for Ddc2, as also concluded from our molecular fitting. Another striking difference between these two structures is the orientation of the head regions within the dimer. The two kinase domains are fully separated in Tel1, thereby suggesting no impediment for substrate recruitment in this model. On the other hand, the individual kinase domains in Mec1 are in close proximity, enclosing only a small cavity between the two domains.

Discussion

Mec1 and Tel1 serve as key regulators of the DNA damage response. Together with other members of the PIKK family, they share a conserved domain arrangement of the N-terminal arrays of HEAT repeats followed by the C-terminal globular kinase flanked with the FAT and FATC domains.

Our EM reconstructions of Mec1·Ddc2 and Tel1 reveal their dimeric architecture and provide the first structural insights supporting earlier biochemical findings on Mec1·Ddc2$^{ATR\text{-}ATRIP}$ and Tel1^{ATM}. Both models adopt a similar architecture with the head region comprising the FAT, kinase, and FATC domains, as well as the curved arm region consisting of large stretches of the N-terminal HEAT repeats. Our models are consistent with the 6.6 Å crystal structure of DNA-PKcs (14), as well as structures of other PIKKs such as SMG-1 (10). The DNA-PKcs structures show that the head region also consists of the kinase and FATC domain with additional HEAT repeats extending from the head domain and curving back onto it, encircling a large cavity. SMG1 is also shown to consist of a head region with

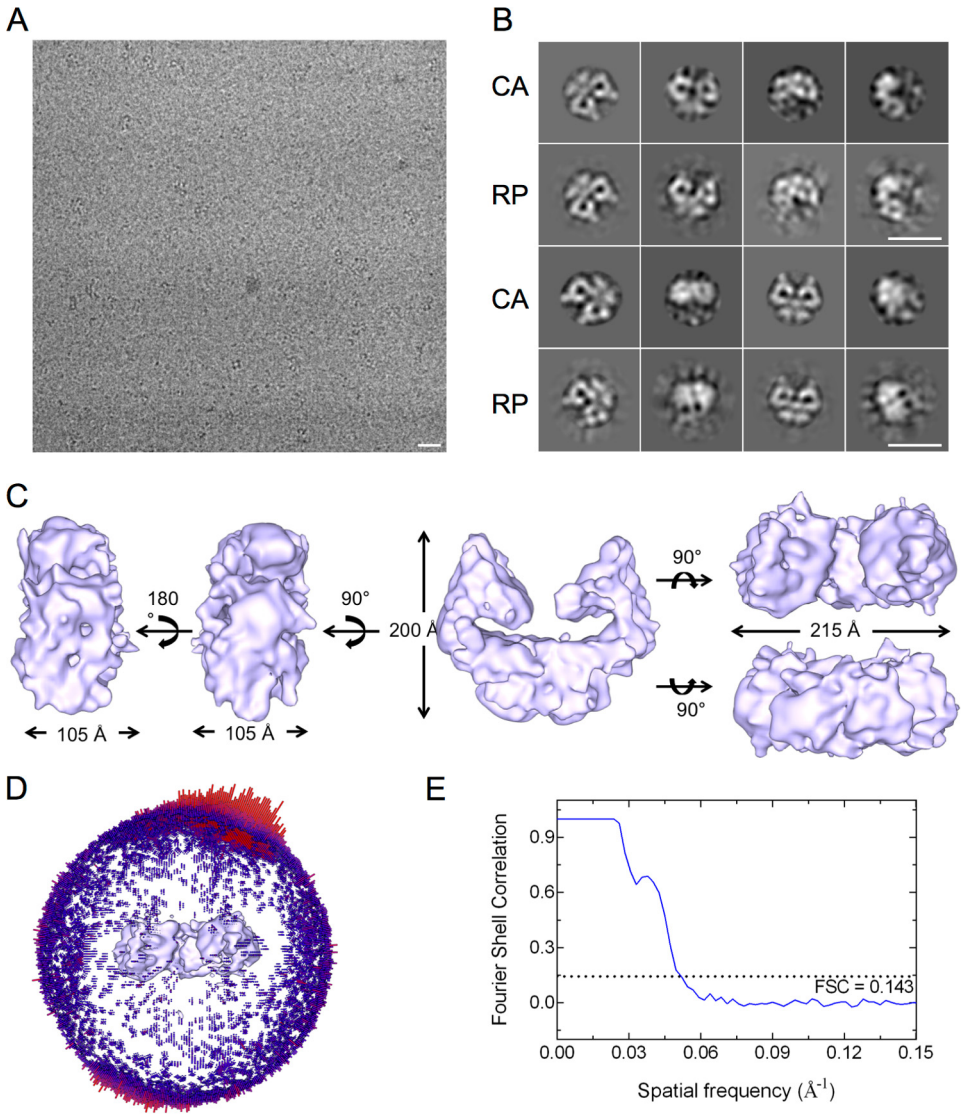

FIGURE 4. **Cryo-EM three-dimensional reconstruction of Tel1 dimer.** *A*, a representative micrograph of cryofrozen Tel1 particles on carbon-coated grids. *B*, a comparison between two-dimensional CA and their corresponding RP generated from the three-dimensional model. *Scale bars* in *A* and *B* correspond to 200 Å. *C*, different views of the three-dimensional structure of Tel1 dimer. The *two left panels* show the side views, the *middle panel* shows the front view, and the *upper* and *lower right panels* show top and bottom views, respectively. *D*, Euler angle distribution of all particles used in refinement of the non-symmetrized three-dimensional model. *E*, Fourier shell correlation curve used to calculate the model resolution of 19.2 Å according to the gold standard FSC (0.143 criterion).

a body comprising of tubular density that curves back toward the head domain. Although Mec1 exists in a complex with its obligatory binding protein Ddc2, it exhibits a similar structural organization. The C-terminal Ddc2 is predicted to contain HEAT repeats. Because Ddc2 interacts with the N-terminal Mec1, as previously reported biochemically (35), it might form a natural extension of the N-terminal HEAT repeats of Mec1. Based on our fitting of the 5.9 Å atomic model of mTOR (Fig. 6*B*) into the EM density of the Mec1·Ddc2 dimer, there is a remaining unassigned density extending from the N-terminal HEAT repeats of Mec1 that could accommodate the Ddc2 subunit. Then similar to DNA-PKcs and SMG-1, Ddc2 could possibly fold back into Mec1, positioning its N terminus in close proximity to the head region of Mec1. All PIKKs thus stabilize their C-terminal catalytic domains by using extended HEAT repeats, either within the same polypeptide chain as in Tel1^{ATM} and DNA-PKcs or by merging with an additional polypeptide chain such as Ddc2^{ATRIP}.

Dimers of Mec1·Ddc2 and Tel1 represent a PIKK in a functional form that exhibits basal kinase activity prior to activation (Fig. 1*B*, *inset*). The oligomerization of ATR-ATRIP through the ATRIP coiled-coil region is required for localization into foci of radiation-induced damage sites, as well as stalled replication forks (37, 38). Ddc2 also contains a coiled-coil region and thereby likely contributes to the dimeric interface of Mec1·Ddc2. Our domain assignment of Mec1·Ddc2 (Fig. 6*B*) locates HEAT repeats at the dimeric interface. It is also seen in Tel1 structure that the HEAT repeats form the major dimer interface at the arm region (Fig. 6*C*). Similar findings have also been observed in the EM structures of mTORC1 (16) and TORC2 (13), and mutations within the HEAT repeats of Mec1 lead to defective DNA damage responses in the G_1/S and intra-S checkpoints (61). Interestingly, we found that the dimeric interactions via HEAT repeats are likely to be stabilized by close vicinity of the FAT domain. Our Mec1·Ddc2 reconstruction shows that the kinase domains could also contribute

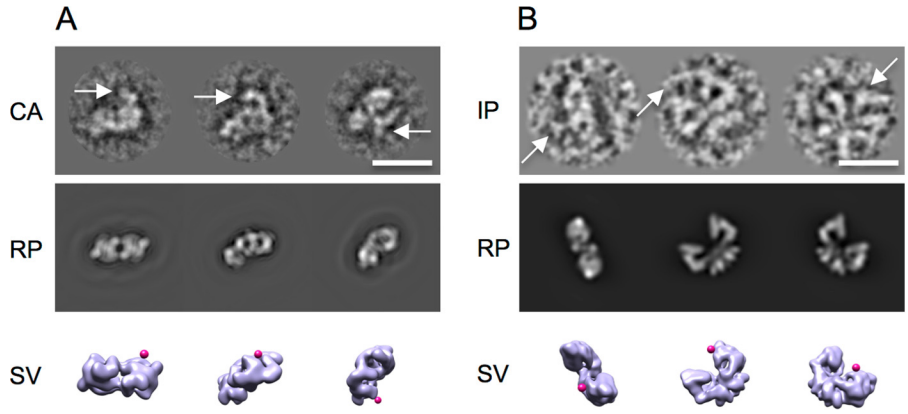

FIGURE 5. **Antibody labeling of the Mec1·Ddc2 and Tel1 reconstructions.** *A*, antibody labeling against the C terminus of Mec1. CA of anti-FATC antibody-labeled Mec1·Ddc2 show a clear extra density highlighted by *white arrows*. The density is missing in RP generated from the unlabeled Mec1·Ddc2 dimeric model along the same Euler angles as assigned to CA. *Magenta markers* indicate the location of the anti-FATC antibody as shown by surface views (*SV*) of Mec1·Ddc2 along the same Euler angles as in CA and RP. *B*, antibody labeling against the C terminus of Tel1. Individual particles (*IP*) show a clear extra density highlighted by *white arrows*. The density is missing in RP generated from the unlabeled Tel1 dimeric model along the same Euler angles as assigned to IP. *Magenta markers* indicate the location of the anti-FATC antibody as shown by surface views of Tel1 along corresponding angles. *Scale bars* correspond to 200 Å.

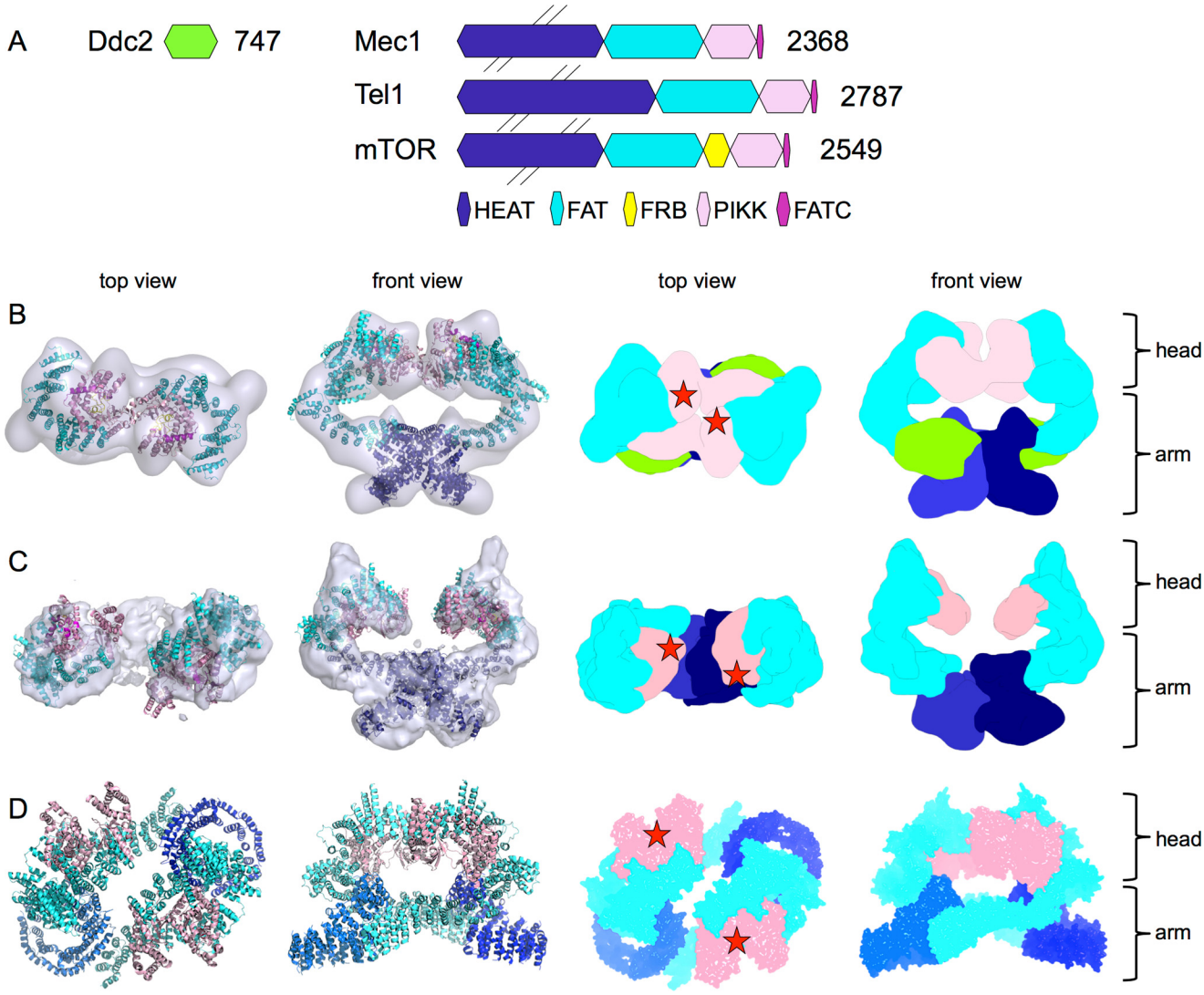

FIGURE 6. **Comparison of Mec1·Ddc2, Tel1, and mTORC1.** *A*, schematic domain arrangement of Ddc2, Mec1, Tel1, and mTOR. *B*, top and front views of the Mec1·Ddc2 EM reconstruction. *C*, top and front views of the Tel1 EM reconstruction with mTOR structures fitted in, as well as the top and front views of the segmented maps based on domain locations. *Pink*, FATC and kinase domain; *cyan*, FAT and HEAT repeats; *dark blue*, N-terminal HEAT repeats. The extra tubular density in Mec1·Ddc2 compared with Tel1, which accounts for Ddc2, is shown in *light green*. *D*, top and front views of the atomic model of mTOR (Protein Data Bank code 5FLC) fitted into the 5.9 Å cryo-EM structure of mTORC1 (EMD-3213). Densities corresponding to Raptor and mLST8 subunits of the complex, as well as the FKBP protein, have been removed. Top and front views of the segmented map of mTOR. *Red stars* indicate the positions of the active sites.

to the dimer interface and could thus regulate substrate binding through the association or dissociation of the kinase domains without the requirement for a complete dissociation of the dimer. The recent cryo-EM reconstruction of mTORC1 (16) also shows a dimeric structure. The dimeric architecture is distinct from the one reported here. In Mec1·Ddc2 and Tel1, there is one major dimer interface, formed by HEAT repeats into a large intertwined density region. Although in mTORC1, at least two distinct dimer interfaces form by HEAT repeats, encircling a large cavity (Fig. 6*D*). In mTORC1, the two kinase domains are located similarly to that of Mec1 and Tel1, although the active sites are facing away from the dimer interface (Fig. 6, *B–D*). It is possible that, depending on the number of HEAT repeats, different forms of dimerization exist for the PIKKs. Alternatively, the different dimeric forms observed in our work and in mTORC1 could represent different functional states of the PIKKs.

A number of the PIKKs were reported to autophosphorylate via residues in the C-terminal domain as a molecular switch for their kinase activity (17, 43, 62, 63). Our reconstructions show that the two head domains can adapt very different conformations within the dimer, suggesting that one monomer can phosphorylate the adjacent monomer within the dimer. Upon DNA damage, ATM has been inferred to exist as a dimer in its inactive form, and dimer dissociation by autophosphorylation is associated with activation of kinase activity (17). However, in the presence of the oxidative stress, ATM dimerizes via a disulfide bridge in the FATC region and compensates for the loss of the Mre11·Rad50·Nbs1-dependent activity (50). The seemingly conflicting requirement for dimers is consistent with our results presented here. We show that kinase domains could contribute to the dimer interface but substrate binding and possibly activation do not necessarily require a complete dissociation of the dimer, which is formed primarily through the HEAT repeats. It is possible that phosphorylation might disrupt a subset of the dimer interface, thereby affecting the stability of the dimer, which could manifest in different oligomeric states *in vitro*.

Our data here suggest a putative model for Mec1 and Tel1. Although dimerization through these HEAT repeats brings the kinase domains of Mec1·Ddc2 in close proximity, perhaps suggesting that activation may require the separation of these domains, in Tel1, the kinase domains are separated by 35 Å. Therefore, activation of these PIKKs may proceed through a more complex mechanism rather than a simple separation of the kinase domains. There are certain mechanistic advantages to maintaining the dimer through the HEAT repeats anchor while allowing possible repositioning and activation of the kinase domains. A dimer could increase the interaction surface with cofactors or support cooperativity to allow a more efficient recruitment. Furthermore, a complete dissociation of dimers to monomers would imply that to deactivate Mec1 or Tel1 or to recycle it for other activities, reassociation into dimers would be required. A tethered dimer could ensure that it can be readily recycled between an inactive and an active state, allowing rapid multiple rounds of controlled activation/deactivation. However, understanding the exact activation mechanisms requires structural and biochemical data on a reconstituted complex involving the PIKK bound to its activator.

Author Contributions—M. S., V. C. D., P. H. W., E. T., S. H., and D. B. designed and performed the experiments, and M. S., V. C. D., P. H. W., P. M. B., and X. Z. analyzed the data. P. M. B. and X. Z. conceived and designed the study. M. S. and V. C. D. performed the majority of electron microscopy, and M. S. did the antibody labeling studies, while D. B. collected the initial negative stain EM data for the Mec1·Ddc2 complex. P. H. W., E. T., A. V. M., and S. H. purified the proteins and performed biochemical analysis. M. S., V. C. D., X. Z., and P. M. B. wrote the manuscript.

Acknowledgments—We thank T. Pape for help with electron microscopy data acquisition, R. L. Perera and other members in X. Z.'s group for input and useful discussions, and C. Stith for expert technical assistance with Mec1 expression and purification.

References

1. Abraham, R. T. (2004) PI 3-kinase related kinases: "big" players in stress-induced signaling pathways. *DNA Repair* **3,** 883–887
2. Lempiäinen, H., and Halazonetis, T. D. (2009) Emerging common themes in regulation of PIKKs and PI3Ks. *EMBO J.* **28,** 3067–3073
3. Llorca, O., Rivera-Calzada, A., Grantham, J., and Willison, K. R. (2003) Electron microscopy and 3D reconstructions reveal that human ATM kinase uses an arm-like domain to clamp around double-stranded DNA. *Oncogene* **22,** 3867–3874
4. Lau, W. C., Li, Y., Liu, Z., Gao, Y., Zhang, Q., and Huen, M. S. (2016) Structure of the human dimeric ATM kinase. *Cell Cycle* **15,** 1117–1124
5. Boskovic, J., Rivera-Calzada, A., Maman, J. D., Chacón, P., Willison, K. R., Pearl, L. H., and Llorca, O. (2003) Visualization of DNA-induced conformational changes in the DNA repair kinase DNA-PKcs. *EMBO J.* **22,** 5875–5882
6. Spagnolo, L., Rivera-Calzada, A., Pearl, L. H., and Llorca, O. (2006) Three-dimensional structure of the human DNA-PKcs/Ku70/Ku80 complex assembled on DNA and its implications for DNA DSB repair. *Mol. Cell* **22,** 511–519
7. Rivera-Calzada, A., Maman, J. D., Spagnolo, L., Pearl, L. H., and Llorca, O. (2005) Three-dimensional structure and regulation of the DNA-dependent protein kinase catalytic subunit (DNA-PKcs). *Structure* **13,** 243–255
8. Williams, D. R., Lee, K. J., Shi, J., Chen, D. J., and Stewart, P. L. (2008) Cryo-EM structure of the DNA-dependent protein kinase catalytic subunit at subnanometer resolution reveals α helices and insight into DNA binding. *Structure* **16,** 468–477
9. Arias-Palomo, E., Yamashita, A., Fernández, I. S., Núñez-Ramírez, R., Bamba, Y., Izumi, N., Ohno, S., and Llorca, O. (2011) The nonsense-mediated mRNA decay SMG-1 kinase is regulated by large-scale conformational changes controlled by SMG-8. *Genes Dev.* **25,** 153–164
10. Melero, R., Uchiyama, A., Castaño, R., Kataoka, N., Kurosawa, H., Ohno, S., Yamashita, A., and Llorca, O. (2014) Structures of SMG1-UPFs complexes: SMG1 contributes to regulate UPF2-dependent activation of UPF1 in NMD. *Structure* **22,** 1105–1119
11. Deniaud, A., Karuppasamy, M., Bock, T., Masiulis, S., Huard, K., Garzoni, F., Kerschgens, K., Hentze, M. W., Kulozik, A. E., Beck, M., Neu-Yilik, G., and Schaffitzel, C. (2015) A network of SMG-8, SMG-9 and SMG-1 C-terminal insertion domain regulates UPF1 substrate recruitment and phosphorylation. *Nucleic Acids Res.* **43,** 7600–7611
12. Yip, C. K., Murata, K., Walz, T., Sabatini, D. M., and Kang, S. A. (2010) Structure of the human mTOR complex I and its implications for rapamycin inhibition. *Mol. Cell* **38,** 768–774
13. Gaubitz, C., Oliveira, T. M., Prouteau, M., Leitner, A., Karuppasamy, M., Konstantinidou, G., Rispal, D., Eltschinger, S., Robinson, G. C., Thore, S., Aebersold, R., Schaffitzel, C., and Loewith, R. (2015) Molecular basis of the rapamycin insensitivity of target of rapamycin com-

plex 2. *Mol. Cell* **58,** 977–988
14. Sibanda, B. L., Chirgadze, D. Y., and Blundell, T. L. (2010) Crystal structure of DNA-PKcs reveals a large open-ring cradle comprised of HEAT repeats. *Nature* **463,** 118–121
15. Yang, H., Rudge, D. G., Koos, J. D., Vaidialingam, B., Yang, H. J., and Pavletich, N. P. (2013) mTOR kinase structure, mechanism and regulation. *Nature* **497,** 217–223
16. Aylett, C. H., Sauer, E., Imseng, S., Boehringer, D., Hall, M. N., Ban, N., and Maier, T. (2016) Architecture of human mTOR complex 1. *Science* **351,** 48–52
17. Bakkenist, C. J., and Kastan, M. B. (2003) DNA damage activates ATM through intermolecular autophosphorylation and dimer dissociation. *Nature* **421,** 499–506
18. Morrow, D. M., Tagle, D. A., Shiloh, Y., Collins, F. S., and Hieter, P. (1995) TEL1, an S. cerevisiae homolog of the human gene mutated in ataxia telangiectasia, is functionally related to the yeast checkpoint gene MEC1. *Cell* **82,** 831–840
19. Sun, Z., Fay, D. S., Marini, F., Foiani, M., and Stern, D. F. (1996) Spk1/Rad53 is regulated by Mec1-dependent protein phosphorylation in DNA replication and damage checkpoint pathways. *Genes Dev.* **10,** 395–406
20. Lydall, D., Nikolsky, Y., Bishop, D. K., and Weinert, T. (1996) A meiotic recombination checkpoint controlled by mitotic checkpoint genes. *Nature* **383,** 840–843
21. Santocanale, C., and Diffley, J. F. (1998) A Mec1- and Rad53-dependent checkpoint controls late-firing origins of DNA replication. *Nature* **395,** 615–618
22. Sanchez, Y., Desany, B. A., Jones, W. J., Liu, Q., Wang, B., and Elledge, S. J. (1996) Regulation of RAD53 by the ATM-like kinases MEC1 and TEL1 in yeast cell cycle checkpoint pathways. *Science* **271,** 357–360
23. Sanchez, Y., Bachant, J., Wang, H., Hu, F., Liu, D., Tetzlaff, M., and Elledge, S. J. (1999) Control of the DNA damage checkpoint by chk1 and rad53 protein kinases through distinct mechanisms. *Science* **286,** 1166–1171
24. Paciotti, V., Lucchini, G., Plevani, P., and Longhese, M. P. (1998) Mec1p is essential for phosphorylation of the yeast DNA damage checkpoint protein Ddc1p, which physically interacts with Mec3p. *EMBO J.* **17,** 4199–4209
25. Brush, G. S., Morrow, D. M., Hieter, P., and Kelly, T. J. (1996) The ATM homologue MEC1 is required for phosphorylation of replication protein A in yeast. *Proc. Natl. Acad. Sci. U.S.A.* **93,** 15075–15080
26. Flott, S., Kwon, Y., Pigli, Y. Z., Rice, P. A., Sung, P., and Jackson, S. P. (2011) Regulation of Rad51 function by phosphorylation. *EMBO Rep.* **12,** 833–839
27. Mills, K. D., Sinclair, D. A., and Guarente, L. (1999) MEC1-dependent redistribution of the Sir3 silencing protein from telomeres to DNA double-strand breaks. *Cell* **97,** 609–620
28. Moser, B. A., Chang, Y. T., Kosti, J., and Nakamura, T. M. (2011) Tel1ATM and Rad3ATR kinases promote Ccq1-Est1 interaction to maintain telomeres in fission yeast. *Nat. Struct. Mol. Biol.* **18,** 1408–1413
29. Zou, L., and Elledge, S. J. (2003) Sensing DNA damage through ATRIP recognition of RPA-ssDNA complexes. *Science* **300,** 1542–1548
30. Rivera-Calzada, A., Lopez-Perrote, A., Melero, R., Boskovic, J., Munoz-Hernandez, H., Martino, F., and Llorca, O. (2015) Structure and assembly of the PI3K-like protein kinases (PIKKs) revealed by electron microscopy. *AIMS Biophys.* **2,** 36–57
31. Mordes, D. A., Glick, G. G., Zhao, R., and Cortez, D. (2008) TopBP1 activates ATR through ATRIP and a PIKK regulatory domain. *Genes Dev.* **22,** 1478–1489
32. Seidel, J. J., Anderson, C. M., and Blackburn, E. H. (2008) A novel Tel1/ATM N-terminal motif, TAN, is essential for telomere length maintenance and a DNA damage response. *Mol. Cell. Biol.* **28,** 5736–5746
33. Paciotti, V., Clerici, M., Lucchini, G., and Longhese, M. P. (2000) The checkpoint protein Ddc2, functionally related to S. pombe Rad26, interacts with Mec1 and is regulated by Mec1-dependent phosphorylation in budding yeast. *Genes Dev.* **14,** 2046–2059
34. Rouse, J., and Jackson, S. P. (2000) LCD1: an essential gene involved in checkpoint control and regulation of the MEC1 signalling pathway in *Saccharomyces cerevisiae*. *EMBO J.* **19,** 5801–5812
35. Wakayama, T., Kondo, T., Ando, S., Matsumoto, K., and Sugimoto, K. (2001) Pie1, a protein interacting with Mec1, controls cell growth and checkpoint responses in *Saccharomyces cerevisiae*. *Mol. Cell. Biol.* **21,** 755–764
36. Ball, H. L., Myers, J. S., and Cortez, D. (2005) ATRIP binding to replication protein A-single-stranded DNA promotes ATR-ATRIP localization but is dispensable for Chk1 phosphorylation. *Mol. Biol. Cell* **16,** 2372–2381
37. Ball, H. L., and Cortez, D. (2005) ATRIP oligomerization is required for ATR-dependent checkpoint signaling. *J. Biol. Chem.* **280,** 31390–31396
38. Itakura, E., Sawada, I., and Matsuura, A. (2005) Dimerization of the ATRIP protein through the coiled-coil motif and its implication to the maintenance of stalled replication forks. *Mol. Biol. Cell* **16,** 5551–5562
39. Mordes, D. A., Nam, E. A., and Cortez, D. (2008) Dpb11 activates the Mec1-Ddc2 complex. *Proc. Natl. Acad. Sci. U.S.A.* **105,** 18730–18734
40. Ball, H. L., Ehrhardt, M. R., Mordes, D. A., Glick, G. G., Chazin, W. J., and Cortez, D. (2007) Function of a conserved checkpoint recruitment domain in ATRIP proteins. *Mol. Cell. Biol.* **27,** 3367–3377
41. Nakada, D., Hirano, Y., Tanaka, Y., and Sugimoto, K. (2005) Role of the C terminus of Mec1 checkpoint kinase in its localization to sites of DNA damage. *Mol. Biol. Cell* **16,** 5227–5235
42. Sun, Y., Xu, Y., Roy, K., and Price, B. D. (2007) DNA damage-induced acetylation of lysine 3016 of ATM activates ATM kinase activity. *Mol. Cell. Biol.* **27,** 8502–8509
43. Liu, S., Shiotani, B., Lahiri, M., Maréchal, A., Tse, A., Leung, C. C., Glover, J. N., Yang, X. H., and Zou, L. (2011) ATR autophosphorylation as a molecular switch for checkpoint activation. *Mol. Cell* **43,** 192–202
44. Lee, J. H., and Paull, T. T. (2004) Direct activation of the ATM protein kinase by the Mre11/Rad50/Nbs1 complex. *Science* **304,** 93–96
45. Navadgi-Patil, V. M., and Burgers, P. M. (2009) A tale of two tails: activation of DNA damage checkpoint kinase Mec1/ATR by the 9-1-1 clamp and by Dpb11/TopBP1. *DNA Repair* **8,** 996–1003
46. Pfander, B., and Diffley, J. F. (2011) Dpb11 coordinates Mec1 kinase activation with cell cycle-regulated Rad9 recruitment. *EMBO J.* **30,** 4897–4907
47. Kumar, S., and Burgers, P. M. (2013) Lagging strand maturation factor Dna2 is a component of the replication checkpoint initiation machinery. *Genes Dev.* **27,** 313–321
48. Navadgi-Patil, V. M., and Burgers, P. M. (2008) Yeast DNA replication protein Dpb11 activates the Mec1/ATR checkpoint kinase. *J. Biol. Chem.* **283,** 35853–35859
49. Navadgi-Patil, V. M., Kumar, S., and Burgers, P. M. (2011) The unstructured C-terminal tail of yeast Dpb11 (human TopBP1) protein is dispensable for DNA replication and the S phase checkpoint but required for the G_2/M checkpoint. *J. Biol. Chem.* **286,** 40999–41007
50. Guo, Z., Kozlov, S., Lavin, M. F., Person, M. D., and Paull, T. T. (2010) ATM activation by oxidative stress. *Science* **330,** 517–521
51. Majka, J., Niedziela-Majka, A., and Burgers, P. M. (2006) The checkpoint clamp activates Mec1 kinase during initiation of the DNA damage checkpoint. *Mol. Cell* **24,** 891–901
52. Ludtke, S. J., Baldwin, P. R., and Chiu, W. (1999) EMAN: semiautomated software for high-resolution single-particle reconstructions. *J. Struct. Biol.* **128,** 82–97
53. Tang, G., Peng, L., Baldwin, P. R., Mann, D. S., Jiang, W., Rees, I., and Ludtke, S. J. (2007) EMAN2: an extensible image processing suite for electron microscopy. *J. Struct. Biol.* **157,** 38–46
54. Mindell, J. A., and Grigorieff, N. (2003) Accurate determination of local defocus and specimen tilt in electron microscopy. *J. Struct. Biol.* **142,** 334–347
55. van Heel, M., Harauz, G., Orlova, E. V., Schmidt, R., and Schatz, M. (1996) A new generation of the IMAGIC image processing system. *J. Struct. Biol.* **116,** 17–24
56. Scheres, S. H. (2012) RELION: implementation of a Bayesian approach to cryo-EM structure determination. *J. Struct. Biol.* **180,** 519–530
57. Scheres, S. H., and Chen, S. (2012) Prevention of overfitting in cryo-EM structure determination. *Nat. Methods* **9,** 853–854
58. Shaikh, T. R., Gao, H., Baxter, W. T., Asturias, F. J., Boisset, N., Leith, A., and Frank, J. (2008) SPIDER image processing for single-particle reconstruction of biological macromolecules from electron micrographs. *Nat. Protoc* **3,** 1941–1974

59. Scheres, S. H. (2012) A Bayesian view on cryo-EM structure determination. *J. Mol. Biol.* **415,** 406–418
60. Pettersen, E. F., Goddard, T. D., Huang, C. C., Couch, G. S., Greenblatt, D. M., Meng, E. C., and Ferrin, T. E. (2004) UCSF Chimera–a visualization system for exploratory research and analysis. *J. Comput. Chem.* **25,** 1605–1612
61. Paciotti, V., Clerici, M., Scotti, M., Lucchini, G., and Longhese, M. P. (2001) Characterization of mec1 kinase-deficient mutants and of new hypomorphic mec1 alleles impairing subsets of the DNA damage response pathway. *Mol. Cell. Biol.* **21,** 3913–3925
62. Chan, D. W., Chen, B. P., Prithivirajsingh, S., Kurimasa, A., Story, M. D., Qin, J., and Chen, D. J. (2002) Autophosphorylation of the DNA-dependent protein kinase catalytic subunit is required for rejoining of DNA double-strand breaks. *Genes Dev.* **16,** 2333–2338
63. Soliman, G. A., Acosta-Jaquez, H. A., Dunlop, E. A., Ekim, B., Maj, N. E., Tee, A. R., and Fingar, D. C. (2010) mTOR Ser-2481 autophosphorylation monitors mTORC-specific catalytic activity and clarifies rapamycin mechanism of action. *J. Biol. Chem.* **285,** 7866–7879

The Dimeric Architecture of Checkpoint Kinases Mec1^{ATR} and Tel1^{ATM} Reveal a Common Structural Organization

Marta Sawicka, Paulina H. Wanrooij, Vidya C. Darbari, Elias Tannous, Sarem Hailemariam, Daniel Bose, Alena V. Makarova, Peter M. Burgers and Xiaodong Zhang

J. Biol. Chem. 2016, 291:13436-13447.
doi: 10.1074/jbc.M115.708263 originally published online April 28, 2016

Structure of nucleotide-bound Tel1^{ATM} reveals the molecular basis of inhibition and structural rationale for disease mutations

Luke A. Yates[1,3], Rhys M. Williams[1,3], Sarem Hailemariam[2], Rafael Ayala[1], Peter Burgers[2], Xiaodong Zhang[1,4]

[1]Section of Structural Biology, Faculty of Medicine, Imperial College London, London SW7 2AZ, UK.
[2]Department of Biochemistry and Molecular Biophysics, Washington University School of Medicine, St Louis, MO 63110, USA
[3]These authors contributed equally
[4] Lead Contact
Correspondence: Xiaodong Zhang, xiaodong.zhang@imperial.ac.uk

SUMMARY

Yeast Tel1 and its highly conserved human orthologue ATM are large protein kinases central to the maintenance of genome integrity. Mutations in ATM are found in ataxia-telangiectasia (A-T) patients and ATM is one of the most frequently mutated genes in many cancers. Using cryo electron microscopy, we present the structure of Tel1 in a nucleotide-bound state. Our structure reveals molecular details of key residues surrounding the nucleotide binding site and provides a structural and molecular basis for its intrinsically low basal activity. We show that the catalytic residues are in a productive conformation for catalysis, but the PIKK-regulatory domain-Insert (PRD-I) restricts peptide-substrate access and the N-lobe is in an open conformation, thus explaining the requirement for Tel1 activation. Structural comparisons with other PIKKs suggest a conserved and common allosteric activation mechanism. Our work also provides a structural rationale for many mutations found in A-T and cancer.

KEYWORDS

Kinase, DNA Damage Response, CryoEM, Phosphatidylinositol-3-kinase-like kinase,

INTRODUCTION

Saccharomyces cerevisiae Tel1 and its highly conserved human orthologue Ataxia-Telangiectasia-Mutated (ATM), are major kinases responsible for maintaining genome

integrity and is highly conserved in Eukaryotes. Tel1^{ATM} is recruited to sites of DNA damage by the MRX/N complex, a key element in double-strand (ds)DNA break repair comprising of Mre11, Rad50, and Xrs2 (Nbs1 in human) (Falck et al., 2005). MRX/N is also the major activator of Tel1^{ATM}, which subsequently phosphorylates hundreds of targets that contain a S/T-Q motif (Lee and Paull, 2004; Matsuoka et al., 2007). Many of these targets, including CHK1/2, ATM, BRCA1, PALB2, p53 and H2AX, are tumour suppressors involved in cell cycle control and dsDNA break repair through homologous recombination (Lavin and Kozlov, 2007; Matsuoka et al., 2007). The precise mechanism of Tel1^{ATM} activation is not fully understood, but is suggested to involve autophosphorylation (Kozlov et al., 2006), lysine acetylation (Sun et al., 2005) and dissociation of homodimers into monomers (Bakkenist and Kastan, 2003). Critically, mutations in ATM are found in Ataxia-Telangiectasia (A-T), a rare disease primarily associated with immunodeficiency and progressive neurological decline. A-T patients also have an increased susceptibility to malignancy due to genomic instability, and ATM is one of the most frequently mutated genes in many cancers (Choi et al., 2016).

Tel1^{ATM} belongs to a family of PI-3K (phosphatidylinositol-3-kinase)-like kinases that also includes ATR (ATM-Rad3-related, and its yeast orthologue Mec1), DNA-PKc, mTOR (mammalian target of Rapamycin), TRRAP/Tra1 and SMG1 (Baretić and Williams, 2014). All PI-3K kinases contain a canonical two-lobed kinase domain, with the smaller N-lobe containing the highly conserved Glycine-rich loop (Gly-rich loop), whilst the larger C-lobe possesses the catalytic and activation loops (Walker et al., 1999). A number of additional conserved and functional elements within the kinase domain have been identified in PIKKs including the LBE (LST8-binding element) (Yang et al., 2013) and the PRD (PIKK regulatory domain) (Mordes et al., 2008). Flanking the kinase domain are the N-terminal HEAT repeats, followed by a FAT (FRAP [FKBP12-rapamycin associated protein], ATM, TRRAP [transformation/transcription domain associated protein]) domain and a ~35 residue FATC domain at the C-terminus (Imseng et al., 2018). Due to their large sizes, structural and mechanistic studies on these kinases have been challenging. A number of high-resolution structures (< 4.0 Å, where many side chains can be resolved) are available, mostly of those involving mTOR, including its complexes with a number of activator proteins (Yang et al., 2017). The 4.3 Å crystal structure of DNA-PKcs revealed the architecture of this large PIKK (Sibanda et al., 2017) whereas the 3.9 Å cryoEM structure of Mec1-Ddc2 provided a structural basis for how ATR^{Mec1} might be kept in an inhibited state (Wang et al., 2017). The cryoEM structures of Tel1 (Xin et al., 2019) and human ATM (Baretić et al., 2017) in the absence of nucleotides have shed some light into kinase function but do not provide a complete understanding of the role of the regulatory elements in maintaining an auto-inhibited state.

Here we present the cryoEM structure of *Saccharomyces cerevisiae* Tel1 in complex with an ATP analogue, AMP-PNP, with sufficient resolution (3.7 – 4.0 Å) to resolve the bound nucleotide and allow most of the side chains in the conserved FAT-Kinase-FATC (FAT-KIN) to be resolved (**Figure 1, Figure S1 and S2**). The structure reveals that the active site residues of Tel1 are in a productive conformation with the exception that the N-lobe, which also contributes to catalytic activities, is likely to undergo further closure upon activation. Significantly, a conserved insertion in the PRD (PRD-I) obscures peptide substrate access to the active site. This explains the low intrinsic activity of Tel1 and its requirement for activation by the binding of MRX and DNA. Comparisons with mTORC1 and DNA-PK structures suggest a common allosteric activation mechanism that could lead to the closure of N-lobe as well as the relocation of the PRD-I domain, leading to an active site that is fully accessible for peptide substrate binding. Due to the high degree of structural conservation between ATM and the Tel1 FAT-KIN regions, where a large number of pathogenic mutations are located, our structure also provides a structural basis for many disease mutations found in ATM.

RESULTS AND DISCUSSION

Structure of the Tel1 dimer

Tel1 was expressed and purified as reported previously (Sawicka et al., 2016) and its kinase activity shown to be stimulated synergistically by both double-stranded (ds) DNA and MRX (Hailemariam et al., 2019). The overall Tel1 dimer structure was refined to a global resolution of 4.0 Å (**Figure S2**). Using localised masking around density regions corresponding to the FAT-KIN domains as well as regions of HEAT repeats, an improved resolution of 3.7 Å was obtained for these regions, which correspond to two thirds of the whole protein. In key functional regions around the kinase domain and the dimer interface, the local resolution estimates are better than 3.5 Å; and densities for bulky side-chains are clearly visible (**Figure S2**). Consequently, we could build side chains into the majority of the FAT, kinase and FATC domains (residues 1527- 2787) and place confident sequence assignment between residues 968 and 1526. The N-terminal HEAT repeats are flexible, as was also shown in ATM structures, and left as Cα trace only due to the lack of clear side chain density. Our structure is in excellent agreement with that of an ATM closed dimer, which was limited to Cα-Cβ atoms (Baretić et al., 2017). Interestingly, we did not observe an open dimer conformation or monomers in our analysis.

Different subdomain terminologies have been used to describe PIKKs, including ATM. For simplicity, we use rigid bodies to define subdomains within the HEAT repeats and the FAT domain, which was originally assigned by multiple sequence alignments (Bosotti et al., 2000). Specifically, by comparing the structure of Tel1 and those of ATM and mTOR, the N-terminal HEAT repeats can be separated into two rigid bodies, which we term N-HEAT (residues 1-1162) and C-HEAT (residues 1163-1437) (**Figure 1**). There is a connecting region, denoted a bridge domain (residues 1438-1600) before the FAT domain, which we have extended and also divided into several rigid bodies: N-FAT (N-terminal FAT, 1600-1786), M-FAT (Middle-FAT, 1787-2128) and C-FAT (C-terminal FAT, 2129 -2355) (**Figure 1 and Figure S3**). The C-FAT consists of the FLAP-BE (as defined in (Baretić et al., 2017)) and HRD domain (**Figure 1**).

The Tel1 dimer interface is extensive and can be divided into three layers (**Figure 2A**); the top layer consists of PRD-I and LBE of one protomer interacting with a long helical antenna specific to $Tel1^{ATM}$ called FLAP-BE, of the adjacent protomer (FLAP-BE', where ' denotes elements from the adjacent protomer) (**Figure 2**); the middle layer mainly consists of FATC of one protomer and the adjacent M-FAT' (immediately preceding FLAP-BE) of the other protomer, while the bottom layer consists of M-FAT-M-FAT' interactions **(Figure 2A**). The buried surface area at the dimer interface is extensive with over 3000 $Å^2$ per protomer. The bottom layer of the dimer interface is exclusively hydrophobic in nature, with a vast array of large bulky hydrophobic residues (Phe and Leu) forming a well-buried core around the 2-fold symmetry axis (**Figure 2B**). The middle layer employs a mixture of polar and hydrophobic residues (**Figure 2C**), whereas the upper layer, which has the smallest interface surface area and is the least well resolved, interacts via charge complementarity (**Figure 2D**). Given the characteristics of the dimer interface, it seems that a dimer-to-monomer transition would be energetically unfavourable. Furthermore, the hydrophobic nature of the bottom layer enables some conformational flexibility at the bottom layer of the dimer interface, whereas the top layer, which is polar in nature, can be broken or rearranged. Indeed, a relative rotation of the FAT-KIN regions in the ATM dimer has been observed in the open dimer conformation (Baretić et al., 2017).

Tel1 nucleotide-bound kinase domain is in a catalytically productive conformation

Similar to the other PIKKs such as mTOR, ATM, DNA-PKc and Mec1, the kinase domain is surrounded by the FAT domains that form a C-shaped cradle surrounding the kinase domain (**Figure 3A**). It is worth noting that N-FAT contacts the kinase C-lobe whereas C-FAT

contacts the N-lobe (**Figure 3A, Figure 1A**). M-FAT sits away from the kinase domain and instead contacts C-HEAT and is in close proximity with N-HEAT and could therefore transmit conformational changes from the HEAT region to the kinase domain (**Figure 3A**, **Figure 1A**).

The structure of nucleotide-bound Tel1 shows the catalytic residues of the C-lobe in a catalytically productive conformation, with clear density for AMP-PNP **(Figure 3B-C)**. The catalytic loop, containing the highly conserved ^{2612}DRH^{2614} motif, adopts a similar conformation to that observed in mTOR structures **(Figure S4)** (Yang et al., 2013, 2017), where D2612 is well-positioned to act as the catalytic base for deprotonation of the hydroxyl group from the peptide substrate, and the side chains of H2614 and N2616 co-ordinate the γ-phosphate of AMP-PNP (**Figure 3B-C**) (Kenyon et al., 2012). The Mg^{2+}-binding ^{2631}DLG^{2633} motif and the adjacent activation loop are well-ordered, allowing us to confidently model in two Mg^{2+} ions co-ordinating the β-/γ- (Mg1) and α-/γ-phosphates (Mg2) of AMP-PNP into the density, using nucleotide-bound structures of PKA and mTORC1 as a guide (**Figure 3B**) (Das et al., 2015; Yang et al., 2013). The activation loop, which is ordered in this kinase, wraps around the catalytic loop and supports kinase activity via several interactions. Most notably, residues E2646 and I2634 of the activation loop sandwich the catalytic loop, and there is an apparent interaction between R2613 of the catalytic loop (^{2612}DRH^{2614} motif) and the main chain of the activation loop, close to the ^{2631}DLG^{2633} motif. The catalytic loop is further constrained by two aromatic residues (W2783 and Y2787) from the C-terminus of FATC (**Figure 3C**). These structural constraints explain the highly conserved nature of FATC and why mutations in this region abolish Tel1^{ATM} activity (Jiang et al., 2006).

The binding pocket for the adenosine ring of AMP-PNP is formed by a number of hydrophobic residues from both N- and C-lobes of the Tel1 kinase domain, with the glycine-rich loop from the N-lobe forming a partial lid over the bound nucleotide (**Figure 3B**). The highly conserved residue K2465 from the N-lobe contributes to α-/β- phosphate coordination of the bound AMP-PNP and is equivalent to K72 of PKA, which is essential for catalysis (Iyer et al., 2005) (**Figure 3B**). Interestingly, comparison of the Tel1 active site with nucleotide-bound mTOR in non-activated and RHEB-activated states (Yang et al., 2017) shows that the N-lobe and the glycine-rich loop of Tel1 most closely resemble that of non-activated mTOR (**Figure S4**). Further closure of the mTOR N-lobe and glycine-rich loop occur upon activation**.** It is therefore likely that the N-lobe and glycine-rich loop of Tel1 will also undergo further closure as part of the catalytic cycle. In addition to the glycine-rich loop, the active

site is further surrounded by LBE, PRD and FLAP-BE' (**Figure 3**), highlighting the importance of these elements in regulating active site access.

Tel1^{ATM} PRD-I and FATC regulate substrate binding

In addition to the open N-lobe, our structure shows that the active site cleft of the Tel1 kinase domain is restricted by the PIKK-regulatory domain (PRD), which we have denoted as the PRD-Insert (PRD) (see below, Figure 3B). The PRD is a PIKK-specific feature that was originally identified in ATR as an element between the kinase domain and the FATC that is essential for the binding of the activator TopBP1 (Mordes et al., 2008). Subsequent PIKK structures have revealed that the regions proposed to be involved in TopBP1 binding are in the highly conserved Kα10 helix, whereas the regions between Kα9 and Kα10 are variable in length and composition between different PIKKs **(Figure S5)**. Therefore we denote this variable region as the PRD-Insert (PRD-I), which is equivalent to Kα9b, Kα9c and Kα9d identified in mTOR and ATM structures (Baretić et al., 2017; Yang et al., 2013, 2017).

In the Tel1 and ATM closed dimer structures, the PRD-I, although only partly resolved, is predicted to occupy the position of a peptide substrate (Baretić et al., 2017; Xin et al., 2019). In the nucleotide-bound Tel1 structure, the complete PRD-I could be resolved. It structurally connects Kα9-Kα10 at the back of the kinase domain to the LBE and FATC at the front of the kinase domain (**Figure 3B**). Starting from Kα9, the PRD-I displays an extended loop followed by a single α-helix, situated directly above the activation loop, reaching towards LBE and FLAP-BE' before returning to Kα10 via a loop (**Figure 3B**). Importantly, PRD-I interacts with many of the key functional and structural elements, including the activation loop, the FATC, the LBE and the FLAP-BE' (**Figure 3B and 3D**). At its N-terminus, an invariant W2702 of PRD-I inserts into the hydrophobic pocket between Kα9 and Kα10, (**Figure 3B**). Towards the C-terminal end, acidic residues in PRD-I (^{2715}EEEHE^{2719}) are in close proximity to a positively charged patch in FLAP-BE' (^{2197}KRHYHR^{2202}) (**Figure 2D**). Together these elements occlude the access to the active site of Tel1.

To estimate the path of a bound Tel1 peptide substrate, we aligned the Tel1 kinase domain with the catalytic and activation loops of substrate-bound structures of PKA (PDB: 3x2u) (Das et al., 2015), Cdk2 (PDB: 3qhw) (Bao et al., 2011) and Pak-4 (PDB: 4jdh) (Chen et al., 2014) **(Figure 3D)**. It is clear that PRD-I in Tel1 overlaps with the peptide substrate-binding site, whereas the γ-phosphate of AMP-PNP and the catalytic aspartate (D2612) are suitably

close to the predicted location of the target Ser/Thr (P0) for phosphotransfer to occur (Das et al., 2015) (**Figure 3D**). The PRD-I, together with the LBE and FLAP-BE', thus occludes the active site and occupies substrate binding site. It is therefore the major determinant for inhibition and the requirement of Tel1 activation by MRX-dsDNA. Furthermore, Y2780 within the FATC sits close to the predicted P+1 peptide substrate position, suggesting a potential role in determining substrate specificity. This is consistent with a Y2780A mutant Tel1 demonstrating significantly defective levels of Rad53 phosphorylation, supporting the idea that this part of FATC may be involved in target recognition (Ogi et al., 2015). We thus suggest a dual role for FATC, being important for constraining the catalytic loop conformation as well as substrate peptide recognition.

Proposed activation mechanism of Tel1^{ATM}

Among the PIKK enzymes, only mTOR has a set of high-resolution structures that enable side chain assignments for both non-active and activated states. Comparisons of mTORC1 and the activator bound mTORC1-RHEB complex reveal that RHEB binding induces allosteric conformational changes to C-FAT that, via a clockwise rotation around the kinase C-lobe, results in the closure of the N-lobe and glycine-rich loop, thus realigning the active site (Yang et al., 2017). RHEB binds at a significant distance away from the kinase domain, close to N-FAT (Yang et al., 2017). Upon binding of RHEB there is little conformational change in N-FAT. Instead, through HEAT domain relocation, significant conformational changes occur in M-FAT and are subsequently transmitted to C-FAT (Yang et al., 2017). DNA-PKc also binds to its activator, Ku70-Ku80-DNA, through its HEAT repeats and structural comparisons between mTOR and DNA-PKc alone and in complex with their activators reveal a common mode of allosteric activation involving domain movement of M-FAT and C-FAT (Sharif et al., 2017; Sibanda et al., 2017; Yin et al., 2017). Despite the structural and sequence divergence of the N-HEAT region, the FAT-KIN domains of PIKKs are highly conserved in their structures (**Figure S6**). Furthermore, the conserved conformational changes in mTOR and DNA-PKc, irrespective of their distinct activator binding sites, suggest similar conformational changes might occur in Tel1 as a means for activation.

Intact MRX/MRN complexes along with dsDNA are required to stimulate Tel1^{ATM} activity (Hailemariam et al., 2019; Lee and Paull, 2004, 2005; Lee et al., 2003; Uziel et al., 2003). Tel1^{ATM} interacts with MRX/N via direct associations with the complex (Lee and Paull, 2004), and recent studies indicate that each of the three MRX subunits binds Tel1, suggesting an extensive MRX-Tel1 interaction interface (Hailemariam et al., 2019). The interaction

between Tel1 and the C-terminus of Xrs2/Nbs1, has been mapped to regions in the N-HEAT and C-HEAT domains in Tel1^{ATM} (You et al., 2005) in a similar location to DNA-PK and mTORC1 activator binding sites (**Figure S6**)**.** When we align the Tel1 and the inactive mTORC1 structures on their kinase C-lobes, N-FAT and C-FAT align reasonably well, with the largest differences in M-FAT (**Figure S6**). It is therefore plausible that binding of MRN/X would result in a concerted motion of HEAT and M-FAT which is propagated to C-FAT, resulting in the N-lobe and glycine-rich loop closure analogous to RHEB-activated mTORC1 (Yang et al., 2017). Distinct from mTOR, these movements would involve FLAP-BE within the C-FAT, which subsequently could affect PRD-I conformation and the dimer interface, presumably releasing inhibition for substrate binding and active site access. Recent cryoEM structures of apo-Tel1 suggested domain motions which are reminiscent of those observed during mTOR activation, with these intrinsic motions also resulting in increased PRD-I disorder (Xin et al., 2019). Interestingly, we did not observe similar domain movement or PRD-I disorder when Tel1 is nucleotide-bound. This lack of domain movement and a consistently ordered PRD-I maintaining autoinhibition are consistent with observed low-level kinase activity of Tel1 in the absence of activators (~0.065 phosphates transferred per minute per protomer) (Hailemariam et al., 2019).

Structural basis for hyperactive mutations of Tel1 and disease associated mutants in ATM

The role of PRD-I in inhibiting the activity of Tel1 and a proposed allosteric activation mechanism are supported by Tel1 hyper-active mutations identified in a genetic screen to rescue Mec1 deficient cells (Baldo et al., 2008). Many mutations are in similar positions to cancer-associated mTOR hyper-activating mutations known to increase sensitivity to allosteric activation (Yang et al., 2017). Several mutations map onto Kα9 and Kα10 and surrounding regions (**Figure 4A**). Among the mutant strains, three possess only single amino acid substitutions (N2692D, F2576V and Q2764H), that hyper-activate Tel1 activity. In one such mutant, N2692 of Kα9 is next to G2252 of C-FAT, which is also mutated in one of the strains, and therefore N2692D or G2252C could affect Kα9 conformation and consequently affect the PRD-I position (**Figure 4B**). Q2764 is within the FATC and also located at the dimer interface with M-FAT', specifically in a region just before the FLAP-BE'. A Q2672H substitution could affect FLAP-BE' to aid the relocation of PRD-I. There are also a number of mutations at the interface between N-FAT and C-lobe, close to the LBE and activation loop. These mutations could also affect substrate access (**Figure 4A**). Several mutations, e.g. I2336T and A2287V, are found within the C-FAT, close to the N-lobe and are

similar to known mTOR hyper-activating mutations (Yang et al., 2017). Presumably these mutations could allow the N-lobe to move closer to the active site in the absence of activator proteins.

The high structural homology between Tel1 and ATM FAT-KIN regions allows us to map pathogenic A-T missense and cancer-associated mutations onto the structure (**Figure 4C**). Ataxia telangiectasia is caused by bi-allelic mutation of the *ATM* gene and a significant proportion of A-T mutations result in abolished ATM expression, via truncation, incorrect splicing or incorrect frame-shifts (McKusick, 2007; Sandoval et al., 1999; Stankovic et al., 1998), suggesting that the molecular basis of A-T is loss of ATM protein. The majority of A-T missense mutations are found within the FAT-KIN domains (Choi et al., 2016) and ATM is often mutated in multiple cancers, with the FAT-KIN regions exhibiting some of the highest mutational frequency (Forbes et al., 2015; McKusick, 2007). Consistent with loss of activity in A-T and possibly in some cancers, some of the cancer-associated mutations are present in the highly conserved glycine-rich loop, the catalytic loop as well as the activation loop, thus affecting catalytic activity directly. A good example is the A-T mutation G2867R (G2609 in Tel1), which sits within the catalytic loop at a sharp turn just below the activation loop (**Figure 4D**). The introduction of a large charged side-chain would certainly alter the structure of these elements critical for catalysis.

A large number of disease-associated substitutions are found outside the Kinase active site and are distributed within the FAT domain and Kinase-FAT interface. Strikingly, there is a large cluster of mutations within the FLAP-BE and others around PRD-I, especially in Kα9 and Kα10 and regions surrounding them (**Figure 4**, **Table S1**). Presumably these mutations affect PRD-I, thus substrate phosphorylation. The AT mutation, V2424G (L2179 in Tel1), sits close to the cancer-associated mutations E2423, R2443Q, E2444K and D2448Φ (A2178, Q2206, R2209, D2210 in Tel1, respectively) (**Figure 4C**, **Table S1**) and are likely to disrupt the FLAP-BE structure as they hold the two helices together through salt-bridges or hydrophobic interactions. Disrupting the FLAP-BE would likely alter the PRD-I within the context of a dimer and would therefore alter peptide substrate access. Another cluster of mutations exists around LBE and FATC. Mutations in these regions would also affect substrate access by affecting PRD-I. Interestingly, similar to hyperactive mutations, several pathogenic mutations are concentrated around the interfaces between the C-lobe and N-FAT; again these mutations could affect key elements including LBE and the activation loop or prevent allosteric activation.

The nucleotide-bound structure presented here reveals that Tel1 exists as an auto-inhibited dimer that is likely activated via an allosteric mechanism found in other PIKKs. With the exception of N-lobe, the nucleotide co-ordinating residues and the catalytic site in the C-lobe are positioned to allow catalysis. However, the PRD-I competes with peptide-substrates and occludes the access to the active site, and is likely the major determinant of the low basal activity of Tel1. The PRD-I is held in place by a number of PIKK-specific features, with mutations in these regions leading to altered activity and disease phenotypes. The movement of the PRD-I is clearly necessary for full kinase activity and based on other related PIKKs may occur through an allosteric mechanism that is common to this family of kinases. Hyper-activating mutations and disease-associated mutations of Tel1 and ATM clearly suggest the FAT-domain is involved in regulating the activity of this kinase. Further structural work on an activator-bound Tel1^{ATM} will be required to resolve how the PRD-I is evicted from the active site to allow peptide-substrate binding.

ACKNOWLEDGMENTS

Initial screening of samples was carried out at Imperial College London Centre for Structural Biology EM facility. High-resolution data were collected at the eBIC (proposal EM19865), Diamond Light Source and we thank Drs C. Alistair Seibert and Yuriy Chaban for their support in collecting the data. eBIC is funded by the Wellcome Trust, MRC and BBSRC. This work is funded by the Wellcome Trust Investigator Award to XZ (210658/Z/18/Z), the National Institutes of Health (GM118129 to PB) and a NSF Graduate Research Fellowship (2014157291 to SH).

AUTHOR CONTRIBUTIONS

XZ and LAY designed the studies. SH and LAY prepared the samples. LAY with RA carried out initial cryoEM studies. LAY and RMW performed the cryoEM analysis, built and refined the structural models. XZ and PB supervised the studies. XZ, LAY and RMW wrote the manuscript with input from all the authors.

DECLARATION OF INTERESTS

The authors declare no competing interests.

REFERENCES

Adams, P.D., Afonine, P.V., Bunkóczi, G., Chen, V.B., Davis, I.W., Echols, N., Headd, J.J., Hung, L.W., Kapral, G.J., Grosse-Kunstleve, R.W., et al. (2010). PHENIX: a comprehensive Python-based system for macromolecular structure solution. Acta Crystallogr D Biol Crystallogr *66*, 213–221.

Afonine, P.V., Klaholz, B.P., Moriarty, N.W., Poon, B.K., Sobolev, O.V., Terwilliger, T.C., Adams, P.D., and Urzhumtsev, A. (2018). New tools for the analysis and validation of cryo-EM maps and atomic models. Acta Crystallogr D Struct Biol *74*, 814–840.

Bakkenist, C.J., and Kastan, M.B. (2003). DNA damage activates ATM through intermolecular autophosphorylation and dimer dissociation. Nature *421*, 499–506.

Baldo, V., Testoni, V., Lucchini, G., and Longhese, M.P. (2008). Dominant TEL1-hy mutations compensate for Mec1 lack of functions in the DNA damage response. Mol Cell Biol *28*, 358–375.

Bao, Z.Q., Jacobsen, D.M., and Young, M.A. (2011). Briefly bound to activate: transient binding of a second catalytic magnesium activates the structure and dynamics of CDK2 kinase for catalysis. Structure *19*, 675–690.

Baretić, D., and Williams, R.L. (2014). PIKKs--the solenoid nest where partners and kinases meet. Curr Opin Struct Biol *29*, 134–142.

Baretić, D., Pollard, H.K., Fisher, D.I., Johnson, C.M., Santhanam, B., Truman, C.M., Kouba, T., Fersht, A.R., Phillips, C., and Williams, R.L. (2017). Structures of closed and open conformations of dimeric human ATM. Sci Adv *3*, e1700933.

Bosotti, R., Isacchi, A., and Sonnhammer, E.L. (2000). FAT: a novel domain in PIK-related kinases. Trends Biochem Sci *25*, 225–227.

Chen, C., Ha, B.H., Thévenin, A.F., Lou, H.J., Zhang, R., Yip, K.Y., Peterson, J.R., Gerstein, M., Kim, P.M., Filippakopoulos, P., et al. (2014). Identification of a major determinant for serine-threonine kinase phosphoacceptor specificity. Mol Cell *53*, 140–147.

Chen, V.B., Wedell, J.R., Wenger, R.K., Ulrich, E.L., and Markley, J.L. (2015). MolProbity for the masses-of data. J Biomol NMR *63*, 77–83.

Choi, M., Kipps, T., and Kurzrock, R. (2016). ATM mutations in cancer: therapeutic implications. Mol Cancer Ther *15*, 1781–1791.

Das, A., Gerlits, O., Parks, J.M., Langan, P., Kovalevsky, A., and Heller, W.T. (2015). Protein Kinase A Catalytic Subunit Primed for Action: Time-Lapse Crystallography of Michaelis Complex Formation. Structure *23*, 2331–2340.

Emsley, P., and Cowtan, K. (2004). Coot: model-building tools for molecular graphics. Acta Crystallogr D Biol Crystallogr *60*, 2126–2132.

Falck, J., Coates, J., and Jackson, S.P. (2005). Conserved modes of recruitment of ATM, ATR and DNA-PKcs to sites of DNA damage. Nature *434*, 605–611.

Forbes, S.A., Beare, D., Gunasekaran, P., Leung, K., Bindal, N., Boutselakis, H., Ding, M., Bamford, S., Cole, C., Ward, S., et al. (2015). COSMIC: exploring the world's knowledge of somatic mutations in human cancer. Nucleic Acids Res *43*, D805–11.

Hailemariam, S., Kumar, S., and Burgers, P.M. (2019). Activation of Tel1^{ATM} kinase requires Rad50 ATPase and long nucleosome-free DNA, but no DNA ends. Journal of Biological Chemistry jbc.RA119.008410.

Imseng, S., Aylett, C.H., and Maier, T. (2018). Architecture and activation of phosphatidylinositol 3-kinase related kinases. Curr Opin Struct Biol *49*, 177–189.

Iyer, G.H., Garrod, S., Woods, V.L., and Taylor, S.S. (2005). Catalytic independent functions of a protein kinase as revealed by a kinase-dead mutant: study of the Lys72His mutant of cAMP-dependent kinase. J Mol Biol *351*, 1110–1122.

Jiang, X., Sun, Y., Chen, S., Roy, K., and Price, B.D. (2006). The FATC domains of PIKK proteins are functionally equivalent and participate in the Tip60-dependent activation of DNA-PKcs and ATM. J Biol Chem *281*, 15741–15746.

Kenyon, C.P., Roth, R.L., van der Westhuyzen, C.W., and Parkinson, C.J. (2012). Conserved phosphoryl transfer mechanisms within kinase families and the role of the C8 proton of ATP in the activation of phosphoryl transfer. BMC Res Notes *5*, 131.

Kozlov, S.V., Graham, M.E., Peng, C., Chen, P., Robinson, P.J., and Lavin, M.F. (2006). Involvement of novel autophosphorylation sites in ATM activation. EMBO J *25*, 3504–3514.

Krissinel, E., and Henrick, K. (2007). Inference of macromolecular assemblies from crystalline state. J Mol Biol *372*, 774–797.

Lavin, M.F., and Kozlov, S. (2007). ATM activation and DNA damage response. Cell Cycle *6*, 931–942.

Lee, J.H., and Paull, T.T. (2004). Direct activation of the ATM protein kinase by the Mre11/Rad50/Nbs1 complex. Science *304*, 93–96.

Lee, J.H., and Paull, T.T. (2005). ATM activation by DNA double-strand breaks through the Mre11-Rad50-Nbs1 complex. Science *308*, 551–554.

Lee, J.H., Xu, B., Lee, C.H., Ahn, J.Y., Song, M.S., Lee, H., Canman, C.E., Lee, J.S., Kastan, M.B., and Lim, D.S. (2003). Distinct functions of Nijmegen breakage syndrome in ataxia telangiectasia mutated-dependent responses to DNA damage. Mol Cancer Res *1*, 674–681.

Matsuoka, S., Ballif, B.A., Smogorzewska, A., McDonald, E.R., Hurov, K.E., Luo, J., Bakalarski, C.E., Zhao, Z., Solimini, N., Lerenthal, Y., et al. (2007). ATM and ATR substrate analysis reveals extensive protein networks responsive to DNA damage. Science *316*, 1160–1166.

McKusick, V.A. (2007). Mendelian Inheritance in Man and its online version, OMIM. Am J Hum Genet *80*, 588–604.

Mordes, D.A., Glick, G.G., Zhao, R., and Cortez, D. (2008). TopBP1 activates ATR through ATRIP and a PIKK regulatory domain. Genes Dev *22*, 1478–1489.

Ogi, H., Goto, G.H., Ghosh, A., Zencir, S., Henry, E., and Sugimoto, K. (2015). Requirement of the FATC domain of protein kinase Tel1 for localization to DNA ends and target protein recognition. Mol Biol Cell *26*, 3480–3488.

Pei, J., and Grishin, N.V. (2007). PROMALS: towards accurate multiple sequence alignments of distantly related proteins. Bioinformatics *23*, 802–808.

Pettersen, E.F., Goddard, T.D., Huang, C.C., Couch, G.S., Greenblatt, D.M., Meng, E.C., and Ferrin, T.E. (2004). UCSF Chimera—a visualization system for exploratory research and analysis. J Comput Chem *25*, 1605–1612.

Ramlaul, K., Palmer, C.M., and Aylett, C.H.S. (2019). A local agreement filtering algorithm for transmission EM reconstructions. J Struct Biol *205*, 30–40.

Sandoval, N., Platzer, M., Rosenthal, A., Dörk, T., Bendix, R., Skawran, B., Stuhrmann, M., Wegner, R.D., Sperling, K., Banin, S., et al. (1999). Characterization of ATM gene mutations in 66 ataxia telangiectasia families. Hum Mol Genet *8*, 69–79.

Sawicka, M., Wanrooij, P.H., Darbari, V.C., Tannous, E., Hailemariam, S., Bose, D., Makarova, A.V., Burgers, P.M., and Zhang, X. (2016). The dimeric architecture of checkpoint kinases mec1atr and tel1atm reveal a common structural organization. J Biol Chem *291*, 13436–13447.

Scheres, S.H., and Chen, S. (2012). Prevention of overfitting in cryo-EM structure determination. Nat Methods *9*, 853–854.

Sharif, H., Li, Y., Dong, Y., Dong, L., Wang, W.L., Mao, Y., and Wu, H. (2017). Cryo-EM structure of the DNA-PK holoenzyme. Proc Natl Acad Sci USA *114*, 7367–7372.

Sibanda, B.L., Chirgadze, D.Y., Ascher, D.B., and Blundell, T.L. (2017). DNA-PKcs structure suggests an allosteric mechanism modulating DNA double-strand break repair. Science *355*, 520–524.

Sievers, F., Wilm, A., Dineen, D., Gibson, T.J., Karplus, K., Li, W., Lopez, R., McWilliam, H., Remmert, M., Söding, J., et al. (2011). Fast, scalable generation of high-quality protein multiple sequence alignments using Clustal Omega. Mol Syst Biol *7*, 539.

Stankovic, T., Kidd, A.M., Sutcliffe, A., McGuire, G.M., Robinson, P., Weber, P., Bedenham, T., Bradwell, A.R., Easton, D.F., Lennox, G.G., et al. (1998). ATM mutations and phenotypes in ataxia-telangiectasia families in the British Isles: expression of mutant ATM and the risk of leukemia, lymphoma, and breast cancer. Am J Hum Genet *62*, 334–345.

Sun, Y., Jiang, X., Chen, S., Fernandes, N., and Price, B.D. (2005). A role for the Tip60 histone acetyltransferase in the acetylation and activation of ATM. Proc Natl Acad Sci USA *102*, 13182–13187.

Uziel, T., Lerenthal, Y., Moyal, L., Andegeko, Y., Mittelman, L., and Shiloh, Y. (2003). Requirement of the MRN complex for ATM activation by DNA damage. EMBO J *22*, 5612–5621.

Walker, E.H., Perisic, O., Ried, C., Stephens, L., and Williams, R.L. (1999). Structural insights into phosphoinositide 3-kinase catalysis and signalling. Nature *402*, 313–320.

Wang, X., Ran, T., Zhang, X., Xin, J., Zhang, Z., Wu, T., Wang, W., and Cai, G. (2017). 3.9 Å structure of the yeast Mec1-Ddc2 complex, a homolog of human ATR-ATRIP. Science *358*, 1206–1209.

Xin, J., Xu, Z., Wang, X., Tian, Y., Zhang, Z., and Cai, G. (2019). Structural basis of allosteric regulation of Tel1/ATM kinase. Cell Res.

Yang, H., Rudge, D.G., Koos, J.D., Vaidialingam, B., Yang, H.J., and Pavletich, N.P. (2013). mTOR kinase structure, mechanism and regulation. Nature *497*, 217–223.

Yang, H., Jiang, X., Li, B., Yang, H.J., Miller, M., Yang, A., Dhar, A., and Pavletich, N.P. (2017). Mechanisms of mTORC1 activation by RHEB and inhibition by PRAS40. Nature *552*, 368–373.

Yin, X., Liu, M., Tian, Y., Wang, J., and Xu, Y. (2017). Cryo-EM structure of human DNA-PK holoenzyme. Cell Res *27*, 1341–1350.

You, Z., Chahwan, C., Bailis, J., Hunter, T., and Russell, P. (2005). ATM activation and its recruitment to damaged DNA require binding to the C terminus of Nbs1. Mol Cell Biol *25*, 5363–5379.

Zhang, K. (2016). Gctf: Real-time CTF determination and correction. J Struct Biol *193*, 1–12.

Zheng, S.Q., Palovcak, E., Armache, J.P., Verba, K.A., Cheng, Y., and Agard, D.A. (2017). MotionCor2: anisotropic correction of beam-induced motion for improved cryo-electron microscopy. Nat Methods *14*, 331–332.

Zivanov, J., Nakane, T., Forsberg, B.O., Kimanius, D., Hagen, W.J., Lindahl, E., and Scheres, S.H. (2018). New tools for automated high-resolution cryo-EM structure determination in RELION-3. Elife *7*.

Zivanov, J., Nakane, T., and Scheres, S.H.W. (2019). A Bayesian approach to beam-induced motion correction in cryo-EM single-particle analysis. IUCrJ *6*, 5–17.

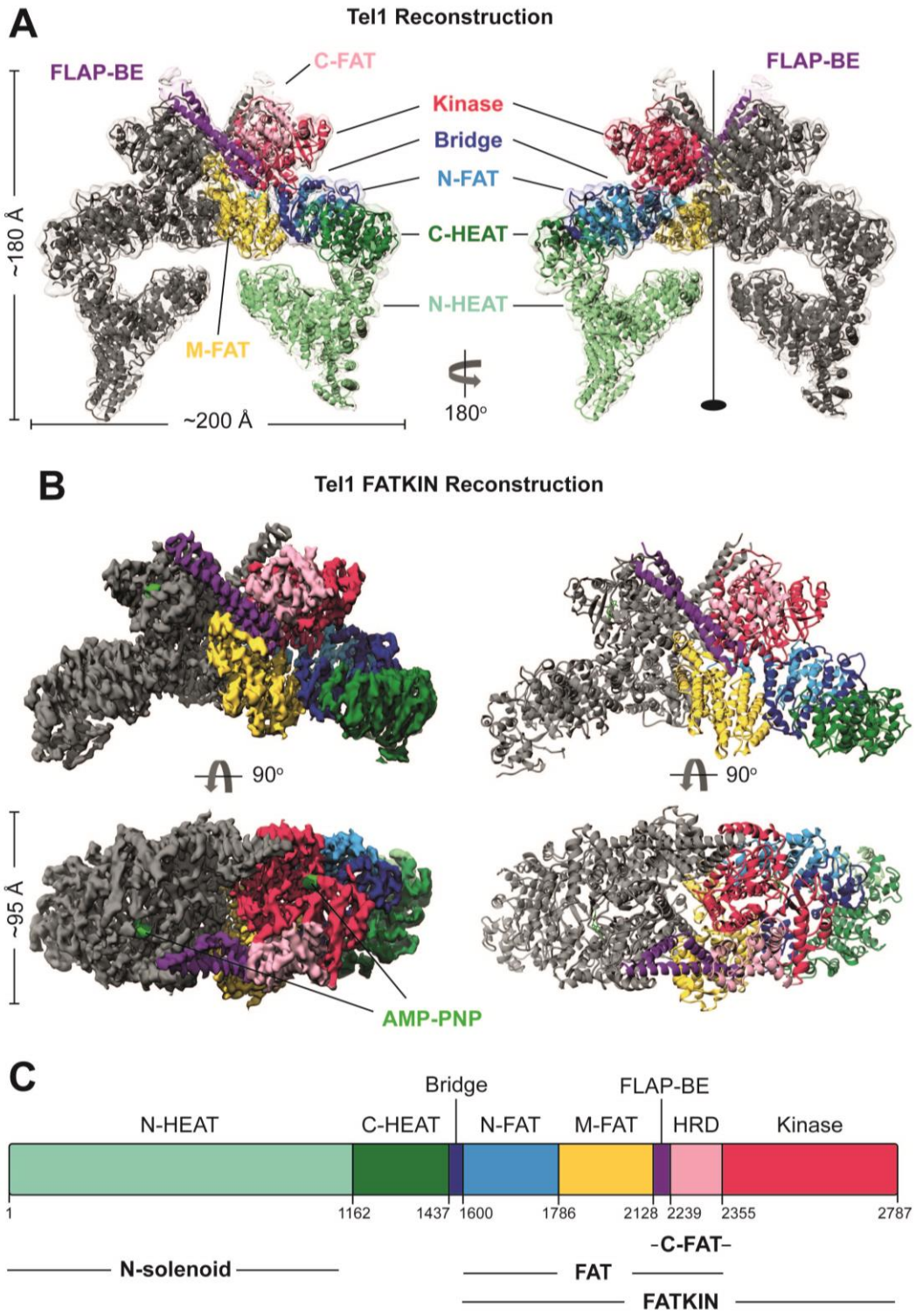

Figure 1 – Structure of Tel1 Dimer. (A) Overall structure of the nucleotide bound (AMP-PNP) Tel1 dimer structure determined by cryoEM to 4.0 Å resolution by Gold Standard Fourier shell correlation (GS-FSC). Regions of the structure are coloured according to domains; Kinase, red; C-FAT, pink; FLAP-BE, purple; N-FAT, blue; Bridge, dark blue; C-HEAT, green; N-HEAT, light green. Approximate dimensions of the protein are also given. (B) Reconstruction of the FATKIN region determined to 3.7 Å resolution by GS-FSC, coloured as in (A). (C) Domain arrangement of Tel1.

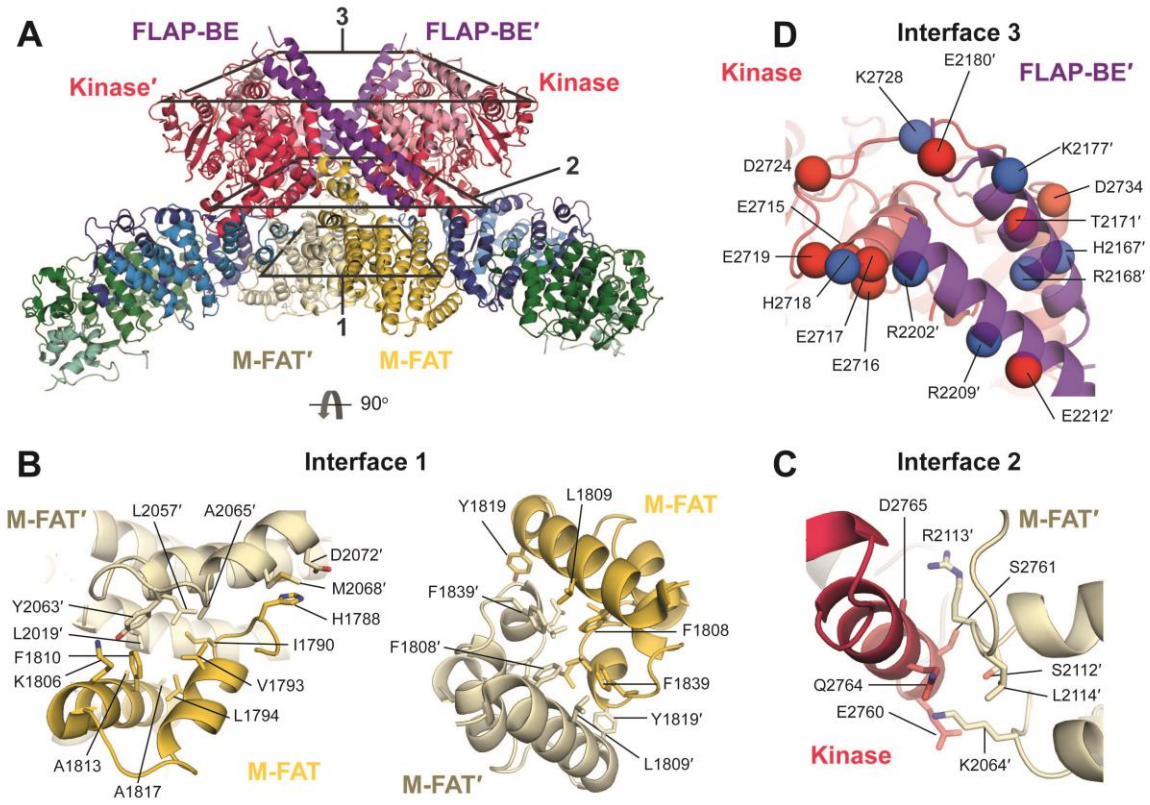

Figure 2 – Tel1 Dimer Interface. (A) FATKIN dimer structure coloured by domain as in Fig1, and for clarity M-FAT' is coloured in pale yellow to distinguish it clearly. Different layers of the dimer interface are boxed and detailed views of the nature of the interface are shown in (B-D).

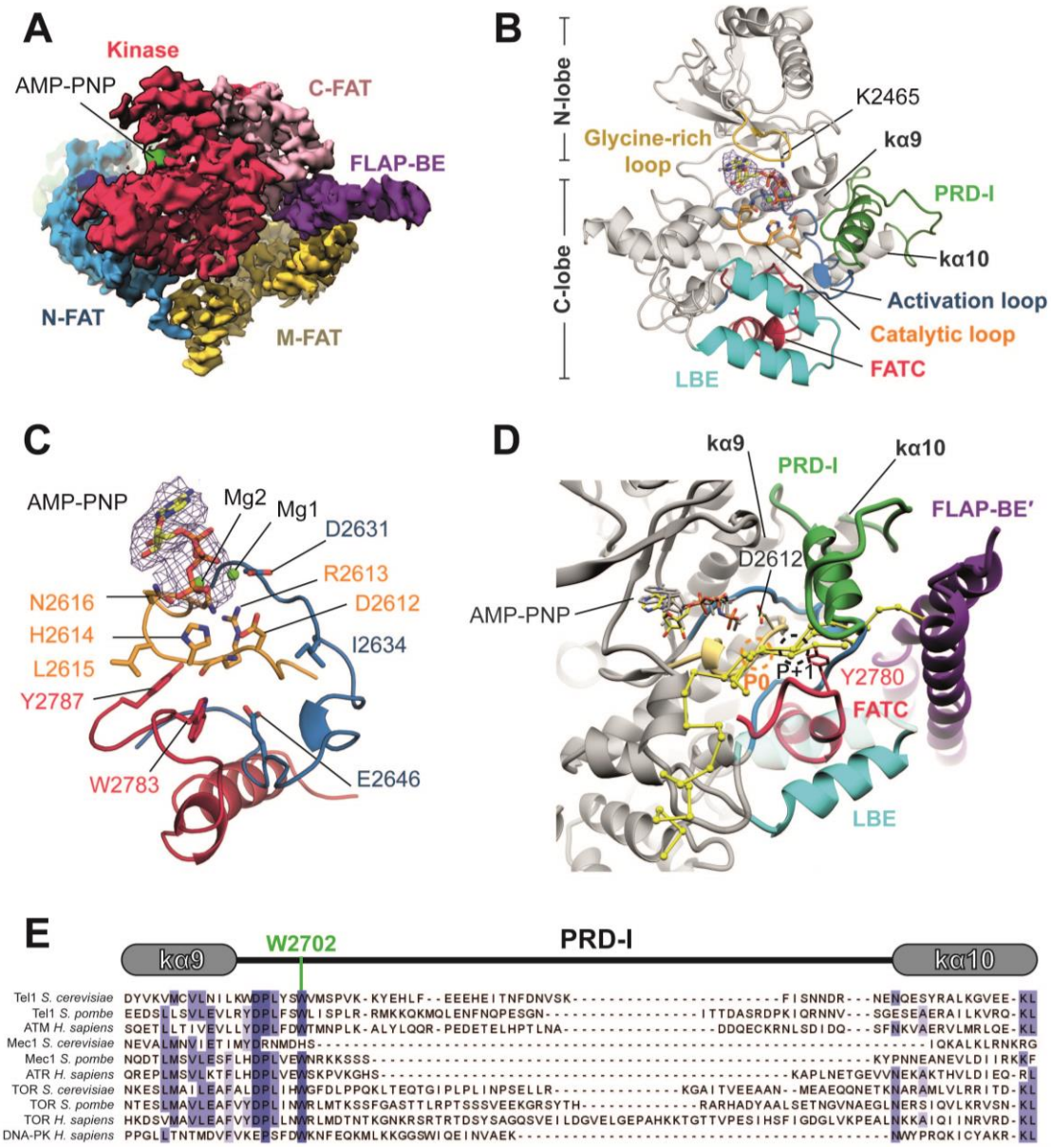

Figure 3 – Details of the Tel1 Kinase Domain and the PRD-I. (A) CryoEM density of Tel1 FAT-KIN shows the FAT domains cradle the kinase domain. Domains are coloured as in Fig1. (B) Structural details of the AMP-PNP bound (with cryo EM density shown as mesh) kinase domain (grey) with key structural features highlighted and labelled. (C) Molecular details of interacting residues with AMP-PNP, the activation loop (blue) and FATC (red) which support the catalytic loop (yellow). (D) Predicted peptide binding using superimposition of kinase-substrate peptide complex crystal structures of PKA, Pak-4 and Cdk2. The target serine/threonine is shown and labelled (P0) and the predicted location of the P+1 residue is highlighted and is close to Y2780 of the FATC. (E) Sequence alignment of the structurally conserved kα9 and kα10 and the intervening PRD of several PIKKs. An invariable tryptophan (W2702) that anchors the PRD is highlighted.

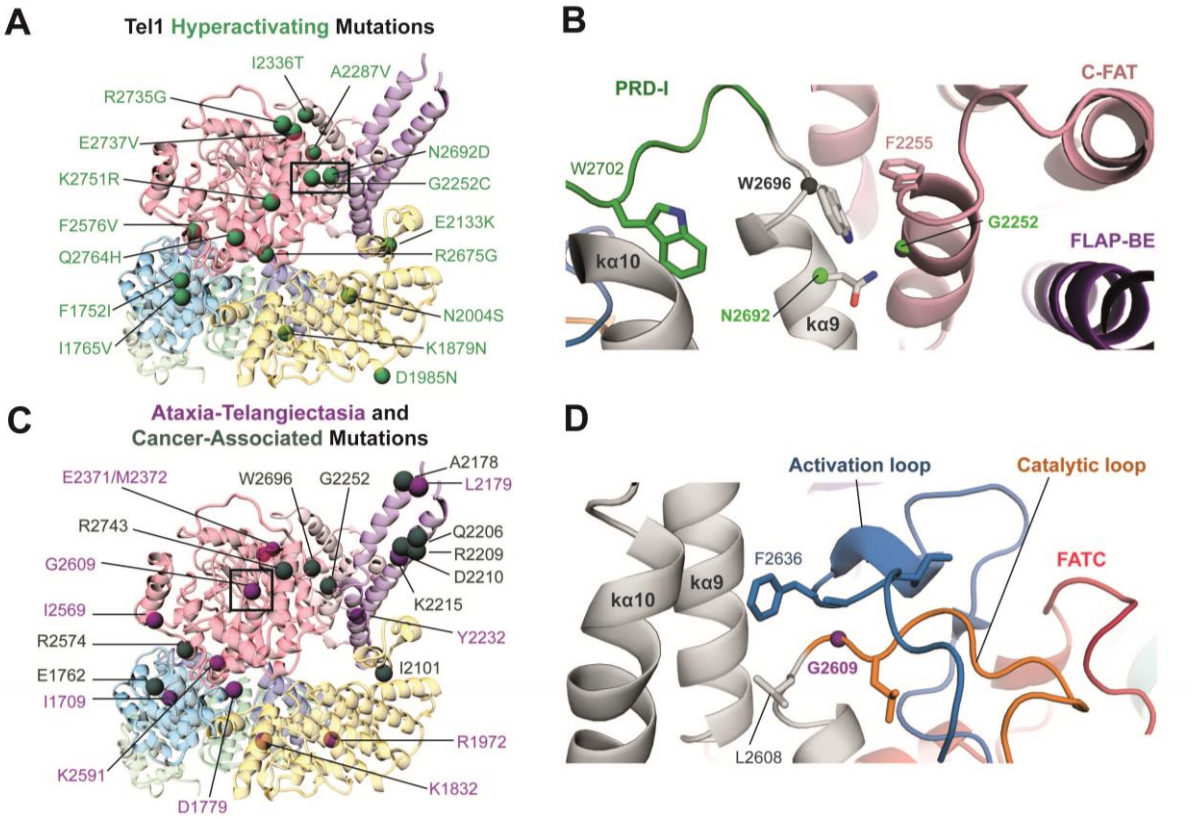

Figure 4 – Mapping of Tel1 hyper-activating and ATM disease associated mutations. (A) Tel1 FAT-KIN protomer is shown coloured as in Fig1 with Hyper-activating mutations found in (Baldo et al., 2008) mapped and shown as green spheres. (B) Molecular details of a cluster of mutations in kα9 found in cancer and described in hyper-activating Tel1 phenotypes. (C) Cancer-associated (dark grey spheres) and Ataxia Telangiectasia-associated (A-T, purple spheres) mutations at structurally equivalent locations (see Table S1 for details). (D) Molecular details of G2609 (G2867 in ATM), which is mutated to Arginine in A-T.

Table 1 – Data collection and Refinement statistics

Data Acquisition			
Dataset Number	Dataset 1	Dataset 2	Dataset 3
Sample	Tel1-AMP-PNP		
Microscope	Titan KRIOS (eBIC, Oxfordshire, UK)		
Voltage (kV)	300	300	300
Number of Micrographs	4508	2445	5656
Nominal Magnification	75,000 (129032)	75,000 (129032)	75,000 (129032)
Detector	Falcon III (linear mode)	Falcon III (linear mode)	Falcon III (linear mode)
Pixel size	1.085 A/pix	1.085 A/pix	1.085 A/pix
Dose rate	105 $e^-/Å^2/s$	120 $e^-/Å^2/s$	102 $e^-/Å^2/s$
Frames (dose/frame)	23 (3.8 $e^-/Å^2$/frame)	34 (2.6 $e^-/Å^2$/frame)	34 (2.6 $e^-/Å^2$/frame)
Total Dose	88.8 $e^-/Å^2$	88.4 $e^-/Å^2$	88.9 $e^-/Å^2$
Integration time	0.59 s	0.87 s	0.87 s
Defocus Range	-1.1 to -3.2	-1.1 to -3.2	-1.2 to -3.2

Image Processing		
Reconstruction	Tel1 Dimer (EMD-XXXX)	FAT-KIN (EMD-XXXX)
Software	RELION-3.0	RELION-3.0
Particles	167596	167596
Box Size (pixels)	380 x 380 x 380	380 x 380 x 380
Symmetry	C2	C2
Map Resolution (Å)	4.0	3.7
Map Resolution range (Å)	3.6 – 5.6	3.4 – 4.6
Map Sharpening B-Factor ($Å^2$)	-75	-165

Coordinate Refinement		
Software	PHENIX	
Algorithm	REAL SPACE REFINEMENT	
Resolution (Å)	4.0	3.7
$FSC_{model\ vs.\ map}$ = 0.5 (Å)	4.1	3.9
Correlation Co-efficient	0.84	0.81

Model	
PDB Code	XXXX
Number of Residues	

Protein	5158 (2579 per monomer)
Ligand (AMP-PNP)	2 (1 per monomer)
B-factors Overall	243.7 (82.2 for FAT-KIN)
Protein	243.7 (82.2 for FAT-KIN)
AMP-PNP	223.3 (79.0 for FAT-KIN)
RMS deviations	
Bond Length (Å)	0.006
Bond Angles (°)	0.99
Validation	
Molprobity Score	1.86
Molprobity Clashscore	5.87
Rotamer Outliers (%)	0.8
C_β deviations (%)	0
Ramachandran Plot	
Favoured (%)	90.4
Allowed (%)	9.5
Outliers (%)	0.1

METHODS

Electron Microscopy grid preparation

A frozen aliquot of *Saccharomyces cerevisiae* Tel1 (800nM, stored in 40mM HEPES 7.8, 10% Glycerol, 200mM NaCl, 2mM DTT, 0.1% Tween-20, 0.01% NP40, 1mM EDTA, 0.5mM EGTA) was diluted 8-fold using sequential addition of 10 µl volumes of buffer (50mM Tris-HCl, 50mM NaCl, pH 7.4 supplemented with AMP-PNP and Magnesium Acetate), and was incubated for 30 minutes on ice. The final concentration of Tel1 was 100nM; 1mM AMP-PNP; 4mM $Mg(OAc)_2$. Samples (4 µl) were deposited onto Lacey Carbon 300 mesh gold grids that also have an additional ultrathin carbon support layer (Ted Pella Inc. USA), which were plasma-cleaned, for 30 seconds in air, prior to sample application. Samples were vitrified in liquid ethane at liquid nitrogen temperature using a Vitrobot Mk IV (FEI) set with a blotting force of -6, a waiting time of 60 s and a blotting time of 2 seconds. Plunge freezing was performed at 4 °C and 100% humidity.

CryoEM Data Acquisition

High-resolution data were collected for Tel1 over three sessions at eBIC (Oxfordshire, UK) on an FEI Titan KRIOS (Thermo Fisher) and are summarised in Table 1. For all three datasets, the microscopes were operated at 300kV with the specimen at cryogenic temperatures (approximately -180 °C) with images recorded at 1-3 µm underfocus on a Falcon III direct electron detector in linear mode at a nominal magnification of 75,000 X, corresponding to a calibrated pixel size of 1.09 Å, and a cumulative total electron dose of ~90 $e^-/Å^2$. We collected a total of 12,609 micrographs, which were fractionated into frames (dataset 1, 4508, 23 frames; dataset 2; 2445, 34 frames; dataset 3; 5656, 34 frames). A representative micrograph is shown in Figure S1A.

CryoEM Image Processing

Movie frames were aligned, corrected for drift, beam induced motion and dose-weighted using MotionCor2 (Zheng et al., 2017) using a 5 x 5 patch implemented in RELION-3.0 (Zivanov et al., 2018). Contrast transfer function (CTF) fitting was performed using Gctf (Zhang, 2016). Particles were picked with Gautomatch using re-projections of a low resolution Tel1 EM structure (Sawicka et al., 2016) for selection. Particles were extracted in RELION-3.0 using a box size of 400 x 400 pixels and binned four times for initial processing. The number of particles picked per dataset are summarised in Table 1. Reference-free 2D classification of particles from a single dataset was performed in RELION-3.0 and revealed two major views (Figure S1A) and subsequent 3D volumes after refinement showed preferential orientation issues. Therefore, 2D classification was omitted as a first step and 3D classification with an initial Tel1 model (Sawicka et al., 2016), filtered to 60 Å, was performed instead for all datasets. Particle star files were sub-divided to speed up the processing pipeline, as the datasets still contained non-particles and 'junk' not removed by 2D classification. Initial 3D classification with 4 classes produced a single class (23% particles) that exhibited features expected for this protein. Similar 3D classes from each batch/dataset were selected, re-extracted twice binned, and joined before an initial consensus 3D refinement. After 3D refinement the particle stack was further cleaned using 3D classification in RELION-3.0 using local angular searches, higher T-factors (T=8) and sub-dividing into six classes. Of the 6 classes many displayed over-fitted and noisy features, however a single class (29%, ~160K particles) showed clear secondary structure and was selected for further refinement. Particles corresponding to the best 3D class were re-extracted (1.085 Å/pixel) in a slightly smaller box size (380 x 380 pixels) and were refined according to the gold-standard refinement procedure implemented in RELION-3.0 applying C2 symmetry and using a soft mask (C2 symmetric) corresponding to the protein, resulting in a 4.4 Å reconstruction after post-processing according to the FSC = 0.143 criterion (Scheres and Chen, 2012). Beam-induced particle polishing (Zivanov et al., 2019) followed

by CTF refinement (Zivanov et al., 2018) improved the map resolution to 4.0 Å. Local resolution estimates calculated in RELION-3.0 showed that density regions corresponding to the N-terminal HEAT repeats were of lower resolution (~5 Å) as compared to the kinase-containing C-terminal half (~3.6 – 4.4 Å, Figure S2A). Using a soft mask (C2 symmetrized) encompassing some of the HEAT repeat regions, the FAT domain and the C-terminal kinase domain of the dimer, 3D refinement (gold-standard) improved the resolution yielding a 3.7 Å reconstruction after post-processing (according to FSC = 0.143 criterion), corresponding to approximately two thirds of the protein. Angular accuracy and angular distribution plots suggest that rare views were captured by omitting initial 2D classification steps and that the early preferential orientation issues were circumvented. Local resolution estimates show that the best resolution regions are better than 3.5 Å and the map shows defined secondary structure features and clearly resolved bulky side chains (Figure S2). A set of 167596 particles images (~47% from dataset 1, ~12% from dataset 2, ~41% from dataset 3) were used for the final reconstructions.

Tel1 Model Building and Refinement

The final 3.7 Å and 4.0 Å EM maps were sharpened with a negative B-factor of -165, as determined by RELION-3.0, or less to avoid high-resolution noise and therefore over fitting of a model. A structure of dimeric human ATM (pdb 5np0) was docked into the maps in the first instance. It was clear from this initial fitting that AMP-PNP was bound in the active site. The ATM model, which is restricted to Cα-Cβ only, was manually fitted as rigid body regions into our maps and residues that did not fit the density or that clearly differed between species were trimmed in Coot (Emsley and Cowtan, 2004). The high-resolution maps permitted accurate model building and therefore we built the structure manually starting with the kinase bound to AMP-PNP using the high-resolution nucleotide-bound X-ray structures of mTOR (Yang et al., 2013) and PKA (Das et al., 2015) as guides alongside side-chain density in our maps to model the correct location of the catalytic loop, activation loop and the glycine-rich loop. The kinase domain was subsequently built manually by using residues at the AMP-PNP bound active site as a start point and using bulky side chains as landmarks for correct sequence assignment against UNIPROT accession code P38110. We also made use of a local agreement filtering program (Local Agreement Filtering Algorithm for Transmission EM Reconstructions [LAFTER]) (Ramlaul et al., 2019) that produces a map filtered to maintain consistent features between the two independent half-maps from gold-standard refinement and recovers more signal. This allowed us to confidently place residues in loops and regions where sharpening did not aid model building. We were able to build co-ordinates with the majority of side chains corresponding to residues 1527-2787 and place residues with sequence assignment (but occasional side chains) to 967-1526. The N-HEATs

were more challenging to build and so these were built as a poly-Alanine trace. The co-ordinates for the model corresponding to the FAT-Kinase regions of the dimer were first real space refined in PHENIX (Adams et al., 2010; Afonine et al., 2018) against the 3.7 Å map (sharpened with -165 B-factor). The Tel1 Dimer co-ordinates (which include the previously refined FAT-Kinase region) were refined against the 4.0 Å map (sharpened with -75 B-factor). In both cases data used in refinement was limited to spatial frequencies to the RELION estimated resolution to prevent over-fitting. Ramachandran, C_β, non-crystallographic symmetry (NCS), and secondary structure restraints (generated in PHENIX using caBLAM) were used throughout the refinement to ensure good model geometry and the coordinates were validated using MOLPROBITY (Chen et al., 2015) in PHENIX. Typically 3-cycles of real space refinement were run (3 macro cycles of global and local optimization and B-factor refinement), with PHENIX automatically estimating relative weighting of the restraints and map to prevent over-fitting (Afonine et al., 2018). Refinement and model statistics are given in Table 1. Map vs model FSC curves were also generated in PHENIX as part of the refinement procedure and given in Figure S2.

Model Interpretation and Analysis

Figures were created using PyMOL (Schrodinger, LLC) and UCSF Chimera (Pettersen et al., 2004). Structural superposition of structures was performed in PyMOL aligning kinases by their C-lobes. Dimer interface buried surface area estimates were calculated using PISA (Krissinel and Henrick, 2007). Multiple sequence alignments were performed using Clustal Omega (Sievers et al., 2011) and displayed in Jalview. Structure-based sequence alignments were performed in PROMALS3D (Pei and Grishin, 2007).

Table S1

Tel1 Hyperactivity Mutations - found in reference (Baldo et al., 2008)				
Variant	**Mutation(s)**	**Region**	**Effect on Catalysis**	**Structural comments**
Tel1-hy385	N2692D	Kα9	Increase	
Tel1-hy394	I1765V	M-FAT	Increase	Could prevent allosteric activation
	K1879N	M-FAT		
	N2004S	M-FAT		
	R2675G	Kinase C-lobe		
Tel1-hy680	Q2764H	Kinase C-lobe	Increase	
Tel1-hy909	A2287V	HRD	Increase	ATM K3016 is Acetylated during activation
	I2336T	HRD		
	K2751R	Kinase		
Tel1-hy184	F1752I	M-FAT	None	PRD-I conformation may be altered
	D1985N	M-FAT		
	E2133K	M-FAT/FLAP-BE		
	R2735G	Close to PRD-I		
	E2737V	Close to PRD-I		
Tel1-hy628	N2185H	FLAP-BE loop (Not modelled)	None	*Cancer mutation, see below
	G2252C*	HRD packs against Kα9		
Tel1-hy544	F2576V	Kinase C-lobe	Reduction	
ATM Disease-Associated Mutations				
ATM mutation	**Tel1**	**Region**	**Disease**	**Structural comments**
G2867R	G2609	Kinase-Catalytic loop	AT	Disrupt activation and catalytic loop
R2849P	K2591	Kinase domain	AT	Kinase - M-FAT interface
F2827C	I2569	LBE (Kα4c)	AT	LBE contacts PRD
D2625E/A2626P	E2371/M2372	Kα1	AT	Disrupts N-lobe
V2424G	L2180	FLAP-BE	AT	Likely contacting PRD
Y2470D	Y2232	FLAP-BE	AT	Disrupts FLAP-BE
A2067D	K1833	M-FAT, Dimer interface	AT	
D2016G	D1780	M-FAT	AT	Interface with C-lobe
R2227C	R1973	M-FAT	AT	
V1913G	I1710	N-FAT	AT	N-FAT/M-FAT boundary
N1983S/Y	~E1763	Shoulders?	Cancer	See R2832C
C2337R	I2102	Close to FLAP-BE	Cancer	M-FAT/FLAP-BE junction
E2423G	A2179	FLAP-BE	Cancer	Likely contacting PRD
R2443Q	R2209	FLAP-BE	Cancer	Holding FLAP-BE helices together
E2444K	Q2206	FLAP-BE	Cancer	
D2448Φ/N	D2210	FLAP-BE	Cancer	
R2453H/P	K2215	FLAP-BE	Cancer	

S2489F	G2252	HRD	Cancer	Packs against Kα9. Likely similar effect as mutation Y2954C in Kα9.
G2694R/E	Gly-rich loop		Cancer	Disruption of active site
G2695X				
P2699X				
D2708N/Y	Hairpin at rear of Gly-rich loop			
G2709D				
D721X (+ neighbours)	Kα3 (PKA αC equivalent)			
N2875T/S	Catalytic loop (Mg2-binding)			
D2289X	DLG motif (Mg1-binding)			
L2890X				
G2891X				
R2832C	R2574	Kα6	Cancer	Likely interacts with region around P1759. ATM has an extended helix here, could be linked to allostery. This region also contains N1983S/Y.
Y2954C	W2696	Kα9	Cancer	Beginning of PRD, packs against HRD. See S2489F.
R3008H/C	R2743	Kα10	Cancer	Helix after PRD